

**Sensitivity Analysis and Standard Error Development of a River Temperature Model  
(FLUVIAL-EB): Understanding Predicted River Temperature Response to Atmospheric  
Observations at the Basin Scale**

A Thesis submitted to the faculty of  
San Francisco State University  
In partial fulfillment of  
the requirements for  
the Degree

Master of Science

In

Geoscience

by

Nicholas Modar

San Francisco, California

May 2023

Copyright by  
Nicholas Modar  
2023

## Certification of Approval

I certify that I have read Sensitivity Analysis and Standard Error Development of a River Temperature Model (FLUVIAL-EB): Understanding Predicted River Temperature Response to Atmospheric Observations at the Basin Scale. by Nicholas Modar, and that in my opinion this work meets the criteria for approving a thesis submitted in partial fulfillment of the requirement for the degree Master of Science in Geoscience at San Francisco State University.

---

Dr. Erin Bray, Ph.D.  
Associate Professor,  
Thesis Committee Chair

---

Jeff Dozier, Ph.D.  
Emeritus

---

Leora Nanus, Ph.D.  
Associate Professor

## Abstract

This thesis encompasses three chapters that aim to improve the understanding of a large-lowland river's radiative energy balance and the atmospheric-water surface interactions that control it. In Chapter 1, we develop a sensitivity analysis of a physically-based numerical energy balance model (FLUVIAL-EB) that takes a detailed account of heat energy fluxes in a river system to assess the role of atmospheric variables in river temperature change. We calculate the sensitivity of predicted river temperature to small individual perturbations to several meteorological variables across different seasons, including shortwave radiation, longwave radiation, air temperature, wind speed, vapor pressure, and air pressure. We pay special attention to the perturbation values as early results highlight the need to develop a specialized methodology for perturbing atmospheric variables because each variable operates on differing magnitudes. The coefficient of variation (CV) term is applied to each atmospheric dataset to determine the perturbation value of each variable for each season. We conclude that the CV method provides a standardized measure of the distribution of the observed weather variables and encompasses the seasonal variability within each atmospheric record. Results show that predicted river temperature is particularly susceptible to positive changes in shortwave radiation ( $+2.6^{\circ}\text{C}$ , 25km river distance and  $+10.3^{\circ}\text{C}$ , 150 km river distance) in summer seasons at the longitudinal river basin scale. In Chapter 2, we present a novel Gaussian variance-based, multi-variable error decomposition scheme on the simple standard error equation to account for the contribution of weather data to the error in predicted river temperature. The FLUVIAL-EB model incorporates key atmospheric variables for energy flux and river temperature predictions from the California Irrigation Management Information System (CIMIS) data network. We examine a possible source of error due to the utilization of this data set by using Taylor Series expansion approximations under finite-difference assumptions, where we expand the basic standard error equation to calculate the standard error of predicted river temperature. The equation includes 1) a weighting term (partial derivatives calculated in Chapter 1 that provide a measure of influence on the standard error based on predicted river temperature sensitivities to each atmospheric variable, 2) a Pearson's correlation coefficient term which measures the direction and magnitude of the correlation between two uncorrelated atmospheric variables, and 3) a standard error value for each atmospheric variable that characterizes error due to misrepresentation of the atmosphere directly over the river channel, which we call standard error due to geographic displacement between the weather stations and river channel. Assuming predicted river temperature is only a function of the six critical atmospheric variables, results show error values to be small across all seasons and distances of the river. The most significant error in predicted river temperature occurs during the winter months ( $\pm 0.12^{\circ}\text{C}$ ) followed by spring, summer, and fall ( $\pm 0.08^{\circ}\text{C}$ ,  $\pm 0.03^{\circ}\text{C}$ ,  $\pm 0.05^{\circ}\text{C}$ , respectively) at the 150 km river distance. Chapter 3 introduces the FLUVIAL-EB model's ability to predict energy fluxes and river temperature along river distance by replacing CIMIS data with gridded regional climate model output. Initially, we hoped to present modeled river temperatures based on atmospheric predictions derived under a high greenhouse gas emission scenario (RCP 8.5) from the fifth-generation Canadian Regional Climate Model (CRCM5). The results presented in Chapter 3 highlight the FLUVIAL-EB model's efficacy in utilizing gridded climate data and motivate future work to incorporate climate predictions into the FLUVIAL-EB model to observe how river temperature reacts under a high-

emission greenhouse gas scenario. To conclude, results from this work highlight the need to improve the accuracy and representativeness of weather time-series observations to improve FLUVIAL-EB model predictions of temperature along the length of a river and to incorporate more sources of error to prediction results and model inputs. Results also emphasize the importance of a seasonally based approach to making water management decisions as river temperature sensitivity to the atmosphere fluctuates by a substantial amount depending on the seasons ( $\pm 10.3$  °C, in summer at river distance 150km given a  $+ 1.1 \text{ Wm}^{-2}$  perturbation to shortwave radiation). Finally, the FLUVIAL-EB model can incorporate gridded climate data representing atmospheric conditions derived from high greenhouse gas emission scenarios, making it a valuable tool to assess changes in energy fluxes and river temperature of a large-lowland river in anthropogenic-induced climatic conditions.

## **Acknowledgements**

I would like to express my sincere gratitude to my thesis committee for their invaluable support and guidance throughout this research project. I am grateful to my supervisor, Dr. Erin Bray, for their constant encouragement, feedback, and patience during the ups and downs of my research journey. Their insights, expertise, and guidance were essential in shaping the direction of this thesis and helping me navigate the complexities of the research process.

I would also like to thank the other members of my thesis committee, Dr. Jeff Dozier, for their valuable advice, and expertise on the modeling portion of this project. I am also grateful to, Dr. Leora Nanus, for their time, effort, and valuable feedback. Their expertise and insights from their respective fields were essential in helping me develop this thesis.

Additionally, I would like to thank the Earth and Climate Science Department for their support. Along with the Monteverdi family whose John A. and Anna Monteverdi Fellowship in the Atmospheric and Oceanic Sciences allowed me to dedicate myself to this research and maximize my potential as a graduate student at San Francisco State University.

Finally, I would like to express my heartfelt appreciation to my family and friends who supported me throughout this journey. Your love, encouragement, and patience were crucial in helping me overcome the challenges of this research project, and I am deeply grateful for your unwavering support.

## Table of Contents

<b>List of Tables</b>	<b>ix</b>
<b>List of Figures</b>	<b>x</b>
<b>Chapter 1 – A Sensitivity Analysis: Understanding how atmospheric conditions impact predicted river temperature within the FLUVIAL-EB model, a physically-based numerical model</b>	<b>1</b>
Introduction	1
Background	3
A chronological review of hydrological modeling	5
Physically-based numerical energy balance models	6
How atmospheric conditions affect the energy fluxes within rivers	8
FLUVIAL-EB model, a physically-based numerical energy balance model	9
What is a sensitivity analysis?	11
Research Goals	13
Study Region	13
Overview of the San Joaquin River Basin	13
The spatial extent of the FLUVIAL-EB model	14
<i>Overview of seasonal atmospheric variability of the San Joaquin Valley</i>	15
Data	16
HEC-RAS version 4.1.0	16
<i>California Irrigation Management Information System (CIMIS)</i>	17
United States Geological Survey (USGS) and the California Data Exchange Center (CDEC)	18
Methods	19
Choosing consistent flow for FLUVIAL-EB model stability	19
Choosing temporal ranges for model experiments based on consistent flow from a USGS stream gauge	19
FLUVIAL-EB model stability.	19
Estimating FLUVIAL-EB model boundary temperatures	20
Execute FLUVIAL-EB model simulations.	20
Sensitivity analysis	21
Partial Derivative Equation	21
Estimating unique perturbation values for partial derivatives	24
Results	27
General findings on scaled partial derivatives	31
Normalized partial derivatives	32
Atmospheric energy fluxes	33
Limitations	34
Conclusion	35
<b>Chapter 2 – Developing a Standard Error Equation for FLUVIAL-EB Predicted River Temperatures</b>	<b>38</b>
Introduction	38
Uncertainty analysis and sources of error in physically-based numerical river temperature models	39
Data	40
Methods	40
Definition of the standard error equation in the context of the FLUVIAL-EB model	40

Defining a standard error equation – Taylor series, variance-based expansion of the basic standard error equation	41
Components of the standard error equation	50
Error due to geographic proximity – a possible source of error in FLUVIAL-EB model predictions due to misrepresentation of the atmosphere directly over the river channel	51
Limitations	53
Results	54
Discussion	56
<b>Chapter 3 – Applying Gridded Climate Data to a Physically-based Numerical Energy Balance Model (FLUVIAL-EB)</b>	<b>58</b>
Introduction	58
Climate change and FLUVIAL-EB model predictions	60
Methods	61
Data	62
Canadian Regional Climate Model version 5 (CRCM5)	62
ERA-Interim reanalysis-driven data	63
Limitations	63
Results	64
Conclusion	65
<b>Figures</b>	<b>67</b>
<b>Tables</b>	<b>85</b>
<b>Appendices</b>	<b>96</b>
Appendix A: Auxiliary Figures	97
Appendix B: Auxiliary Tables	107

## List of Tables

<b>Table 1. Notation Table</b>	<b>85</b>
<b>Table 2. Observed hydrometeorological data from 11 sites and observed water temperature from 8 sites used to predict the energy balance continuously along the San Joaquin River, CA, USA. Denair II and Patterson are not within the study area and therefore are not considered part of the standard error calculations. Data sources include the California Irrigation Management Information System (CIMIS), the US Bureau of Reclamation (USBR), the US Geological Survey (USGS), the CA Dept. of Fish and Game (CADFG), the CA Dept. of Water Resources (CADWR), and the California Data Exchange Center (CDEC)</b>	<b>86</b>
<b>Table 3. Periods of consistent flow from SJF stream gauge data.</b>	<b>87</b>
<b>Table 4. Selected periods of consistent flow from SJF stream gauge station. Start and end times will be used for model simulation.</b>	<b>88</b>
<b>Table 5. Mean water temperature values from USGS station: SJF for initial boundary conditions across all seasons.</b>	<b>89</b>
<b>Table 6. FLUVIAL-EB model run commands for prescribed flow profile, temporal range, spatial and temporal resolution, and initial and boundary temperatures specified</b>	<b>90</b>
<b>Table 7. Scaled sensitivity terms along river distance and across seasons for each atmospheric variable. Scaled 7-day mean partial derivative terms at different distances along the river for the 7-day DJF, MAM, JJA, and SON model simulation periods. Color gradient corresponds to negative terms (green) and positive terms (red).</b>	<b>91</b>
<b>Table 8. Normalized sensitivity terms along river distance and across seasons for each atmospheric variable. Normalized 7-day mean partial derivative terms at different distances along the river for the 7-day DJF, MAM, JJA, and SON model simulation periods. Normalized partial derivatives are unitless. Color gradient corresponds to the negative terms (green) and positive terms (red).</b>	<b>92</b>
<b>Table 9. Summary of perturbation values for sensitivity analysis.</b>	<b>93</b>
<b>Table 10. Standard error values across all seasons and select distances along the river.</b>	<b>94</b>
<b>Table 11. CRCM5 gridded climate data.</b>	<b>95</b>
<b>Table 7. Sensitivity terms along river distance and across seasons for each atmospheric variable. Scaled 7-day mean partial derivative terms at different distances along the river for the 7-day DJF, MAM, JJA, and SON model simulation periods. Color gradient corresponds to negative terms (green) and positive terms (red).</b>	<b>108</b>

## List of Figures

<b>Figure 1. Overview of the San Joaquin River (black) and major tributaries (blue). Also shown (orange lines) are the Friant-Kern Canal and the Madera Canal.</b>	<b>68</b>
<b>Figure 2. Overview of the Sacramento-San Joaquin River Delta system</b>	<b>69</b>
<b>Figure 3. Overview of the model extent. The FLUVIAL-EB model predicts energy fluxes and river temperature from Friant Dam to the confluence of the Merced Riverd</b>	<b>70</b>
<b>Figure 5. Perturbation Theory. Perturbed predicted river temperature values are subtracted from baseline predicted river temperature values for each time and distance along the river. The difference is divided by the unique perturbation value. The result is a partial derivate value for each time and distance along the river, representing river temperature sensitivity to an atmospheric variable.</b>	<b>72</b>
<b>Figure 6. Scaled partial derivatives representing predicted river temperature sensitivity along river distance for the 7-day DJF (Winter) model simulation period.</b>	<b>73</b>
<b>Figure 7. Scaled partial derivatives representing predicted river temperature sensitivity along river distance for the 7-day MAM (Spring) model simulation period.</b>	<b>74</b>
<b>Figure 8. Scaled partial derivatives representing predicted river temperature sensitivity along river distance for the 7-day JJA (Summer) model simulation period.</b>	<b>75</b>
<b>Figure 9. Scaled partial derivatives representing predicted river temperature sensitivity along river distance for the 7-day SON (Fall) model simulation period.</b>	<b>76</b>
<b>Figure 10. Normalized partial derivatives representing predicted river temperature sensitivity along river distance for the 7-day MAM (Spring) model simulation period.</b>	<b>77</b>
<b>Figure 11. Normalized partial derivatives representing predicted river temperature sensitivity along river distance for the 7-day MAM (Spring) model simulation period.</b>	<b>78</b>
<b>Figure 12. Normalized partial derivatives representing predicted river temperature sensitivity along river distance for the 7-day MAM (Spring) model simulation period.</b>	<b>79</b>
<b>Figure 12. Normalized partial derivatives representing predicted river temperature sensitivity along river distance for the 7-day MAM (Spring) model simulation period.</b>	<b>80</b>
<b>Figure 14. Baseline energy fluxes (<math>Wm^{-2}</math>) for each of 4 seasonal simulation periods.</b>	<b>81</b>
<b>Figure 15. Methodology map for error due to geographic proximity to the river channel. Weather values from Firebaugh and Westland CIMIS stations are used to calculate the standard error of each weather variable.</b>	<b>82</b>

<b>Figure 16. Total standard error due to uncertainties in weather values collected from the CIMIS station network within the study area along river distance and across all seasons.</b>	<b>83</b>
<b>Figure A1. Interpolated weather values at distance along the river for a mean 7-day model simulation period for the DJF season.</b>	<b>98</b>
<b>Figure A2. Interpolated weather values at distance along the river for a mean 7-day model simulation period for the MAM season.</b>	<b>99</b>
<b>Figure A3. Interpolated weather values at distance along the river for a mean 7-day model simulation period for the JJA season.</b>	<b>100</b>
<b>Figure A4. Interpolated weather values at distance along the river for a mean 7-day model simulation period for the SON season.</b>	<b>101</b>
<b>Figure A5. Partial derivatives representing predicted river temperature sensitivity along river distance for the 7-day DJF (Winter) model simulation period.</b>	<b>102</b>
<b>Figure A6. Partial derivatives representing predicted river temperature sensitivity along river distance for the 7-day MAM (Spring) model simulation period.</b>	<b>103</b>
<b>Figure A7. Partial derivatives representing predicted river temperature sensitivity along river distance for the 7-day JJA (Summer) model simulation period.</b>	<b>104</b>
<b>Figure A8. Partial derivatives representing predicted river temperature sensitivity along river distance for the 7-day SON (Fall) model simulation period.</b>	<b>105</b>
<b>Figure A9. Predicted river temperature (blue line) simulated during the winter (DJF) season. Grey area represents how confident we are in predicted river temperature (<math>\pm^{\circ}\text{C}</math>) for the DJF seasons assuming that predicted river is only a function of the six atmospheric variables used in this study and uncertainty in predictions only come from error due to geographic proximity between weather station and channel.</b>	<b>106</b>

## **List of Appendices**

<b>Appendix A: Auxiliary Figures</b>	<b>97</b>
<b>Appendix B: Auxiliary Tables</b>	<b>107</b>

# **Chapter 1 – A Sensitivity Analysis: Understanding how atmospheric conditions impact predicted river temperature within the FLUVIAL-EB model, a physically-based numerical model**

## **Introduction**

The atmosphere strongly impacts local hydrology and ecosystems, influencing agricultural productivity, municipal water supply, and fisher and wildlife management (Bunn & Arthington, 2002; Daniels & Danner, 2020; Lettenmaier & Gan, 1990). The San Joaquin River in California's Central Valley is susceptible to anthropogenic disruptions as the river has long been diverted for agricultural and municipal use. It is necessary to re-establish natural flow to the region in a way that focuses on ecosystem management while maintaining infrastructure that supports the agrarian economies and municipal functions provided by the San Joaquin River. Understanding the relationships and dynamics that govern local hydrological systems is vital to protecting regional ecosystems and informing regional policy (Rosbjerg & Rodda, 2019).

Analytical and computational modeling techniques are increasingly utilized in research to establish scientifically based policies for managing water use and protecting endangered ecosystems. In this study, we employed a physically-based river energy balance model that accounts for multiple components of heat exchanges, absorptions, and transmissions between the atmosphere and water, as well as the bed and water surface. The selection of hydrological models should align with the specific research objectives, which often focus on watershed-scale projects, including total flow and water balance (Beven, 1989; Dugdale, Hannah, & Malcolm, 2017). While it is important to consider all components of the instream hydrologic system including groundwater infiltration, rainfall inputs, and biotic fluctuations, this study focuses

specifically on atmosphere-water surface interactions to predict river temperature along river distance and across seasons, therefore, we selected a model that focuses only on the radiative energy balance of a large-lowland river.

Regardless of the research goals and model type employed, it is necessary to perform a sensitivity analysis on the association between the model inputs and outputs in hydrological modeling (Devak & Dhanya, 2017). Examining the connection between model inputs and outputs provides a quantifiable degree of comprehension of how the input values utilized to initiate model computations impact the forecasts, which authenticate the model and improves the efficacy of the model results. Failure to provide such an analysis causes an incomplete understanding of predictions, which can significantly impact water resource management and environmental decision-making. Therefore, a sensitivity analysis is imperative to ensure the robustness and validity of the energy balance model presented in this study.

This study investigates the physically-based numerical model (FLUVIAL-EB) that calculates the energy balance and river temperature along a 150 km section of the San Joaquin River. Specifically, the model assesses atmospheric control on predicted river temperature by developing a sensitivity analysis where we examine how sensitive predicted river temperature change is to adjustments to six important atmospheric variables. The results of this study will aid in a better understanding of the atmospheric variables that govern FLUVIAL-EB model-predicted river temperature change so that we can provide local governments with scientifically-based research that aids in water use management and maintaining healthy ecosystems.

This study evaluates the physically-based numerical model FLUVIAL-EB, which estimates energy balance and river temperature along a 150 km stretch of the San Joaquin River.

The main objective of Chapter 1 is to investigate the relationship between the atmosphere and predicted river temperature by conducting a sensitivity analysis. Specifically, we examine how small, positive perturbations of six critical atmospheric variables affect predicted river temperature change. The findings of this study provide valuable insights into the impact of atmospheric variables on river temperature, which can aid in developing effective management strategies for the San Joaquin River and other large-lowland river systems.

## **Background**

Hydrology models are increasingly developed and utilized as predictive tools to make informed decisions about water allocations for municipalities, agriculture, and ecological systems (Gleick, 1989; Taheri, Mohammadian, Ganji, Bigdeli, & Nasser, 2022). Scientists use hydrological models to answer questions involving water storage, sediment transport, surface water-atmosphere interaction, and water chemistry. The environment these models are structured to replicate is unpredictable, making developing or selecting a model difficult (Horton, Schaeffli, & Kauzlaric, 2022). It is essential for a hydrologist to choose or create a model that suits the needs of the research goals and subsequently analyze model functions and results to establish confidence in their research. We elected to utilize a physically-based energy balance model to assess the atmosphere's role in effecting changes to predicted river temperatures and in Chapter 2, to ascertain possible sources of error that stem from the atmospheric dataset used for model predictions.

Energy balance models have emerged as a valuable tool for assessing the relationship between the atmosphere and water temperature changes due to their ability to incorporate various physical and meteorological factors. These models estimate stream temperature by quantifying

the energy fluxes between the water surface and the surrounding environment, considering factors such as shortwave radiation, air temperature, wind speed, the albedo of the bed, suspended solids within the water column, and flow.

Numerous studies have evaluated the performance of different energy balance models for predicting stream temperatures. For example, Christian E. Torgersen (2000) compared several energy balance models and found that more complex models produced more accurate predictions, which accounted for more environmental factors. Others observe the thermal structure of a proglacial river through energy balance modelling techniques by incorporating timelapse thermal imagery of snowmelt to study the relationship between the atmosphere, warm glacial melt, and the radiative energy balance of a river (Cardenas et al., 2014)

The relationship between atmospheric datasets and river temperature predictions in energy balance models has also been studied. Studies have investigated the influence of air temperature on river temperatures, finding that air temperature, shortwave radiation, and wind speed are critical factors in determining stream temperature within energy balance models (Brown, 1969; Caissie, 2006; Datt, Srivastava, Negi, & Satyawali, 2008; Verburg & Antenucci, 2010).

Despite the advances in energy balance modeling, there are still limitations in accurately predicting stream temperatures, particularly in complex river systems with heterogeneous conditions. Limitations often stem from a lack of high-resolution meteorological data for remote or poorly monitored river systems, which can limit the accuracy of energy balance models (Wang et al., 2020). Additionally, energy balance model predictions are often highly parameterized which makes their output dependent on parameterizations. Therefore, the quality of model predictions are a function on how well the model is parameterized (Sun, Salvucci,

Entekhabi, & Farhadi, 2011). The FLUVIAL-EB energy balance model used here specifically avoid parameterization of hydrologic components to avoid this common limitation. The model relies instead on a set of physically based equations that do not incorporate along stream parametrized features. Albedo of the bed surface is the only parameterized function and is held constant for the purposes of this work because we are only concerned with atmosphere-water surface interactions.

Energy balance stream temperature models have shown great promise in predicting river temperatures but are sometimes limited by spatial and temporal coverage of meteorological datasets. Chapter 1 of this paper focuses on learning as much as possible about the relationship between an atmospheric dataset and FLUVIAL-EB model river temperature predictions.

### ***A chronological review of hydrological modeling***

In this initial review of hydrological modeling, we will visit the types of models and their uses in past and current literature. First published in 1856, Henry Darcy was one of the first hydrologists to apply simple mathematical statements to represent a hydrological process (Simmons, 2008). In the 1960s, scientists began to recognize the potential of computer modeling, and in 1966, N. H. Crawford and Linsley (1966) developed the first watershed model called the Stanford Watershed Model (SWM). The SWM was one of the first models to create a continuous numerical simulation of interacting hydrology processes such as infiltration, soil moisture, evaporation, and channel flow hydraulics to arrive at physical and mathematical descriptions of the flow regime for a specific area (Norman H. Crawford, 2004). Some modern hydrology models utilize machine learning or neural network algorithms such as the LSTM-based Hydrological Model (LHSM) to predict river flow (Li, Marshall, Liang, Sharma, & Zhou, 2021).

The application of hydrology models should include specific research goals and spatial considerations. We chose to focus on physically-based numerical energy balance models as we consider the spectral energy balance of a large lowland river to be a first-order control of river temperature.

### ***Physically-based numerical energy balance models***

What are a physical-based numerical energy balance model's defining characteristics and applications? First, a physically-based model is a mathematical model used to simulate the hydrological cycle and can predict the movement of water through the atmosphere, land, and reservoirs. These models are based on fundamental physics principles and utilize equations that describe the physical processes that control water transport, such as precipitation, evaporation, infiltration, surface runoff, and groundwater flow. Freeze and Harlan (1969) help define a few seminal descriptions of a physically-based hydrological response model which are still perpetuated in the literature:

1. A physically-based mathematical model represents time-dependent hydrological progressions defined by the continuity and conservation of mass and momentum equations.
2. Also defined is a series of boundary conditions that delineate the overall shape of a particular basin. (i.e., elevation, channel depths, channel widths, vegetation, soil type, stream bed type.)
3. Physically-based numerical models specify spatial nodes in which the discrete temporal aspect of the model is used to approximate model response at time =  $t_n$ .

4. Often, meteorological observations are incorporated at each defined spatial node so that weather data can be utilized in the model set of physically representative governing equations.

Physically-based numerical energy balance models are valuable tools for predicting various hydrological processes by simulating the energy balance of waterbodies. These models consider the energy inputs and outputs through equations representing the physical laws governing heat transfer between water, atmosphere, and land. A literature review of past and current energy balance modeling research shows that physically-based energy balance modeling has mainly focused on snow melt processes, although more recent work incorporated spectral energy balance equations for river temperature predictions. Arnold, Richards, Willis, and Sharp (1998) investigated glacial hydrology and found that physically-based energy balance models perform well in predicting detailed spatial and temporal patterns of subglacial processes such as melt rates, water pressures, and velocities. Furthermore, Griessinger et al. (2019) demonstrated that integrating a distributed multi-layer energy balance snow model improves the accuracy of snow simulations for hydrologic modeling in Alpine catchments. Datt et al. (2008) employed an energy balance model to study snowmelt in the Himalayas and found that air temperature and absorbed shortwave radiation from the snowpack led to a high thermal state resulting in higher rates of snow melt.

Recently, researchers have applied spectral energy balance equations to energy flux and river temperature models to understand a water column's absorptive and evaporative characteristics and the radiative fluxes that govern them. (B.W. Webb, 1997; Caissie, 2006; Hannah & Garner, 2015; Webb, Hannah, Moore, Brown, & Nobilis, 2008). These models have

primarily focused on the advection component of the energy balance through approaches like RAFT (Daniels & Danner, 2020; Pike et al., 2013) and statistical forecasting (Null, Ligare, & Viers, 2013). However, these models tend to use simplified methods for calculating the radiation balance, despite it being the most significant component of the energy balance. Water management agencies use stream temperature models such as HEC-5Q (Willey, 1986) or CVTEMP (St-Hilaire, 2017), which utilize lumped exchange coefficients and empirically estimate shortwave absorption in water without specifying the wavelength. Finally, Bray, Dozier, and Dunne (2017) suggest that ignoring wavelength length in the energy balance masks how radiation attenuates through the water column, making it difficult to accurately predict absorption, scattering, and energy transport in and out of different components.

Physically-based numerical energy balance models have drawbacks, as their prediction accuracy depends on the set of physical equations and data used and the spatial and temporal robustness of the data. An interpolation scheme or downscaling/upscaling techniques may be used without complete data, but the strength of these methods affects the results (Dugdale et al., 2017).

### ***How atmospheric conditions affect the energy fluxes within rivers***

This study recognizes that radiative, latent, sensible, and advective heat exchanges display first-order control on river temperature. Other factors control river temperature change, such as managed flow releases from dams, flow, along stream riparian structure, atmospheric disturbances from wildfires, and ground water infiltration but their effects on river temperature change are dictated by the heat exchange between the atmosphere-water surface or atmosphere-land surface interactions. Atmospheric conditions such as air temperature, shortwave radiation,

downwelling longwave radiation, and wind speed all contribute to the partitioning of evaporation and absorption characteristics of the river and affect the rate at which heat energy is exchanged at the bed-water and water-atmosphere surface layers. In sum, the absorptive and evaporative attributes of the water column are dictated by radiative heat exchange at each surface layer of the river which are controlled by the incidental atmospheric conditions acting upon the water surface. The FLUVIAL-EB model accounts for the above-mentioned spectral energy balance components, which are necessary to understand how the atmosphere drives changes to energy fluxes and predicted river temperature.

***FLUVIAL-EB model, a physically-based numerical energy balance model***

The FLUVIAL-EB (FLUVIAL-EB) model is a physically-based numerical river energy balance model previously developed by Bray et al. (2017). The Fluvial Energy Balance model simulates the spatially distributed spectral energy balance over a reach of a clear lowland river (in this case, the San Joaquin River). The model calculates the spectral energy balance through an Eulerian framework where energy fluxes and river temperatures are calculated at prescribed timesteps and distances along the river. The spectral energy balance and river temperature predictions are controlled by absorbed radiative fluxes propagating through the water column and the bed in upward and downward directions. Energy is either added or removed through atmosphere-water surface interactions and at the rate at which the river flow transports and accumulates energy in the water column. The FLUVIAL-EB model couples a spectral radiation balance with turbulent heat fluxes, bed conduction, and a 1D hydraulic model employed over the longitudinal profile of a river of varying depth and velocity with distance downstream of a dam. The model solves the one-dimensional heat advection equation through finite difference methods

from Sridhar, Sansone, LaMarche, Dubin, and Lettenmaier (2004). Equation 1 and the description is adopted from (Bray et al., 2017).

$$\frac{\partial T}{\partial t} + \frac{v}{Q} \frac{\partial(TQ)}{\partial x} = \frac{Q_{net}}{\rho c_p D} + \frac{v}{Q} \frac{\partial}{\partial x} \left[ D_l \frac{Q}{v} \frac{\partial T}{\partial x} \right] \quad (1)$$

$T$  is the average cross-sectional river temperature at time  $t$  and distance  $x$  along the river,  $v$  is flow velocity,  $Q_{net}$  is the net energy exchange between the atmosphere, the bed, and the water,  $Q$  without a subscript is river discharge,  $\rho$  is water density,  $c_p$  is the specific heat of the water,  $D$  is depth, and  $D_l$  is the longitudinal dispersion coefficient. The water is assumed to be clear and well-mixed. Since we are focusing here on the relationship between predicted river temperature and the atmosphere, we are most concerned with the net energy term ( $Q_{net}$ ), which incorporates atmospheric data into its calculations. The net energy term ( $Q_{net}$ ) is shown in Equation 2.

$$Q_{net} = S_{net} + F_{net} + H + L + G \quad (2)$$

$Q_{net}$  is the net shortwave radiation,  $S_{net}$  is the net shortwave radiation,  $F_{net}$  is the net longwave radiation,  $H$  is the sensible heat flux,  $L$  is the latent heat flux, and  $G$  is the bed conduction. The term  $Q_{net}$  is responsible for energy exchanges between the atmosphere and water surface through the entire water column. Bray et al. (2017) gives a detailed account of how the model processes each of the components in the  $Q_{net}$  energy balance term.

The FLUVIAL-EB model couples spatially distributed values of width, depth, and velocity, output from HEC-RAS version 4.1.0 (U.S. Army Corps of Engineers, HEC-RAS, Hydrological Engineering Center, <http://www.hec.usace.army.mil/software/hec-ras/>). Width, depth, roughness, and velocity all vary spatially along the river but are defined based on a few specific discharge values. More information on the HEC-RAS component of the FLUVIAL-EB model is presented in the data section of Chapter 1.

The FLUVIAL-EB model solves Equation 1 by incorporating six vital atmospheric variables that govern atmosphere-water and water-bed interactions. Atmospheric data is first gathered from the available meteorological stations and then spatially interpolated to cover the spatial extent of the channel. The model interpolates measurements taken at each meteorological station for specific moments in time using the *griddedInterpolant* function in MATLAB. As the governing differential equation operates instantaneously at any given time and distance, it necessitates the availability of input variables for all  $x$  and  $t$  values. The model derives instantaneous data from hourly averages by computing a cumulative sum, employing a smoothing spline, and subsequently calculating the derivative. By following this process, we were able to establish a seamless spatial and temporal representation of the entire river, encompassing hourly meteorological data and modeled steady-state hydraulic values. We focus our attention on quantifying relationships between weather input and FLUVIAL-EB river temperature output because 1) this relationship has not yet been studied within the context of the FLUVIAL-EB model and 2) atmospheric time-series data from a network of meteorological stations presents a potential source of error to predicted river temperatures across seasons and along the length of the river.

### ***What is a sensitivity analysis?***

A sensitivity analysis (SA) examines the sensitivity of model output(s) with respect to small changes to model input(s). An SA is developed with specific research questions in mind. Typically, an SA will be specific to the model, or the input type (s) being examined. An SA will 1) provide information on how influential specific input variables are on model results, 2) give

guidance for ongoing changes to model structure and parameterization, and 3) will give the necessary context in which to examine model output (Devak & Dhanya, 2017).

Mathematically, an SA examines the change in output with respect to a given change in its input. The function describes an SA on model predictions:

$$output = f(input),$$

where this input ( $input, \dots, input_i$ ) is the data series that is used to simulate  $i$  number of results that are derived within the numerical structure of the model. Assuming simulated model results are only a function of specific inputs, we can perturb each  $input$  value ( $input, \dots, input_i$ ) by a small perturbation value which we denote as  $input_{perturbation}$ . We then run the model with the adjusted data series  $input_{perturbation}, \dots, input_{perturbation,i}$  to assess model simulation results ( $output_{perturbation}, \dots, output_{perturbation,i}$ ) derived as a function of

$input_{perturbation}, \dots, input_{perturbation,i}$  where,

$$output_{perturbation} = f(input_{perturbation}).$$

The sensitivity of the solution ( $output_{perturbation}$ ) with respect to the  $input_{perturbation}$  perturbation is approximated by the partial derivative,

$$\left[ \frac{(output_{perturbation} - output)}{input_{perturbation}} \right]_{1, \dots, i}.$$

The partial derivatives presented in this work represent how sensitive predicted river temperature is with respect to small perturbations to each atmospheric variable. Partial derivatives are calculated for all times and distances along the river. The partial derivatives aid in understanding the atmosphere-water surface physically-based numerical interactions computed within the FLUVIAL-EB, which provide insights into how a few critical atmospheric variables govern predicted river temperature change.

## ***Research Goals***

The overall scope of Chapter 1 is to advance applications of a recently developed energy balance model (FLUVIAL-EB) by performing a sensitivity analysis on a predicted river temperature and the relative influence of a few critical atmospheric variables across seasons and along river distance. The goals of this study are:

1. To find the best method for developing a partial derivative equation that represents predicted river temperature change with respect to shortwave radiation, longwave radiation, air temperature, wind speed, vapor pressure, and air pressure;
2. To assess a "best value" for perturbing atmospheric variables that follow finite difference assumptions to observe predicted river temperature sensitivity to changes in the atmosphere;
3. To rank which of the six atmospheric variables causes the most change to predicted river temperature, given a small change to each variable to determine which of the six-atmosphere variables cause the most significant change to predicted river temperature, and;
4. To analyze and comment on partial derivative values along all distances of the river reach studied across four different seasons.

## **Study Region**

### ***Overview of the San Joaquin River Basin***

The San Joaquin River is the second longest river in California (530 km) and the second largest river basin by area (82,880 km<sup>2</sup>). Headwaters of the San Joaquin River watershed originate in California's Sierra Nevada Mountain Range. Water flows west of the valley facing

the slopes of the Sierra Nevada Mountain range. As the river reaches the San Joaquin Valley floor, it flows northward, eventually flowing into the San Francisco Bay (Figure 1). The San Joaquin River system is part of a larger Sacramento-San Joaquin delta system, including the Sacramento River. The Sacramento River flows from north to south toward San Francisco Bay. Both river systems converge and drain into the San Francisco Bay delta system before entering the Pacific Ocean (Figure 2).

Tributaries to the mainstem San Joaquin River channel include the Fresno River, Chowchilla River, Merced River, Tuolumne River, Stanislaus River, Calaveras River, Mokelumne River, and the Consumes River (Figure 1). The Merced, Tuolumne, and Stanislaus Rivers are the three major tributaries of the region. Of these eight rivers, the Consumes River (a tributary of the larger Mokelumne River) is the only river in the basin that does not have a significant dam. All other rivers have been heavily modified, and flow diverted for agricultural use, hydroelectric power, and municipal water storage, which serve San Joaquin Valley communities.

### ***The spatial extent of the FLUVIAL-EB model***

The FLUVIAL-EB model is currently developed to predict river temperature along the San Joaquin River, although it has the capability of predicting river temperature for any extensive lowland, clear river once coupled with specific physical characteristics unique to the model region. The modeled river channel begins just below Friant Dam and ends 150 km downstream near the confluence of the Merced River (Figure 3). The spatial extent of the model features, including the meteorological station network that the FLUVIAL-EB model uses to

collect atmospheric data at various distances along the river, encompasses approximately 10,092  $Km^2$  denoted by the dashed black box in Figure 3.

### ***Overview of seasonal atmospheric variability of the San Joaquin Valley***

An overview of the seasonal climatology of the San Joaquin River is provided to understand seasonal patterns reflected in river temperature predictions. The San Joaquin Valley is characterized by hot, dry summers and cool, rainy winters. The region is classified as inland Mediterranean, although due to the longitudinal length of the valley, some regions are categorized as desert conditions (Fernandez-Bou et al., 2021). Over a 30-year period, the National Weather Service reports, the average wintertime air temperature value (DJF) for the region is 13.3 °C (56 °F) with occasional freezing conditions. Springtime (MAM) average daily temperature is 21.8 °C (71.3 °F). Summer (JJA) months air temperature average is 31.1 °C (88.0 °F) with an average of 40 days per year over 37.7 °C (99.9 °F). Fall (SON) months air temperature average is 24.6 °C (76.3 °F) (Baker, 1994).

The weather during the summer season is dictated by the semi-permanent sub-tropical high-pressure feature (Pacific High) that sits off the West coast of North America. Weather associated with the Pacific High includes high temperatures due to compressed, descending air and low relative humidity. In the winter, the Pacific High typically migrates south along the West coast of North America. This allows cool air and low-pressure systems from high latitudes to sweep into the San Joaquin Valley. The subtropical jet stream sometimes also produces wintertime weather events, bringing moist low-pressure systems through the valley. The weather during wintertime is dominated by intermittent periods of cool, rainy days which are dictated by the Pacific High and south-traveling low-pressure features that originate over the North Pacific

Ocean or atmospheric river events dictated by the subtropical jet stream (The Joaquin Valley Air Pollution Control District (SJVUAPCD), 2003).

The atmospheric variables that are the specific focus of this thesis include shortwave radiation, longwave radiation, air temperature, windspeed, vapor pressure, and air pressure (Table 1), all of which vary seasonally as a function of the dominant climatology described in the previous paragraph. (See Appendix A, Figure A1 through Figure A4 for all six atmospheric variables from the surrounding meteorological station network and interpolated across the length of the river for all four seasons.) One of the key features that will be highlighted in the results section is that due to atmospheric governance over the spectral energy balance processes of the FLUVIAL-EB model, we can attribute seasonal variation of predicted river temperature to seasonal variation within the weather data time series, and the background climatology of the region. The dominating climatic features that control the weather within the study area cause stable non-variable weather for much of the summer (dry, stable air mass) as opposed to the winter season (subtropical and polar jet-dominated weather patterns) when weather is more variable. Intermediate months (Spring and Fall seasons) are often more predictable transitional periods between the observed extremes during winter and summer periods.

## **Data**

### ***HEC-RAS version 4.1.0***

The FLUVIAL-EB model makes predictions that utilize river velocity, channel depth, and water surface elevation, which were previously calculated by an HEC-RAS version 4.1.0 (Hydraulic Engineering Center River Analysis System) model developed by the U.S. Army Corps of Engineers (USACE, [www.hec.usace.army.mil](http://www.hec.usace.army.mil)) specifically for the San Joaquin River.

HEC-RAS output includes physical boundaries of the San Joaquin River (SJR) from Friant Dam to the confluence with the Merced River. The FLUVIAL-EB model incorporates HEC-RAS derived channel and flow characteristics to interpolate these hydraulic variables continuously over all distances along the river using the MATLAB function *gridded Interpolant*. River channel variables retrieved from the HEC-RAS model along the river account for estimated flow losses, estimated tributary inflows, and assumed hydraulic operating rules at the structures along the reach (Mussetter Engineering, 2006). The data incorporated into the FLUVIAL-EB model includes 1) hydraulic depth for the cross-section, defined as the area/surface width of the active flow, 2) velocity, and 3) discharge.

### ***California Irrigation Management Information System (CIMIS)***

The meteorological variables used to synthesize energy fluxes and river temperature predictions are pulled from the California Irrigation Management Information System (CIMIS) network of weather stations throughout the San Joaquin Valley. CIMIS is a Department of Water Resources entity that manages a network of over 145 automated weather stations throughout California.

The meteorological variables used in the FLUVIAL-EB model include shortwave radiation ( $S, Wm^{-2}$ ), air temperature ( $T_a, ^\circ C$ ), relative humidity ( $R_h, \%$ ), windspeed at 2 m height ( $U, ms^{-1}$ ), and air pressure ( $p, mbar$ ). The CIMIS meteorological network that is used in this paper is shown in Table 2 and Figure 4. The FLUVIAL-EB model uses relative humidity and temperature to derive vapor pressure ( $V_p, mbar$ ) using methods found in (Hardy, 1998). Net longwave emitted by the atmosphere is also derived internally using techniques found in Dilley and O'Brien (1997).

In Figure 4, the modeled extent of the San Joaquin River is shown in black. The green triangle denotes the location of each CIMIS station. Note that air pressure was not available within the CIMIS weather station network. We used air pressure data from the United States Bureau of Reclamation (USBR). Air pressure data from USBR was only available at the weather station at the beginning of the reach near Friant Dam (station: FRT). The hydrostatic equation calculates air pressure at the remaining stations based on station elevation. Because air pressure is not readily available at each station and must be calculated along the distance of the river, it presents a possible source of error in energy balance predictions. However, we assume that the contribution to the total error in river temperature predictions due to air pressure is relatively small as air pressure does not significantly change from the beginning of reach to the most downstream extent of the modeled river channel. The six meteorological variables used in energy balance calculation within the FLUVIAL-EB model are shown in Table 2. Detailed descriptions of CIMIS equipment and site information can be found online (<https://cimis.water.ca.gov/>).

***United States Geological Survey (USGS) and the California Data Exchange Center (CDEC)***

Flow and temperature data was downloaded from the California Data Exchange Center (CDEC) data portal (<https://cdec.water.ca.gov/>), which is managed by the United States Geological Survey (USGS). Time series data for water temperature and flow from the 2009, 2010, and 2011 water years were used. For this paper, only 2011 data was used. Table 2 and Figure 5 show the location of each stream gauge denoted by an orange diamond. The stream gauge station where the data is collected is located directly beneath the dam, providing flow release values in cubic feet per second (*cfs*). We identify periods of constant flow (within  $\pm 30$  *cfs*) for each of the four seasons (Table 3). We identify periods of continuous flow for

each season to choose model run dates. Table 4 is the select four temporal ranges (for each season) that exhibit constant flow.

Water temperature time-series data was also used from the SJF station for each continuous flow period found in Table 5 so that observed water temperatures could be used as the upstream boundary conditions in the FLUVIAL-EB model. Initial water temperature conditions used in the model simulations were calculated by taking the 14-day average across four seasons for the selected simulation periods.

## **Methods**

### ***Choosing consistent flow for FLUVIAL-EB model stability***

An initial step was taken to find periods of consistent flow release from the dam within the stream gauge time-series data (Table 3). We choose a constant flow release profile of 1530 cfs across all seasons and all model-run experiments. This flow profile mitigates fluvial advective processes that affect river temperature predictions so that we can focus on predicted river temperature change due to the six atmospheric variables used in this study. It also avoids dry riverbed conditions within the model, leading to deterioration in numerical stability.

### ***Choosing temporal ranges for model experiments based on consistent flow from a USGS stream gauge FLUVIAL-EB model stability.***

Hydrological responses vary by season; thus, we observe model output for each of the four seasons. The periods associated with the consistent flow were used to define model prediction periods (Table 4). Model prediction periods include a 15-day modeled period for each season in 2011 (Table 4).

Moreover, to conduct a sensitivity analysis on the sensitivity of predicted river temperature to the atmosphere, a 15-day simulation period within each of the four seasons is deemed adequate for observing predicted river temperature change. The first eight days are removed to spin up the model, which removes equilibrium errors usually present within the first timesteps of model simulations (Seck, Welty, & Maxwell, 2015). The last seven days of the 15-day model simulation period are gathered, and all subsequent results are 7-day simulation periods representing each season in 2011.

### ***Estimating FLUVIAL-EB model boundary temperatures***

Initial boundary conditions for predicted river temperature are selected based on measurements taken downstream of the dam for a 14-day period from each of the four seasons during the year 2011. Water temperature data is collected for each 15 days described in the prior subsection, and the mean river temperature is calculated across the entire time series for each season, as shown in Table 5. Mean observed water temperature values are then used as boundary temperature conditions in the *riverExplicitSoln* MATLAB function, the front-facing command line used to predict river temperature with distance along the river.

### ***Execute FLUVIAL-EB model simulations.***

The *riverExplicitSoln* function is the front-end command line function for the entire FLUVIAL-EB model. The function was executed in MATLAB with the prescribed flow profile, temporal range, spatial and temporal resolution, and initial and boundary temperatures specified in Table 6. We obtain a total of 28 model experiments. The last 7-day period of each simulation is selected for each season. Each simulation provides predicted radiative fluxes and river temperatures along each distance of the river.

All predictions are calculated using different atmospheric conditions. A small positive value perturbs a single atmospheric variable while the remaining variables are implemented as their observed values for each of the four seasons. The *riverExplicitSoln* model function is executed for each of the six atmospheric variables. These runs are referred to as the "perturbation" runs. The model was also executed under normal atmospheric conditions for each of the four seasons, which we refer to as the "baseline" runs. The following section describes how each perturbation and baseline model experiment is used to observe the predicted energy balance and river temperature dependence on the atmosphere.

### ***Sensitivity analysis***

The partial derivatives that are defined here, specific to each of the key atmospheric variables studied, represent the change of simulated FLUVIAL-EB river temperature that results from a small positive unit change of a single atmospheric variable while holding the remaining atmospheric variables constant. Sensitivity coefficients are calculated using the finite-difference method to approximate the partial derivative of predicted river temperature with respect to a small positive perturbation to an atmospheric variable (Figure 5).

### ***Partial Derivative Equation***

One goal of Chapter 1 was to quantify each atmospheric variable's influence on river temperature predictions. To do this, we develop a sensitivity analysis where each atmospheric variable undergoes a small, positive perturbation. River temperature is then simulated using observed weather values except for a single perturbed variable. This output is presented as a partial derivative which represents the total change in predicted river temperature between

baseline atmospheric conditions and perturbed atmospheric conditions with respect to the small positive perturbation made to the atmospheric variable.

First, we perturb each atmospheric variable, one at a time, and run the model for each of the four select seasonal periods within 2011. We approximate the partial derivative by applying the one-sided finite difference method to find the partial derivative. The partial derivative

$$\frac{\partial T}{\partial p} \approx \frac{T(w + p, \dots, w_i + p) - T(w, \dots, w_i)}{p} \quad (3)$$

where  $T$ , is the difference between the predicted river temperature simulated under perturbation conditions for a single atmospheric variable ( $T(w + p, \dots, w_i + p)$ ) and the predicted river temperature simulated under baseline atmospheric conditions ( $T(w, \dots, w_i)$ ).  $T$  is a measure of the amount of change in predicted river temperature between perturbation experiments where one atmospheric variable is perturbed while the rest are constant and the normal observed atmospheric conditions.  $p$ , is the perturbation value for each atmospheric variable. Figure 5 illustrates how the partial derivatives were developed, where a 7-day mean of predicted river temperature run under baseline atmospheric conditions ( $T(w, \dots, w_i)$ , red line) and predicted river temperature run under a hypothetical perturbation to a single atmospheric variable ( $T(w + p, \dots, w_i + p)$ , blue line)

Examining which atmospheric variable most strongly controls river temperature is difficult. The FLUVIAL-EB model operates on a complex series of equations that determines how latent heat, sensible heat, and other radiative fluxes are partitioned into evaporation and absorption, making it challenging to ascertain which atmospheric variable affects the most change in predicted river temperature based on initial partial derivative values. Additionally, baseline magnitudes of each weather variable operate on different scales making it difficult to

compare the influence of each atmospheric variable on predicted river temperature. Therefore, we manipulate the partial derivative values by scaling and normalizing across all times and distances along the river.

We use the interquartile range of each variable's time series to scale the partial term. The interquartile range captures the middle range of the distribution and omits outliers that might make it challenging to assess partial derivative values along the length of the river. This is an effective strategy highlighted best by shortwave radiation, which goes to  $0 \text{ Wm}^{-2}$  at night. By ignoring the lower (and upper) quartile range of the shortwave radiation distribution and scaling all values toward the middle quartile of the distribution, we can more easily observe which atmospheric variables most strongly/weakly control river temperature. Scaling partial derivative values also changes the units to degrees Celsius (river temperature), which makes the scaled partial terms easier to comprehend in the context of actual river temperature change due to atmospheric perturbations.

Additionally, we normalize the scaled terms by the atmospheric variable that exhibits the most considerable contribution to predicted river temperature change, which we find to be shortwave radiation. Normalizing scaled partial derivative terms to the scaled partial derivative that contributes the most to changes in predicted river temperature allows us to standardize partial derivative terms making it easier to assess which atmospheric variable affects the most change to the predicted energy balance and river temperature across all seasons and along river distance.

The scaled partial derivative is presented as

$$\left(\frac{\partial T}{\partial Weather}\right)(IQR_{weather}) \quad (4)$$

Where  $\partial T$  is the river temperature between baseline and perturbed scenarios,  $\partial Weather$  refers to the perturbation value used to adjust the atmospheric variable of interest, and  $IQR$  refers to the interquartile range of the weather time series data for the simulation period. The scaled partial derivatives are expressed in river temperature units, providing readers with a realistic context for interpreting the partial derivative terms. The normalized terms are dimensionless by definition:

$$\frac{Scaled_{weather}}{Scaled_{solar\ radiation}} \quad (5)$$

Expanded normalized term:

$$\frac{\left(\frac{\partial T}{\partial Weather}\right)(IQR_{weather})}{\left(\frac{\partial T}{\partial solar}\right)(IQR_{solar})} \quad (6)$$

And rearrange by term:

$$\left(\frac{\partial T IQR_{wx}}{\partial T IQR_{solar}}\right) \left(\frac{\partial_{solar\ radiation}}{\partial_{weather}}\right). \quad (7)$$

Ultimately, we present original, scaled, and normalized partial derivatives (Figure A5-A8, Table B1, Figure 5-8, Table 7, Figure 10-13, and Table 8, respectively), although the results section of this paper will focus on scaled and normalized values as they are most effective in conveying the contribution of each atmospheric variable to changes in FLUVIAL-EB simulation results.

### ***Estimating unique perturbation values for partial derivatives***

Partial derivatives are derived by adjusting some atmospheric variables ( $w$ ) by a perturbation value ( $p$ ), considering river temperature ( $T$ ) is a function of that atmospheric variable ( $T(w + p, \dots, w_i + p)$ ). How do we decide the best perturbation method and value for

this application? The magnitudes of each weather variable operate on different scales in relation to each other, making it difficult to compare the influence of each atmospheric variable on predicted energy fluxes and river temperatures across all seasons and along river distances. Therefore, the value of  $p$  is given careful consideration.

We undergo a series of trial model runs whereby we observe predicted river temperature simulated under various perturbation values. First, we perturbed all six atmospheric variables by a +1.0-unit change for all variables and all seasons. Given that the goal of this research is to present partial derivatives at all distances along the river for all times and all four seasons, the concern with a +1.0-unit change across all variables and seasons is that a +1.0 unit change does not replicate the natural magnitude of change of the six atmospheric variables at the diurnal and seasonal temporal scale. For example, 7-day average shortwave radiation values are between  $305 \text{ Wm}^{-2}$  and  $340 \text{ Wm}^{-2}$ , while the 7-day averages for windspeed are between  $1.0 \text{ ms}^{-1}$  and  $2.5 \text{ ms}^{-1}$  for the summer months (Figure A3). In other words, a +1.0-unit change to windspeed might show a greater magnitude of change in predicted river temperature than a +1.0-unit change to shortwave radiation. We conducted experiments where we adjusted the perturbation values for several weather variables. As an example, shortwave radiation we perturbed by values of  $+5.0 \text{ Wm}^{-2}$ ,  $+10.0 \text{ Wm}^{-2}$ , and  $+15.0 \text{ Wm}^{-2}$ . All results produced no discernible significance reflected in the partial derivative values for predicted river temperature. There was no discernable difference in sensitivity values at all distances of the river and across all seasons.

Next, following the methods in Rakovec et al. (2014), I perturbed all six atmospheric variables by +1.0% (Equation 7, adopted from (Rakovec et al., 2014)).

$$\frac{\partial T}{\partial p} \approx \frac{T(w_i + w_i(0.01)) - T(w_i)}{w_i(0.01)} \quad (8)$$

Where  $p = w_i(0.01)$ , and  $w_i$  is any of the six atmospheric variables for  $t = i$ . This method was promising as it provided a realistic way of perturbing atmospheric variables within the FLUVIAL-EB model because it preserves the natural variations of the dataset. We also tested another perturbation method called the coefficient of variation (CV) method. The coefficient of variation describes the extent of variability in relation to the mean of the population in question.

$$CV = \frac{\sigma_w}{\bar{w}} \quad (9)$$

Where  $\sigma$  is the standard deviation of a weather variable ( $\bar{w}$ ). This step highlighted the need to define a perturbation method that can 1) encapsulate the natural variability of each weather variable and 2) be adjusted based on seasonal changes in the range of each atmospheric variable. We test both the Rakovec and CV methods. We apply both methods to each weather observation within the time-series of the simulation period. The CV method was ultimately used as it was computationally inexpensive and captured the seasonal variability of each variable. Perturbation values calculated under both methods are presented in Table 9.

Our sensitivity analysis methodology differs from traditional approaches, as we do not apply a single perturbation value to each variable. While such an approach provides insight into the model's response to a constant input change, we recognize that the natural variability of weather variables across seasons and their effects on predicted river temperature are essential considerations. Therefore, we utilize the coefficient of variation method to develop unique individual perturbations and assess predicted river temperature sensitivity to these perturbations. We present the resulting partial derivative values as scaled/normalized versions of the original partial derivatives, referred to as partial derivatives. This approach provides more insight into the model's sensitivity to the atmosphere across each season.

Note: When we originally set up model experiments our partial derivative values were undistinguishable from each other making it difficult to analyze predicted river temperature response to small changes made to the meteorology. We realized that the method in which the FLUVIAL-EB model handled manual changes to the surrounding meteorology was non effective. For this reason, we choose to develop the CV method. Subsequently, we develop a MATLAB script that allows the FLUVIAL-EB model to better interpret manual changes to the meteorology. Future work might allow the user to perform a more classic sensitivity analysis where the perturbation value is the same across each variable and seasons although we still find the methods listed above to be useful in determining seasonal changes to predicted river temperature.

## **Results**

In this study, we performed a sensitivity analysis to investigate the impact of changes in critical atmospheric variables on the spectral energy balance of the water column and predicted river temperature within the FLUVIAL-EB model. We examined the sensitivity of predicted river temperature to air pressure, air temperature, shortwave radiation, longwave radiation, vapor pressure, and windspeed for each of the four seasons (winter (DJF), spring (MAM), summer (JJA), and fall (SON)) using a 7-day mean. We calculated scaled and normalized partial derivatives using the coefficient of variation method, as described in the methods section, to understand better the predicted river temperature's sensitivity to each weather variable adjustment. Table 7 and Figure 6-9 show the 7-day mean of the scaled partial derivatives for each atmospheric variable at every distance of the river (0km – 150 km) calculated at a 10m resolution (x-axis) and presented in terms of degrees Celsius. We estimated the sensitivity terms

by subtracting predicted river temperature values simulated under small positive perturbations made to each atmospheric variable from predicted river temperature values simulated under observed weather conditions. Positive/negative sensitivity values represent a warming/cooling trend in predicted river temperatures simulated under small positive changes to atmospheric variables. Physically speaking, these sensitivity values indicate the impact of each atmospheric variable on the river temperature. Table 8 and Figure 10-13 show the normalized partial derivative values. Normalization was done with respect to shortwave radiation, which exhibited the most change in predicted river temperature. We highlighted shortwave radiation values in grey in each table to emphasize that all other values were scaled to this variable. The normalized partial derivatives provided a better understanding of the quantitative trends in the sensitivity of predicted river temperature to each of the six atmospheric variables. Overall, the sensitivity analysis results provided insight into the atmosphere-water surface interaction occurring within the FLUVIAL-EB model, which is essential for predicting river temperature and understanding how changes influence it in the atmosphere.

### *DJF*

For each season, we assess partial derivative values calculated for predicted river temperature output simulated under small positive perturbations made separately to each of the atmospheric variables used in this study. Figure 6 and Table 7 show scaled sensitivity results along all distances of the river for a 7-day mean in DJF.

At the 150km river distance (end of modelled river), predicted river temperature is most influenced by perturbations made to (1) shortwave radiation followed by (2) air temperature, (3) longwave radiation, (4) windspeed, (5) vapor pressure, and (6) air pressure for the DJF season.

All sensitivity values increase in magnitude along the length of the river, although the direction of river temperature changes with respect to each small positive change made to an atmospheric variable change depending on the variable. All atmospheric perturbation experiments show that under a small change, river temperature is immediately effective by the change within the first few kilometers of the dam.

Windspeed and air pressure sensitivity values are negative along the length of the river, while shortwave radiation, longwave radiation, air temperature, and vapor pressure are positive, showing that river temperature is cooling/heating respectively under a slight positive perturbation made to each atmospheric variable.

#### *MAM*

Figure 7 and Table 7 show scaled sensitivity results along all distances of the river for a 7-day mean in MAM. At the 150km river distance, predicted river temperature is most influenced by perturbations made to (1) shortwave radiation followed by (2) longwave radiation, (3) air temperature, (4) vapor pressure, (5) windspeed, and (6) air pressure for the MAM season.

All predicted river temperature sensitivity values increase in magnitude along the length of the river. Shortwave radiation, longwave radiation, and air pressure depart from zero (no change between baseline and perturbation river temperature experiments) immediately within the first few kilometers from the dam. Air temperature, windspeed, and vapor pressure increase in magnitude gradually with distance away from the dam; thus, their effect on river temperature is gradual along the length of the river for the MAM season compared to all other variables.

Perturbations made to shortwave radiation, longwave radiation, air temperature, vapor pressure, and air pressure all exhibit positive (warming) changes in predicted river temperature

for the MAM season. The MAM perturbation value ( $+0.471 \text{ ms}^{-1}$ ) made to windspeed affects an overall net negative (cooling) change in predicted river temperature. Windspeed is the only variable shown to cause a cooling trend along river distance for the MAM season.

### *JJA*

Figure 8 and Table 7 show scaled sensitivity results along all distances of the river for a 7-day mean in JJA. At the 150km river distance, predicted river temperature is most influenced by perturbations made to (1) shortwave radiation followed by (2) air temperature, (3) longwave radiation, (4) windspeed, (5) vapor pressure, and (6) air pressure for the JJA season.

All partial derivatives increase in magnitude downstream. Positive perturbations made to Shortwave radiation and longwave radiation ( $+1.14 \text{ Wm}^{-2}$  and  $+0.08 \text{ Wm}^{-2}$ , respectively) effect predicted river temperatures immediately downstream of the dam, while a positive perturbation to air temperature, windspeed, vapor pressure, and air pressure ( $+0.27^\circ\text{C}$ ,  $+0.3 \text{ ms}^{-1}$ ,  $+0.074 \text{ hPa}$ ,  $+0.0013 \text{ hpa}$ , respectively) all affect predicted river temperature at a slower rate along the river.

Like the MAM season, the small perturbation applied to windspeed causes a decrease (cooling) in predicted river temperature. Shortwave radiation, longwave radiation, air temperature, vapor pressure, and air pressure all impart positive (warming) values for predicted river temperature.

### *SON*

Figure 9 and Table 7 show scaled sensitivity results along all distances of the river for a 7-day mean in SON. At the 150km river distance, predicted river temperature is most influenced

by perturbations made to (1) shortwave radiation followed by (2) longwave radiation, (3) air temperature, (4) windspeed, (5) vapor pressure, and (6) air pressure for the SON season.

Perturbations made to each of the six atmospheric variables lead to a change in predicted river temperature. Shortwave radiation, longwave radiation, and air pressure all affect predicted river temperature within the first few kilometers from the dam under their unique perturbation values ( $+1.27 \text{ Wm}^{-2}$ ,  $+0.12 \text{ Wm}^{-2}$ ,  $+0.003 \text{ hPa}$ , respectively). A more gradual rate of change of predicted river temperature along the river is shown when air temperature, windspeed, and vapor pressure are perturbed by values of  $+0.25 \text{ }^\circ\text{C}$ ,  $+0.32 \text{ ms}^{-1}$ ,  $+0.13 \text{ hPa}$ , respectively.

Except for the winter season (DJF), where a perturbation to air pressure also leads to a slight cooling of the predicted river temperature, windspeed is the only variable that exhibits a negative (cooling) difference in the predicted river temperature under a perturbation.

Perturbations to all other variables result in a positive (warming) change in the predicted river temperature.

### ***General findings on scaled partial derivatives***

Several key takeaways can be drawn from the sensitivity analysis performed on the FLUVIAL-EB model for all seasons. Firstly, atmospheric factors increasingly influence river temperature as water flows downstream from the dam (0 km). Moreover, river temperature is most sensitive to atmospheric changes at greater distances from the source, indicating that the FLUVIAL-EB model can capture the complex interplay between the atmosphere and the water surface. Secondly, perturbations made to different atmospheric variables elicit varying responses in the rate at which predicted river temperature deviates from its boundary condition temperature at distance = 0km. For instance, changes in downwelling shortwave and longwave radiation

cause immediate increases in predicted river temperature, while fluctuations in air temperature, windspeed, vapor pressure, and air pressure cause a more gradual increase that takes place further downstream.

Lastly, a vital feature of this study is the ability to examine specific spatial and temporal relationships between individual atmospheric variables and river temperature. For example, during the MAM season, a  $+1.4 \text{ Wm}^{-2}$  increase in shortwave radiation causes a net  $+2.04 \text{ }^\circ\text{C}$  change in river temperature along the downstream distances of the river (distance = 75km – 150km), while a change in shortwave radiation causes a net  $+2.1 \text{ }^\circ\text{C}$  change in river temperature along the initial portion of the river (distance = 0km – 50km). Observations such as this underscores the utility of Chapter 1 results to determine river temperature sensitivity to key atmospheric variables at key distances and times along the river which help inform location and seasonal based water management decisions.

### *Normalized partial derivatives*

While the previous analysis focused on scaled partial derivative values, it is essential to highlight the utility of observing normalized values (Table 8 and Figure 10-13). Normalization involves dividing the partial derivative values by the scaled partial derivatives that cause the most significant change to predicted river temperature (i.e., shortwave radiation). This process results in uniform, unitless values ranging from -1 to 1. These normalized values provide context by indicating how sensitive river temperature is in the positive (warming) or negative (cooling) directions when a perturbation is made to an atmospheric variable. Normalized values are beneficial for observing predicted river temperature sensitivity since they offer a simple numerical map of cooling and warming trends. Many other studies utilize this tool. Most notably,

greenhouse gas concentrations are often reported as normalized values where the suite of influential greenhouse gasses are normalized by carbon dioxide. Methane concentrations, for example, exist in a much lower magnitude than their carbon dioxide counterpart. Thus, it becomes necessary to normalize methane values to the magnitude of carbon dioxide's part per mass concentration so that these two gasses are comparable from a global greenhouse gas perspective. Relating the greenhouse normalization analogy to the study, windspeed values have a much lower magnitude than values of shortwave radiation. Thus, to compare the response and sensitivity of predicted river temperature to vital atmospheric variables, it is necessary to normalize them.

### *Atmospheric energy fluxes*

The seasonal variation of atmosphere-water interactions in a river was investigated in this study (Figure 14). The results of the baseline model experiment revealed that net absorbed shortwave radiation ( $S_{net}$ ) is the most significant heat flux in the river energy balance across all seasons. Latent ( $L$ ), sensible ( $H$ ), and net longwave ( $F_{net}$ ) fluxes were found to be negative (i.e., cooling the river) across all seasons. Sensible heat flux alternates between heating (+) and cooling (-) between day and night, but its magnitude remains small in all seasons. The latent heat fluxes exhibited a consistent diurnal cycle, balancing the sensible heat flux in all seasons. The dominant source of cooling is longwave radiation ( $F_{net}$ ), as latent heat fluxes are consistently negative. ( $F_{net}$ ) depends on emissivity calculated from air temperature, vapor pressure, a shortwave index (Prata, 1996), and a cloud correction (T. M. Crawford & Duchon, 1999). From the sensitivity analysis results, longwave radiation is a relatively strong control of river temperature change. However, small perturbation to downwelling longwave from the

atmosphere does not significantly cool predicted river temperature. As the river heats the atmosphere, the vapor pressure above the water surface rises, cooling the river. However, an increase in vapor pressure also increases downwelling longwave radiation, resulting in ( $F_{net}$ ) being less strongly negative and, therefore, less effective cooling.

In conclusion, this analysis provides an understanding of the seasonal variation of atmosphere-water interactions in a river, highlighting the importance of the critical climate variables of interest and their impact on the predicted energy balance and river temperatures.

### **Limitations**

There are a few limitations present in Chapter 1. First, we acknowledge that a 15-day simulation period reduced to a 7-day simulation period to allow for model spin-up is not a sufficiently long enough time period to present a true seasonal analysis. We are limited in data storage capabilities required to handle model output and the computational expense of running the FLUVIAL-EB model. However, results and conclusions presented in Chapter 1 highlight the importance of taking a seasonal based approach in understanding how predicted river temperature changes as a function of the atmosphere along distances of the river. Second, inflow and outflow of water along the main channel are not given enough consideration in this chapter. A key signature that is prevalent across all results for each season is that the rate of change in sensitivity of predicted river temperature follows a uniform increase in magnitude (not necessarily direction) within the 75 km to 100 km river distance. The theory for this reoccurring theme within the sensitivity results is that flow is diverted away from the main channel thus decreasing water depth. Decrease in water depth allows the atmosphere to heat the water column quicker causing predicted river temperatures to rise along the 75 km to 100 km river distance at a

quicker rate compared to the rest of the longitudinal river profile. More consideration should be given here to explain the fluctuation of the sensitivity values so that we can discern the role of the atmosphere on predicted river temperature changes based on water depth fluctuations due to water diversion and input locations along the river channel. Lastly, longwave radiation is the only atmospheric variable that is not empirically calculated. We calculate longwave radiation using air temperature, a solar index, and either vapor pressure or precipitable water following methods laid forth in Dilley and O'Brien (1997). The main limitation here is that as we add a perturbation value to air temperature the longwave radiation value also gets adjusted as a function of air temperature change. We then additionally perturb longwave radiation by a small positive value, which means longwave radiation is perturbed at two different times under the current model calculations. This limits our ability to understand how longwave radiation influences predicted river temperature because it is dependent on air temperature in its calculations.

## **Conclusion**

In conclusion, this study utilized the FLUVIAL-EB model to investigate the sensitivity of predicted river temperature to changes in critical atmospheric variables across four seasons (DJF, MAM, JJA, SON). The results reveal that shortwave radiation has the most significant impact on predicted river temperatures across all seasons. Furthermore, partial derivative values increased in magnitude downstream, and the effect of each atmospheric variable varied depending on season and distance downstream from the dam. Small perturbations to shortwave and longwave radiation cause an immediate change in predicted river temperature within the first 10 km

downstream of the dam. The remaining variables affect change in predicted river temperature at a much slower rate, given their respective small perturbations.

This analysis explains the seasonal variation between the atmosphere and water column relationship as they relate to river temperature and energy balance FLUVIAL-EB model predictions. We highlight the substantial control that absorbed shortwave radiation and incoming shortwave radiation has on river temperature, which implies a top-down atmosphere to the water surface to water column dominance over river temperature. The six atmospheric variables observed here are apportioned through the model to calculate radiative, sensible, and latent heat energy exchange into evaporation and absorption characteristics of the river.

We conclude that incoming shortwave and longwave radiation substantially control river temperature for wide, shallow rivers such as the San Joaquin River. Small rivers and streams are often shaded or bordered by overhanging vegetation which limits the amount of radiation ( $S_{net}$ ) that can be absorbed by the water column. However, it is challenging to prevent the primary heating source in a wide shallow river with clear-sky conditions or where vegetative canopy shading can only influence narrow margins of the river along the banks. We find that radiative heating generally controls river temperature, which can increase predicted river temperature by up to 10.3 °C in the summer months (Table 7).

Finally, this chapter has satisfied the requirements of an SA postulated by Devak and Dhanya (2017) as it provides valuable information on the influence of specific input variables on model results. By identifying which variables have the most significant impact on the output, this SA can guide future FLUVIAL-EB efforts in prioritizing efforts to refine and improve model inputs. Additionally, this SA guides ongoing changes to the model structure as we can now better

understand the top-down influence of each atmospheric variable on the energy balance of the water column. Understanding model sensitivity to atmospheric inputs can focus future work on model adjustments or improvements to the input dataset to improve accuracy and effectiveness. Finally, this SA provided the necessary context for examining energy balance and river temperature by better understanding their sensitivities to each of the six atmospheric variables.

## Chapter 2 – Developing a Standard Error Equation for FLUVIAL-EB Predicted River Temperatures

### Introduction

It is crucial to quantify sources of error in a model experiment to improve the accuracy of model predictions (Pechlivanidis, Jackson, & McIntyre, 2011). Estimating sources of uncertainty and quantifying errors associated with model uncertainty has not yet been done for the FLUVIAL-EB model. This chapter addresses a possible source of error in FLUVIAL-EB energy balance and river temperature predictions, where we develop a novel standard error equation that quantifies data uncertainties within the meteorological time-series data across all seasons and along each distance of the river. We hypothesize that the CIMIS-provided atmospheric dataset does not represent atmospheric conditions directly over the river channel and therefore is not representative of the actual atmospheric conditions directly over the river that affect the absorptive and evaporative characteristics at the water-atmosphere surface level.

Standard error values of predicted river temperatures are calculated using an auto-correlated, variance-based decomposition of the basic standard error equation under first-order Taylor Series assumptions. The expanded standard error equation includes the following:

1. A weighting term (partial derivatives calculated in Chapter 1) that measures the unique influence each atmospheric variable imparts on model predictions;
2. A Pearson's correlation coefficient term, which measures the direction and magnitude of the correlation between two uncorrelated atmospheric variables;

3. A standard error value for each atmospheric variable that characterizes error due to misrepresentation of the atmosphere directly over the river channel, which we call standard error due to geographic displacement between the weather station and the river channel.

It is important to note that this approach for quantifying data uncertainties is an initial effort and does not claim to provide a complete analysis of all possible sources of error in FLUVIAL-EB model predictions. However, the methods presented in Chapter 2 provide a first step in quantifying a source of error inherent to the atmospheric dataset used in this study and further enhances our understanding of the seasonal and distal characteristics of predicted river temperatures along the river.

### ***Uncertainty analysis and sources of error in physically-based numerical river temperature models***

Uncertainty in hydrological model predictions is a well-known challenge that hinders confidence in model results (Pechlivanidis et al., 2011). Uncertainty is quantifiable by examining different sources of error that contribute to the total error in model predictions (Bobba, Singh, & Bengtsson, 1995). Model prediction errors can stem from natural, data, parameter, and structural uncertainties. Bobba et al. (1995) describe natural uncertainties as random natural effects inherent to datasets used to calculate model predictions, such as temporal and spatial variability observed in the natural record. Chapter two assesses natural uncertainties in FLUVIAL-EB model predictions stemming from the CIMIS meteorological data network.

Natural uncertainties of meteorological datasets are prevalent in hydrology literature. Spatial and temporal data resolution limits process-based energy balance model results

(Rivington, Matthews, Bellocchi, & Buchan, 2006; Westhoff et al., 2007). For instance, heat fluxes at the air-water and water-bed surfaces vary by region as a function of the prevailing meteorology/climatology processes within the basin (Dugdale et al., 2017). Therefore, the accuracy of model predictions made by numerical energy balance models mainly depends on the set physical properties that govern heat fluxes. The FLUVIAL-EB radiative scheme is governed by the observed downwelling atmospheric fluxes that act upon the water surface. This motivates the goal of understanding natural errors in river temperature predictions caused by solar radiation, longwave radiation, air temperature, wind speed, vapor pressure, and air pressure.

## **Data**

The data utilized in this chapter is a compilation of sources previously discussed in Chapter 1, focusing on two specific weather stations (Firebaugh and Westlands, Table 2), which are part of the CIMIS meteorological network within the region. The data extracted from the CIMIS network includes air temperature, shortwave radiation, air pressure, and wind speed. As described in the data section of Chapter 1, longwave radiation is determined empirically using a clear-sky algorithm (Prata, 1996) and cloud correction equations from (T. M. Crawford & Duchon, 1999). Additionally, partial derivative values derived from the methodology described in Chapter 1 are used as weighting coefficients in the final standard error equation.

## **Methods**

### ***Definition of the standard error equation in the context of the FLUVIAL-EB model***

The basic standard error equation is a statistical measure of the standard deviation of a sampled distribution. The standard error of predicted river temperature quantifies the error in river temperature predictions due to the natural variability of the atmospheric data and the spatial

array of the CIMIS station network. The basic standard error equation is the standard deviation divided by the square root of the number of samples (Equation 10).

$$SE = \frac{\sigma}{\sqrt{n}} \quad (10)$$

Where  $\sigma$  is the standard deviation of the sample, and  $n$  is the number of samples. We use the standard error equation to measure accuracy in FLUVIAL-EB model river predictions (Equation 11).

$$SE_T = \frac{\sigma_T}{n} \quad (11)$$

$\sigma_T$  is the standard deviation of predicted river temperature, and  $n$  is the number of atmospheric samples used to calculate radiative characteristics of the energy balance scheme of the FLUVIAL-EB model.

We could, in theory, execute the basic standard error equation (Equation 11) on any set of river predictions along each river distance. Doing so would not be particularly useful as the results would not allow us to discern errors in predicted river temperature attributable from the six atmospheric variables used in this study. In order to incorporate atmospheric sources of error into the basic standard error equation (Equation 11), we expand the equation to include terms that account for weather data uncertainties.

***Defining a standard error equation – Taylor series, variance-based expansion of the basic standard error equation***

We present a novel Gaussian variance-based, multi-variable error decomposition scheme on the simple standard error equation to account for the contribution of each meteorological variable on the overall error in river temperature predictions. Using first-order Taylor Series

expansion approximations under the finite-difference assumptions, we expand the basic standard error equation to include a set of variance and covariance terms that incorporate a standard error value that characterizes error due to the possible misrepresentation of the atmosphere directly over the river channel. Again, this error term is the standard error due to geographic displacement between the weather station and the river channel (we explain the methodology used to develop the term below).

First, we assume that predicted river temperature ( $T$ ) and the associated standard error are a function of only the weather inputs: air temperature ( $T_a$ ), air pressure ( $p$ ), longwave radiation ( $\downarrow \Phi$ ), shortwave radiation ( $S$ ), vapor pressure ( $e_0$ ), and windspeed ( $U$ ).

$$T = f(T_a, P, \Phi \downarrow, S, e_0, U)$$

$$SE_T = f(SE_{T_a}, SE_P, SE_{\Phi \downarrow}, SE_S, SE_{e_0}, SE_U) \quad (12)$$

Equation 12 is expanded using first-order Taylor Series expansion:

$$\begin{aligned} T \approx & f(T_a, P, \Phi \downarrow, S, e_0, U) + \frac{\partial T}{\partial T_a} (T_a - \bar{T}_a) + \frac{\partial T}{\partial P} (P - \bar{P}) \\ & + \frac{\partial T}{\partial \Phi \downarrow} (\Phi \downarrow - \bar{\Phi \downarrow}) + \frac{\partial T}{\partial S} (S - \bar{S}) + \frac{\partial T}{\partial e_0} (e_0 - \bar{e}_0) + \frac{\partial T}{\partial U} (U - \bar{U}). \end{aligned} \quad (13)$$

$$\bar{T} \approx f(\bar{T}_a, \bar{P}, \bar{\Phi \downarrow}, \bar{S}, \bar{e}_0, \bar{U}). \quad (14)$$

We assume river temperature operates as a function of the six atmospheric variables of interest. Therefore, we can state that the mean of the river temperature is also a function of the mean of all six atmospheric variables during that same period.

We substitute Equation 14 for the mean predicted river in Equation 13,

$$\begin{aligned}
T \approx & f(\bar{T}_a, \bar{P}, \bar{\Phi} \downarrow, \bar{S}, \bar{e}_0, \bar{U}) + \frac{\partial T}{\partial T_a} (T_a - \bar{T}_a) + \frac{\partial T}{\partial P} (P - \bar{P}) \\
& + \frac{\partial T}{\partial \Phi \downarrow} (\Phi \downarrow - \bar{\Phi} \downarrow) + \frac{\partial T}{\partial S} (S - \bar{S}) + \frac{\partial T}{\partial e_0} (e_0 + \bar{e}_0) \\
& + \frac{\partial T}{\partial U} (U - \bar{U})
\end{aligned} \tag{15}$$

which can be simplified:

$$\begin{aligned}
T - \bar{T} \approx & \frac{\partial T}{\partial T_a} (T_a - \bar{T}_a) + \frac{\partial T}{\partial P} (P - \bar{P}) + \frac{\partial T}{\partial \Phi \downarrow} (\Phi \downarrow - \bar{\Phi} \downarrow) + \frac{\partial T}{\partial S} (S - \bar{S}) \\
& + \frac{\partial T}{\partial e_0} (e_0 + \bar{e}_0) + \frac{\partial T}{\partial U} (U - \bar{U}).
\end{aligned} \tag{16}$$

Using Equation 16, we can decompose the first-order terms by incorporating the variance definition. Variance is the measure of the variability within the time series using the average of the squared deviations from the mean predicted river temperature values:

$$Var(T) = \frac{\sum (T - \bar{T})^2}{N} \tag{17}$$

Substituting the approximation for predicted river temperature as a function of the six atmospheric variables (Equation 16) to the variance equation (Equation 17) yields:

$$\begin{aligned}
Var(T) = & \frac{1}{N} \left[ \frac{\partial T}{\partial T_a} (T_a - \bar{T}_a) + \frac{\partial T}{\partial P} (P - \bar{P}) + \frac{\partial T}{\partial \Phi \downarrow} (\Phi \downarrow - \bar{\Phi} \downarrow) \right. \\
& \left. + \frac{\partial T}{\partial S} (S - \bar{S}) + \frac{\partial T}{\partial e_0} (e_0 + \bar{e}_0) + \frac{\partial T}{\partial U} (U - \bar{U}) \right]^2
\end{aligned} \tag{18}$$

Squaring the numerator in Equation 18 and simplifying yields the fully expanded variance of predicted river temperature

$$\begin{aligned}
Var(T) = \frac{1}{N} & \left[ \left( \frac{\partial T}{\partial T_a} (T_a - \bar{T}_a) \right)^2 + \left( \frac{\partial T}{\partial p} (p - \bar{p}) \right)^2 + \left( \frac{\partial T}{\partial \Phi \downarrow} (\Phi \downarrow - \bar{\Phi \downarrow}) \right)^2 + \left( \frac{\partial T}{\partial S} (S - \bar{S}) \right)^2 + \left( \frac{\partial T}{\partial e_0} (e_0 - \bar{e}_0) \right)^2 + \left( \frac{\partial T}{\partial U} (U - \bar{U}) \right)^2 + \right. \\
& 2 \left( \frac{\partial T}{\partial T_a} \frac{\partial T}{\partial p} (T_a - \bar{T}_a) (p - \bar{p}) \right) + 2 \left( \frac{\partial T}{\partial T_a} \frac{\partial T}{\partial \Phi \downarrow} (T_a - \bar{T}_a) (\Phi \downarrow - \bar{\Phi \downarrow}) \right) + \\
& 2 \left( \frac{\partial T}{\partial T_a} \frac{\partial T}{\partial S} (T_a - \bar{T}_a) (S - \bar{S}) \right) + 2 \left( \frac{\partial T}{\partial T_a} \frac{\partial T}{\partial e_0} (T_a - \bar{T}_a) (e_0 - \bar{e}_0) \right) + \\
& 2 \left( \frac{\partial T}{\partial T_a} \frac{\partial T}{\partial U} (T_a - \bar{T}_a) (U - \bar{U}) \right) + 2 \left( \frac{\partial T}{\partial p} \frac{\partial T}{\partial \Phi \downarrow} (p - \bar{p}) (\Phi \downarrow - \bar{\Phi \downarrow}) \right) + \\
& 2 \left( \frac{\partial T}{\partial p} \frac{\partial T}{\partial S} (p - \bar{p}) (S - \bar{S}) \right) + 2 \left( \frac{\partial T}{\partial p} \frac{\partial T}{\partial e_0} (p - \bar{p}) (e_0 - \bar{e}_0) \right) + 2 \left( \frac{\partial T}{\partial p} \frac{\partial T}{\partial U} (p - \bar{p}) (U - \bar{U}) \right) + \\
& 2 \left( \frac{\partial T}{\partial \Phi \downarrow} \frac{\partial T}{\partial S} (\Phi \downarrow - \bar{\Phi \downarrow}) (S - \bar{S}) \right) + 2 \left( \frac{\partial T}{\partial \Phi \downarrow} \frac{\partial T}{\partial e_0} (\Phi \downarrow - \bar{\Phi \downarrow}) (e_0 - \bar{e}_0) \right) + 2 \left( \frac{\partial T}{\partial \Phi \downarrow} \frac{\partial T}{\partial U} (\Phi \downarrow - \bar{\Phi \downarrow}) (U - \bar{U}) \right) + \\
& 2 \left( \frac{\partial T}{\partial S} \frac{\partial T}{\partial e_0} (S - \bar{S}) (e_0 - \bar{e}_0) \right) + 2 \left( \frac{\partial T}{\partial S} \frac{\partial T}{\partial U} (S - \bar{S}) (U - \bar{U}) \right) + 2 \left( \frac{\partial T}{\partial e_0} \frac{\partial T}{\partial U} (e_0 - \bar{e}_0) (U - \bar{U}) \right) \left. \right] \tag{19}
\end{aligned}$$

Next, we express Equation 19 in terms of variance and covariance. Writing Equation 14 in terms of variance and covariance is helpful in statistics and data analysis for several reasons. First, variance and covariance terms describe the relationships between each atmospheric variable. The variance measures the spread or variability around the mean of the dependent variables. The covariance between the dependent and independent variables measures the degree

to which two variables vary together. Second, observing covariance and variance results allows one to calculate other statistical measures such as correlation coefficients, regression analysis, and hypothesis testing. Third, variance and covariance are widely understood statistical measures. Therefore, expressing an equation in these terms can make it easier to compare results with future work where alternative atmospheric data sets are chosen for river temperature simulations or to compare results with other studies. Lastly, these measures help to identify potential problems with the data. Large covariance and variance terms values indicate outliers or measurement errors with the data, and by identifying these issues, we can improve the accuracy and reliability of FLUVIAL-EB model predictions. We rewrite Equation 19 to include variance (Equation 17) and covariance (Equation 20) terms.

First, the definition of covariance between any two weather variables  $w_{1,i}$  and  $w_{2,i}$  is defined as follows:

$$Cov(w_1, w_2) = \frac{\sum(w_{1,i} - \bar{w}_1)(w_{2,i} - \bar{w}_2)}{N} \quad (20)$$

Rewriting Equation 14 in terms of variance and covariance (Equation 17 and Equation 20) yields:

$$\begin{aligned}
Var(T) = & \left(\frac{\partial T}{\partial T_a}\right)^2 Var(T_a) + \left(\frac{\partial T}{\partial p}\right)^2 Var(p) + \left(\frac{\partial T}{\partial \Phi \downarrow}\right)^2 Var(\Phi \downarrow) \\
& + \left(\frac{\partial T}{\partial S}\right)^2 Var(S) + \left(\frac{\partial T}{\partial e_0}\right)^2 Var(e_0) + \left(\frac{\partial T}{\partial U}\right)^2 Var(U) \\
& + 2\left(\frac{\partial T}{\partial T_a} \frac{\partial T}{\partial p} Cov(T_a, p)\right) + 2\left(\frac{\partial T}{\partial T_a} \frac{\partial T}{\partial \Phi \downarrow} Cov(T_a, \Phi \downarrow)\right) \\
& + 2\left(\frac{\partial T}{\partial T_a} \frac{\partial T}{\partial S} Cov(T_a, S)\right) + 2\left(\frac{\partial T}{\partial T_a} \frac{\partial T}{\partial e_0} Cov(T_a, e_0)\right) \\
& + 2\left(\frac{\partial T}{\partial T_a} \frac{\partial T}{\partial U} Cov(T_a, U)\right) + 2\left(\frac{\partial T}{\partial p} \frac{\partial T}{\partial \Phi \downarrow} Cov(p, \Phi \downarrow)\right) \\
& + 2\left(\frac{\partial T}{\partial p} \frac{\partial T}{\partial S} Cov(p, S)\right) + 2\left(\frac{\partial T}{\partial p} \frac{\partial T}{\partial e_0} Cov(p, e_0)\right) \\
& + 2\left(\frac{\partial T}{\partial p} \frac{\partial T}{\partial U} Cov(p, U)\right) + 2\left(\frac{\partial T}{\partial \Phi \downarrow} \frac{\partial T}{\partial S} Cov(\Phi \downarrow, S)\right) \\
& + 2\left(\frac{\partial T}{\partial \Phi \downarrow} \frac{\partial T}{\partial e_0} Cov(\Phi \downarrow, e_0)\right) \\
& + 2\left(\frac{\partial T}{\partial \Phi \downarrow} \frac{\partial T}{\partial U} Cov(\Phi \downarrow, U)\right) + 2\left(\frac{\partial T}{\partial S} \frac{\partial T}{\partial e_0} Cov(S, e_0)\right) \\
& + 2\left(\frac{\partial T}{\partial S} \frac{\partial T}{\partial U} Cov(S, U)\right) + 2\left(\frac{\partial T}{\partial e_0} \frac{\partial T}{\partial U} Cov(e_0, U)\right)
\end{aligned} \tag{21}$$

Equation 21 helps assess dependent and independent relationships between weather variables and predicted river temperature. However, we still have not incorporated a measure of error that represents error due to the geographic proximity between the weather station network and the river channel. Therefore, we adjust Equation 20 to include Pearson's r correlation

coefficient and the standard error due to the geographic proximity between weather stations and the river channel.

Pearson's  $r$  correlation coefficient and the standard error due to the geographic proximity between weather stations and the river channel are incorporated because they simplify our explanation of the statistical relationship between weather input values and predicted river temperature predictions. Pearson's  $r$  correlation coefficient measures the strength and direction of the linear relationship between two weather variables. The standard error of weather term provides the most significant possible error estimation for error in predicted river temperature due to a geographically-inaccurate representation of the atmosphere directly over the river channel. (See the *Misrepresentation of the atmosphere directly over the river channel (Error due to geographic proximity)* subsection below for a full description of this term. We omit the description in this section to focus on expanding the basic standard error equation.)

We rewrite the variance term on the right-hand side of Equation 21. First, we define variance for each weather variable ( $w$ ) in terms of standard error  $SE_w = \sqrt{\frac{Var(w)}{N}}$ . Squaring both sides and solving for the variance of the weather term yields.

$$Var(w) = N \cdot SE_w^2 \quad (22)$$

The covariance equation (Equation 20) is also changed to include the standard error of weather due to geographic distance from the weather channel and Pearson's  $r$  correlation coefficient.

First, we define Pearson's correlation coefficient. ( $r$ ) In terms of covariance and standard deviation ( $\sigma$ ) between two weather variables:

$$r(w_1, w_2) = \frac{Cov(w_1, w_2)}{\sigma_{w_1} \sigma_{w_2}} \quad (23)$$

Next, we rewrite the denominator of Equation 23 in terms of standard error.

$$SE_w = \frac{\sigma_w}{\sqrt{N}} \quad (24)$$

Solving the identity for standard deviation and substituting Equation 24 into Equation 23 yields:

$$r(w_1, w_2) = \frac{Cov(w_1, w_2)}{N(SE_{w_1} + SE_{w_2})} \quad (25)$$

Finally, rearranging the covariance term results in an expression for covariance written in terms of the standard error of weather due to geographic proximity between weather stations and river channel and Pearson's correlation coefficient.

$$Cov(w_1, w_2) = N(SE_{w_1} + SE_{w_2})r(w_1, w_2) \quad (26)$$

Equation 21 is now rewritten in terms of the standard error and Pearson's correlation coefficient:

$$\begin{aligned}
Var(T) = N & \left[ \left( \frac{\partial T}{\partial T_a} SE_{T_a} \right)^2 + \left( \frac{\partial T}{\partial p} SE_p \right)^2 + \left( \frac{\partial T}{\partial \Phi \downarrow} SE_{\Phi \downarrow} \right)^2 + \left( \frac{\partial T}{\partial S} SE_S \right)^2 \right. \\
& + \left( \frac{\partial T}{\partial e_0} SE_{e_0} \right)^2 + \left( \frac{\partial T}{\partial U} SE_U \right)^2 + \frac{\partial T}{\partial T_a} \frac{\partial T}{\partial p} SE_{T_a} SE_p r(T_a, p) \\
& + \frac{\partial T}{\partial T_a} \frac{\partial T}{\partial \Phi \downarrow} SE_{T_a} SE_{\Phi \downarrow} r(T_a, \Phi \downarrow) \\
& + \frac{\partial T}{\partial T_a} \frac{\partial T}{\partial S} SE_{T_a} SE_S r(T_a, S) + \frac{\partial T}{\partial T_a} \frac{\partial T}{\partial e_0} SE_{T_a} SE_{e_0} r(T_a, e_0) \\
& + \frac{\partial T}{\partial T_a} \frac{\partial T}{\partial U} SE_{T_a} SE_U r(T_a, U) + \frac{\partial T}{\partial p} \frac{\partial T}{\partial \Phi \downarrow} SE_p SE_{\Phi \downarrow} r(p, \Phi \downarrow) \\
& + \frac{\partial T}{\partial p} \frac{\partial T}{\partial S} SE_p SE_S r(p, S) + \frac{\partial T}{\partial p} \frac{\partial T}{\partial e_0} SE_p SE_{e_0} r(p, e_0) \\
& + \frac{\partial T}{\partial p} \frac{\partial T}{\partial U} SE_p SE_U r(p, U) + \frac{\partial T}{\partial \Phi \downarrow} \frac{\partial T}{\partial S} SE_{\Phi \downarrow} SE_S r(\Phi \downarrow, S) \\
& + \frac{\partial T}{\partial \Phi \downarrow} \frac{\partial T}{\partial e_0} SE_{\Phi \downarrow} SE_{e_0} r(\Phi \downarrow, e_0) \\
& + \frac{\partial T}{\partial \Phi \downarrow} \frac{\partial T}{\partial U} SE_{\Phi \downarrow} SE_U r(\Phi \downarrow, U) + \frac{\partial T}{\partial S} \frac{\partial T}{\partial e_0} SE_S SE_{e_0} r(S, e_0) \\
& \left. + \frac{\partial T}{\partial S} \frac{\partial T}{\partial U} SE_S SE_U r(S, U) + \frac{\partial T}{\partial e_0} \frac{\partial T}{\partial U} SE_{e_0} SE_U r(e_0, U) \right] \tag{27}
\end{aligned}$$

Finally, we rewrite the normal standard error equation  $SE = \frac{\sigma}{\sqrt{n}}$  in terms of the variance of predicted river temperature (Equation 22) using the identity  $Var(T) = \sigma^2$ ,

$$SE_T = \sqrt{\frac{Var(T)}{N}}. \tag{28}$$

The methodology described here yields an autocorrelated variance-based decomposition of the standard error equation that approximates the standard error of predicted river temperature as a function of the six atmospheric variables upon which we focus in this study. These terms can be assessed separately by observing correlated and uncorrelated relationships, although we only focus on analyzing the total standard error across each season and along each distance of the river.

### ***Components of the standard error equation***

Equation 28, presented above, is an autocorrelated variance-based decomposition of the standard error equation that approximates the standard error of predicted river temperature as a function of the six atmospheric variables used in this study. These terms can be assessed separately, although we focus on analyzing the total standard error, which is a rewritten composition of both correlated (variance) and uncorrelated (covariance) terms. The total standard error equation is made up of these three terms:

- 1) Partial derivatives: Partial terms are weighting constants that measure the sensitivity of predicted river temperature to the atmosphere. For example, in Chapter 1, shortwave radiation influences predicted river temperature most significantly compared to all other weather variables. Therefore, the partial derivative for predicted river temperature with respect to a small positive perturbation to shortwave radiation will influence the standard error of river temperature in the positive direction more than any other partial derivative value across all seasons and along the distance of the river.
- 2) The standard error of each atmospheric variable might arise due to geographic misrepresentation of the weather over the channel. This term is the standard error due to

the geographic proximity between a meteorology station and the river channel. We develop this term uniquely, which will be discussed in the subsequent subsection.

- 3) Pearson's correlation coefficient ( $r$ ): Pearson's  $r$  measures the direction and magnitude of the correlation between two atmospheric variables. The values of Pearson's  $r$  are always between -1 and 1. At -1 and 1, the relationship is maximized, while 0 indicates no relationship between each variable.

***Error due to geographic proximity – a possible source of error in FLUVIAL-EB model predictions due to misrepresentation of the atmosphere directly over the river channel***

One of the main proposed challenges affecting FLUVIAL-EB model results is the quality of the atmospheric data used to predict energy balance and river temperature. Ideally, we would sample the atmosphere directly over the river channel as these values would better represent the governing weather variables that control the energy balance of the water column. We are, however, limited in the spatial coverage and representativeness of the weather directly over the channel and suggest that the data gathered from the CIMIS stations are not representative of the atmosphere directly over the river channel and therefore present a source of error in predicted river temperature. The data resolution limits the effectiveness of the *griddedInterpolant* MATLAB function in calculating weather values at discrete times and distances along the river. To account for this source of error, we developed a method that accounts for errors from the observed weather data.

We assert that weather data from the Merced CIMIS station introduces the most error in predicted river temperature since it is the farthest station from the river channel. We measure all distances recorded in Table 2 and Figure 15 using the ArcGIS Pro tool, *Generate Near Table*

(*Analysis*), which calculates distances between point (weather stations) and line (river channel) data classes. The Merced weather station is 28.9 km from the channel (Station: Merced, Table 2, Figure 15). Next, we find two weather stations with an equal or similar distance between each other than the distance between Merced station and the channel. We find that a distance of 30.5 km separates Firebaugh and Westlands CIMIS stations (Station: Firebaugh and Westlands, Table 2, Figure 15). The distance separating Firebaugh and Westlands stations characterizes the misrepresentation of the atmosphere due to the geographic proximity between the furthest weather station (Merced) and the channel. Finally, we gather time series data for each season at both stations (Firebaugh and Westlands) for each variable and calculate the standard error values of each weather variable between the two stations.

The standard error value described above represents a combined error value from the difference in weather values between the two stations. Statistically, the values calculated here are the standard error of the difference between the means. The standard error of the difference between the means is a measure of the precision with which the difference between two sample means estimates the difference between two population means. In our case, the sample mean represents weather data gathered from Firebaugh and Westlands, which estimates the population means for all weather data gathered from the CIMIS network. Conveniently, the distance between the two stations (Firebaugh and Westlands, 30.5 km) chosen to represent the sample population is approximately equal to the distance of the furthest weather station from the channel (Merced, 28.5 km). Recall that this distance and the weather values recorded at any of the stations within the CIMIS network represent a possible source of error because data is not representative of the atmosphere directly over the river channel. Therefore, the standard error

calculated for the sample population signifies the maximum possible error introduced from the weather data in energy balance and river temperature predictions. To summarize, the standard error of the difference between the means is a measure of the standard deviation of the sampling distribution of the difference between the two sample means. It reflects how much variability we expect to see in the difference between the means across samples which we then include into the total standard error equation to represent error due to geographic proximity between weather stations and the channel.

Mathematically, the standard error of the difference between weather values gathered from Firebaugh and Westlands stations, which we write in terms of standard deviation, is described as:

$$SE_w = \sqrt{\frac{\sigma_{w,Firebaugh}^2 + \sigma_{w,Westlands}^2}{n}} \quad (29)$$

$\sigma_{w,weather\ station}$  is the standard deviation of a weather variable time-series recorded at either Firebaugh or Westlands,  $n$  is the sample size of the weather variable time-series (in this case, the sample size is the same for all variables), and  $SE_w$  is the standard error of the difference between each weather variable, which we described as the error due to geographic proximity between the weather station and channel.

### **Limitations**

There are a few limitations present in Chapter 2. First, we do not account for error due to elevation differences between the atmosphere over the river channel and the atmosphere recorded at Firebaugh and Westlands meteorological stations. Both stations are ~57 m (averaged elevation of the two stations above channel elevation) above the river channel. The derivation of

the total standard error equation does not include a term for error due to elevation difference and thus our standard error due to the meteorological data is limited. Second, the standard error equation presented in Chapter 2 does not include instrument error. Instrument errors for CIMIS weather stations are provided by CIMIS and can be included into the standard error equation in an additive manner. Future work should consider adding this error to the total standard error values. Third, the error values presented in Chapter 2 are small, which causes questions regarding other possible sources of error. These sources of error might include a misrepresentation of river channel physical features, fluvial dynamics, the weather interpolation scheme, etc. Future error development for this model should consider other sources of error and incorporate them to the current error values presented in this work.

## **Results**

We evaluate the standard error of FLUVIAL-EB predicted river temperature for all seasons and along all river distances. The standard error presented here only represents uncertainties due to the meteorological dataset provided by the CIMIS network. Specifically, we hypothesize that one source of uncertainty in FLUVIAL-EB model results stems from the fact that the weather stations are separated from the main channel (the maximum distance from station to channel is 28.5 km). Therefore, weather data is unrepresentative of the atmosphere directly over the river. To quantify model uncertainty attributed to the meteorological dataset, we present a Gaussian variance-based, multi-variable error expansion of the basic standard error equation that represents the error in predicted river temperature due to the geographic separation between the river channel and weather stations.

FLUVIAL-EB model predictions contain more uncertainty than what we account for in Chapter 2. For example, predicted river temperature error could be due to misrepresenting river channel physical features, fluvial dynamics, weather interpolation, and much more. However, the primary purpose of this paper is to observe the sensitivity of predicted river temperature to each atmospheric variable, so we only focus on presenting errors inherent to the atmospheric dataset in Chapter 2. We consider this work a first step in quantifying error values associated with model predictions, where we assume that predicted river temperature error is only a function of the six atmospheric variables used in this study.

The standard error of the 7-day mean simulation period for the four seasons and along all river distances is plotted in Figure 16 and quantified in Table 10. Table 10 is color-coded to observe the distance-wise trends in standard error values. Green represents a small error value, while red represents a high error value.

At the 150 km river distance, the winter season (DJF) shows the most significant error associated with predicted river temperature at ( $\pm 0.12^{\circ}\text{C}$ ) followed by MAM ( $\pm 0.083^{\circ}\text{C}$ ), SON ( $\pm 0.052^{\circ}\text{C}$ ), and JJA ( $\pm 0.029^{\circ}\text{C}$ ). These results demonstrate that the standard error is highest during the coldest seasonal weather patterns and lowest during the warmest ones. Specifically, the standard error is maximized during the DJF winter season and minimized during the JJA summer season. During the transitional seasons of spring and fall, where climatic maximums/minimums are transitioning, we observe standard error values that fall within the range of those observed during the winter and summer months.

Not surprisingly, error values are small at distance = 0km. The partial derivatives are also trivially small at a distance = 0km because there is very little difference between the perturbed

predicted river temperature experiments and baseline predicted river temperature experiments near the dam. Partial derivative terms utilized as weighting constants are multiplied through the standard error equation, which means that when the partial derivatives are small, so is the error. That is why we observe trivially small error values at river distance = 0km. Standard error values follow the same distance-wise pattern as the partial derivatives along all river distances, where error increases with distance from the dam across all seasons.

Interestingly, the error in predicted river temperature that result from geographic proximity between a weather station and the nearest section of the river is much smaller in magnitude than the changes to predicted river temperature that result from small positive perturbations made to each of the six atmospheric variables used in this study. These variables are shown in Figures 6 through 13 and Tables 7 and 8. The only exception is air pressure, as perturbations made to this variable had a negligible impact on river temperature, with changes ranging from 10.4 to 10.3 °C.

The main takeaway from the results presented in Figure 16 and Table 10 is that standard error values are small across all seasons and distances along the river. We can claim that the total error in predicted river temperature is small and that the FLUVIAL-EB model is accurate if we consider the spatial network of the weather stations used in this work to be the only possible source of uncertainty within model predictions.

## **Discussion**

If seasonal signatures within the observed meteorology data, directly and indirectly, influence the standard error values developed in Chapter 2, can we comment on the role of the background climatology of the San Joaquin region discussed in Chapter 1? The results presented

in Figure 16 shows that standard error values for simulated river temperatures vary with season. Notably, the transitional seasons of MAM and SON, which mark the transition from winter to summer and vice versa, have error values that fall within the range of those observed during the winter and summer months. This suggests that periods of high climatic variability introduce more error into model predictions, and periods of low climatic variability introduce less. Notably, during the DJF, when weather is more variable, the error in predicted river temperature is higher. Conversely, the most minor error in predicted river temperature values is seen during the JJA season when the weather is less variable than other seasons.

Our findings indicate that the DJF winter season has the highest standard error values compared to the other seasons, which could be attributed to the increased variability in climatic conditions during this season. California experiences most of its inclement weather during the winter months due to the shift of the high-pressure ridge towards the Pacific Ocean, allowing low-pressure systems to travel through the state from north to south/southeast. This winter climatology leads to more variability in observed weather conditions in the study area, which could explain why we observe larger error values in DJF.

## **Chapter 3 – Applying Gridded Climate Data to a Physically-based Numerical Energy Balance Model (FLUVIAL-EB)**

The goal of Chapter 3 is to apply gridded climate data to the FLUVIAL-EB model. Applying a gridded climate dataset will allow us to observe how a new atmospheric data set governs energy balance and river temperature results. Additionally, by applying gridded climate data that incorporates climate change predictions to the physical processes that make up the structure of the FLUVIAL-EB model to predict river temperature, we can observe how predicted river temperature will change in altered climate scenarios. Results presented in Chapter 3 show the FLUVIAL-EB model's efficacy in incorporating gridded climate data for river temperature predictions for all four seasons in 2010 which motivates future work to explore how river temperature might change under climate change atmospheric conditions.

### **Introduction**

Water temperature fluctuation in large lowland rivers is partially controlled by atmospheric conditions such as shortwave radiation, longwave radiation, air temperature, wind speed, vapor pressure, and air pressure. The relationship between these six atmospheric variables and predicted river temperature is highlighted in Chapters 1 and 2, but how will climate change affect the absorptive and evaporative characteristics of the water column? To answer this question, we explore the FLUVIAL-EB model's efficacy in predicting river temperature using projected climate change gridded datasets as its atmospheric input rather than the observed weather station CIMIS network.

Gridded climate datasets have become valuable for model applications in regions where station data coverage lacks temporal and spatial consistency. Gridded climate datasets refer to data interpolated into a standardized gridded pattern, typically with a spatial resolution of a few kilometers to tens of kilometers (Daly, 2006). Gridded data can assist in modeling applications that rely on robust data sets to calculate results, such as energy balance terms and river temperature, because they provide a smooth, continuous data set over the entire region in both time and space (Eum, Dibike, Prowse, & Bonsal, 2014). Additionally, gridded climate data may represent an extensive range of atmospheric variables and are often available from historical to future projected periods (Choi, Moore, & Rasmussen, 2007). We incorporate gridded data for FLUVIAL-EB model calculations because they offer high-resolution coverage of the study area in time and space and represent the six atmospheric variables used in this study calculated under projected future climate change scenarios.

We utilized gridded climate data from a regional climate model (RCM). Regional climate models (RCMs) provide gridded climate datasets on smooth temporal and spatial scales by incorporating data from various sources, including weather stations, satellite observations, and other climate models. RCM models use sophisticated mathematical algorithms and physics-based equations to simulate the interactions between earth system processes and predict how they will change over time (Rummukainen, 2010). We are specifically interested in incorporating RCM data, including future climate change projections, into the FLUVIAL-EB model to observe changes to the energy balance along river distances in altered climatic states.

Future climate change projections often include what is known as a Representative Concentration Pathway (RCP). An RCP is a set of scenarios used in climate modeling to project

future greenhouse gas concentrations and associated radiation forcing. There are four scenarios in total. We download the "high emissions" scenario (RCP 8.5), which assumes that greenhouse gas emissions will continue to increase throughout the 21<sup>st</sup> century, leading to a radiation-forcing level of  $8.5 \text{ Wm}^{-2}$  by 2100 (Riahi et al., 2011). Due to time constraints, atmospheric data calculated under RCP8.5 conditions was not incorporated into the FLUVIAL-EB model. However, upcoming work will include future climatic predictions to observe how the radiative structure of the river changes across seasons and along river distance under altered climate conditions.

### ***Climate change and FLUVIAL-EB model predictions***

The San Joaquin River is a central feature of California's hydrologic system. Once a robust wetland environment with many ephemeral rivers and lakes, the San Joaquin Valley has lost 95% of its original wetland environment (Ortiz-Partida et al., 2022). Environmental hardship can be attributed to poor management of water and land use, although climate change is also an increasing concern within the region. According to California's Fourth Climate Change Assessment (Ortiz-Partida et al., 2022), climate change negatively impacts the hydrological regime of the San Joaquin River region. Namely,

1. Deterioration of the Sierra Nevada snowpack due to warmer temperatures and inconsistent snow seasons will change flow dynamics and water temperatures.
2. Moreover, wetlands may experience increased water temperatures and evaporation rates under climate change.

The outcomes documented in the San Joaquin Valley Region Report motivate the need to comprehend the region's fluvial dynamics. The goal of Chapter 3 is broadly aimed at enhancing

our scientific knowledge of how the San Joaquin River's spectral energy balance and river temperature profile might operate under high greenhouse gas emission scenarios, using predictions generated by the FLUVIAL-EB model to assist in the development of targeted restoration of the San Joaquin River.

## **Methods**

Methods for this work largely follow previous methodologies, although we are only concerned with incorporating gridded climate data into the FLUVIAL-EB model, and therefore it is not necessary to conduct the SA presented in Chapter 1. Here, we gather the six key atmospheric variables presented throughout this paper from a particular RCM. We modified the FLUVIAL-EB model with unique functions that allow the model to interpolate the six atmospheric variables from an RCM across the study area, which replaces the need for the CIMIS meteorological network. Finally, the model was executed using 2010 RCM data to prove its efficacy in applying gridded climate data to the energy balance equations to predict radiative fluxes and river temperature.

The most crucial step is that the FLUVIAL-EB model can now interpret gridded climate data. Before, the model utilized the network of weather stations near the river reach. Previously, the model synthesized weather observations through a gridded interpolation scheme. The gridded interpolation scheme incorporated atmospheric values into the physically-based numerical structure of the FLVUAL-EB model based on station proximity to the river's main stem. Now, the model can format and interpolate gridded climate data (NetCDF data formats). NetCDF (Network Common Data From) is a file format commonly used to store climate model output because it can handle large, multidimensional datasets such as the RCM output used in this work.

The updates here allow the FLUVIAL-EB model to accept raw NetCDF data, build an interpolation scheme within a bounding box specific to the region, and execute the main physical and radiative processes based on climate model prediction of the six atmospheric variables used in this study.

## **Data**

We collected gridded climate data to replace the CIMIS meteorological station network and prove the FLUVIAL-EB model's ability to predict radiative fluxes and observe changes in radiative fluxes using gridded climate data.

### ***Canadian Regional Climate Model version 5 (CRCM5)***

Future projected climate change data is collected from the CRCM5 (Canadian Regional Climate Model version 5) regional climate model that simulates the Earth's climate system over the Northern Hemisphere. CRCM5 can simulate a range of climate variables, including the critical atmospheric variable used in this study, in historical and future periods. Its high spatial resolution and ability to simulate local climate processes make it a valuable tool for climate change research and decision-making (Bukovsky & Mearns, 2020; Whan & Zwiers, 2014).

Before predicting river temperature using CRCM5 climate predictions, we want to see how FLUVIAL-EB model results compared when run under CIMIS data versus gridded climate data. The available CIMIS data included 2009, 2010, and 2011 coverage for the six atmospheric variables. Unfortunately, CRCM5's historical output does not include these years, making comparing predicted river temperatures under each dataset challenging. Therefore, we utilize another gridded climate data set to prove the model's ability to incorporate gridded climate data

and to compare predicted river temperatures run under gridded climate data to results calculated under CIMIS observations.

### ***ERA-Interim reanalysis-driven data***

CRCM5 climate model output also includes predictions output driven by ERA-Interim reanalysis data. We used this data set and not the CRCM5 RCP8.5 data set because we needed to compare the predicted river temperature run under the available CIMIS data with the predicted river temperature run under gridded climate data. We could not do so with the CRCM RCP8.5 simulations because the periods between the future climate projection dataset and CIMIS data did not align. ERA-Interim is a global atmospheric reanalysis dataset produced by the European Centre for Medium-Range Weather Forecasts (ECMWF). It provides a comprehensive record of the Earth's atmosphere over 36 years, from 1979 to 2014, and is widely used in climate research (Dee et al., 2011). The Era-Interim reanalysis data set is used to drive CRCM5 model simulations at lower lateral boundaries and includes a proven compilation of reanalysis data that matches the observed record for the suite of climate variables calculated within the CRCM5 model (Martynov et al., 2013).

Table 11 presents all gridded climate model data utilized for the scope of this chapter. The results presented in this chapter compare predicted river temperature calculated using 3-hourly CRCM5 ERA-interim driven climate output calculated at 0.11-degree spatial resolution for the year 2010.

### **Limitations**

The main limitation in Chapter 3 is computational expense. First, one benefit of using gridded climate data is that it provides a complete temporal record of past, present, and future,

atmospheric data. Due to the computational expense of running the FLUVIAL-EB model and the data storage requirements of the model output, we are limited in utilizing the full functionality of the long-term data record provided by gridded climate data. Ideally, we would be able to conduct a full seasonal analysis with gridded climate data in past, present, and future climates to observe seasonal changes in predicted river temperatures. Currently, it is unfeasible to run the FLUVIAL-EB model for this amount of time. Future work might incorporate shorter simulation periods calculated under future gridded climate change data if model validation is conducted under present atmospheric data.

## **Results**

We conduct a model simulation using ERA-interim data to show the total scope of work done regarding adjustments made to allow the FLUVIAL-EB model to accept gridded climate data. This study compared river temperature simulations forced by observed weather data and regional climate model data. The results show that the two datasets produced different river temperature responses. The regional climate model data produces higher predicted temperatures. Specifically, the mean daily temperature forced by the regional climate model data was consistently higher than that forced by observed weather data. This difference was most pronounced in the winter months (DJF) when the mean difference between CRCM and CIMIS forced predicted river temperature values across all times, and river distance was 1.9 °C— followed by a 1.5 °C change in SON °C, a 1.3 change in JJA °C, and a 0.3 °C change in predicted river temperature. The regional climate model data also produced a wider temperature range, with higher maximum and lower minimum temperatures than observed weather data.

## Conclusion

The differences between the two datasets could be attributed to several factors, including spatial and temporal resolution differences and the physical representation of hydrologic processes. For example, the regional climate model may have more accurate representations of regional climate patterns and atmospheric circulation than observed weather data because our sample weather size is so small. Additionally, the regional climate model may better capture the feedback between land surface processes and atmospheric conditions, which can affect the energy balance and river temperature. The gridded climate data application is not necessarily key in this application, where our observed data set is relatively complete. Moving forward, our study aims to expand on this work by incorporating RCM data calculated under high-emission climate scenarios. This will enable us to obtain river temperature and energy flux values representing predicted atmospheric levels. By doing so, we can assess the potential impacts of climate change on river temperatures in the region and develop more informed water resource management strategies. This study serves as a critical first step towards a better understanding of the impacts of climate change on river temperatures in the region. It will be essential for informing future research on hydrological processes and ecosystem management in changing climate conditions.

In conclusion, this study successfully incorporated gridded climate data into the FLUVIAL-EB model to predict river temperatures in a specific region. Comparing predicted river temperatures using observed weather data and regional climate model data highlighted significant differences in predicted temperatures, with the regional climate model data producing consistently higher values. These differences could be attributed to various factors, including

spatial and temporal resolution and the physical representation of hydrologic processes.

Nevertheless, this study provides valuable insights into the potential impacts of climate change on river temperatures in the region, and the incorporation of future climate scenarios will enable us to develop more informed strategies for water resource management.

The successful incorporation of gridded climate data into the FLUVIAL-EB model illustrates the potential for regional climate models to enhance our understanding of hydrological processes and ecosystem management under changing climate conditions. This study is a critical first step toward developing more accurate and reliable models for predicting regional river temperatures. Future research should focus on further refining and expanding the model framework to incorporate additional climate variables and improve accuracy. Overall, the findings of this study have significant implications for the management of water resources and the conservation of ecosystems, emphasizing the need for continued research in this area to address the challenges posed by climate change.

**Figures**

Figure 1. Overview of the San Joaquin River (black) and major tributaries (blue). Also shown (orange lines) are the Friant-Kern Canal and the Madera Canal.

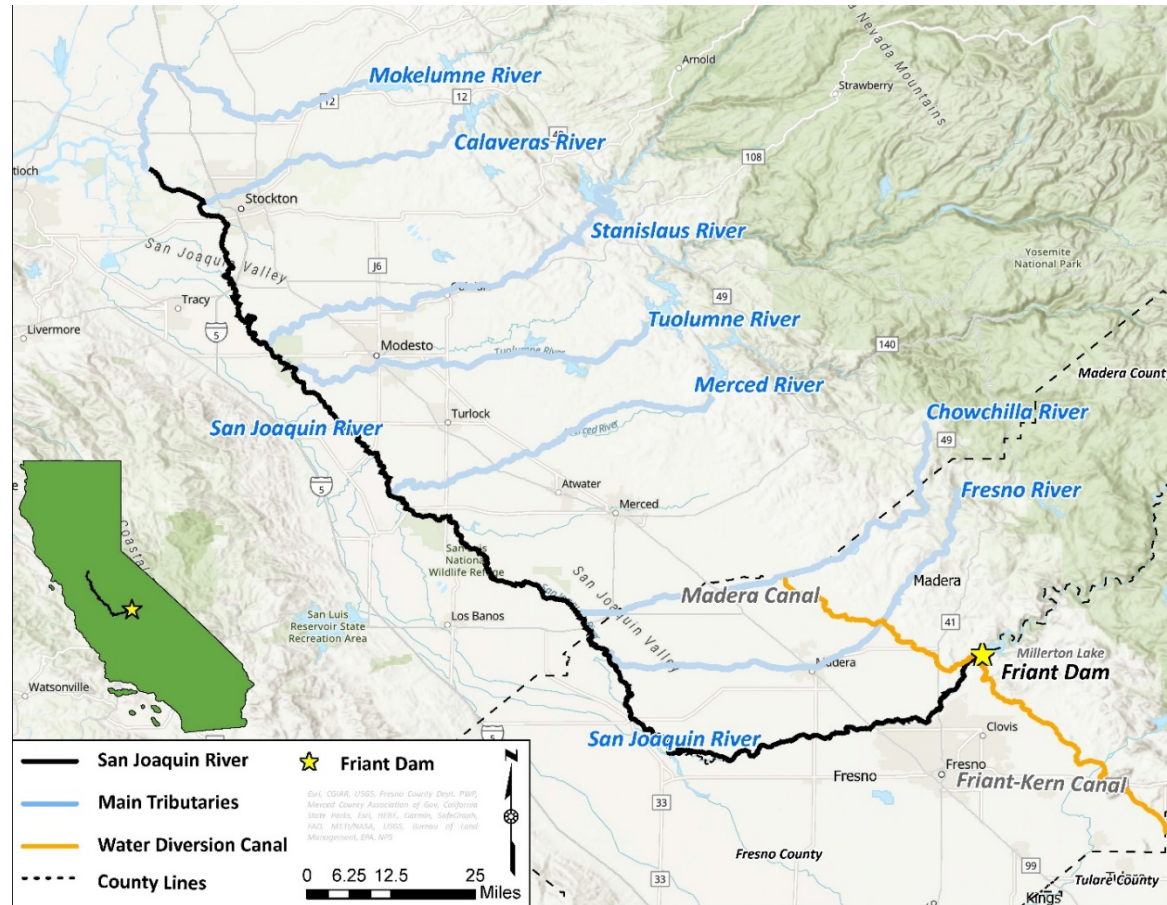
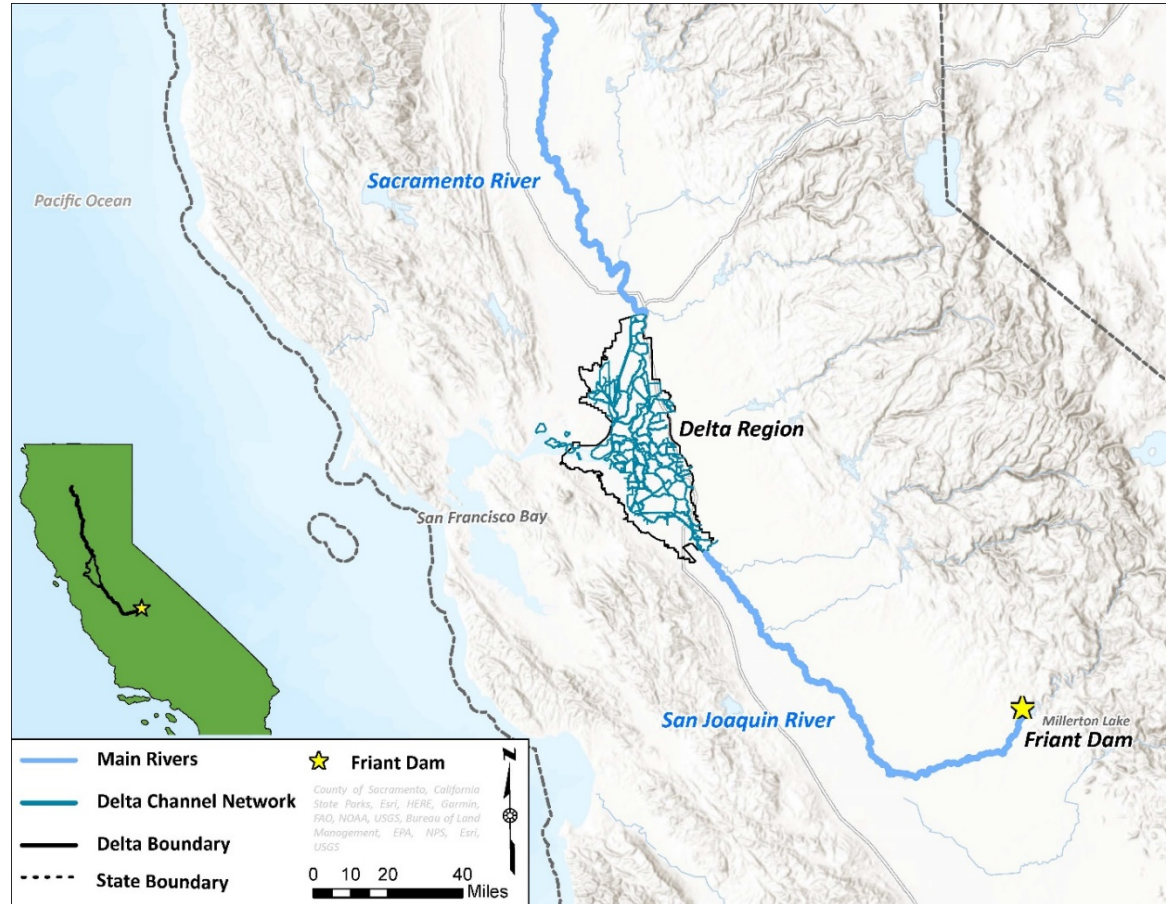
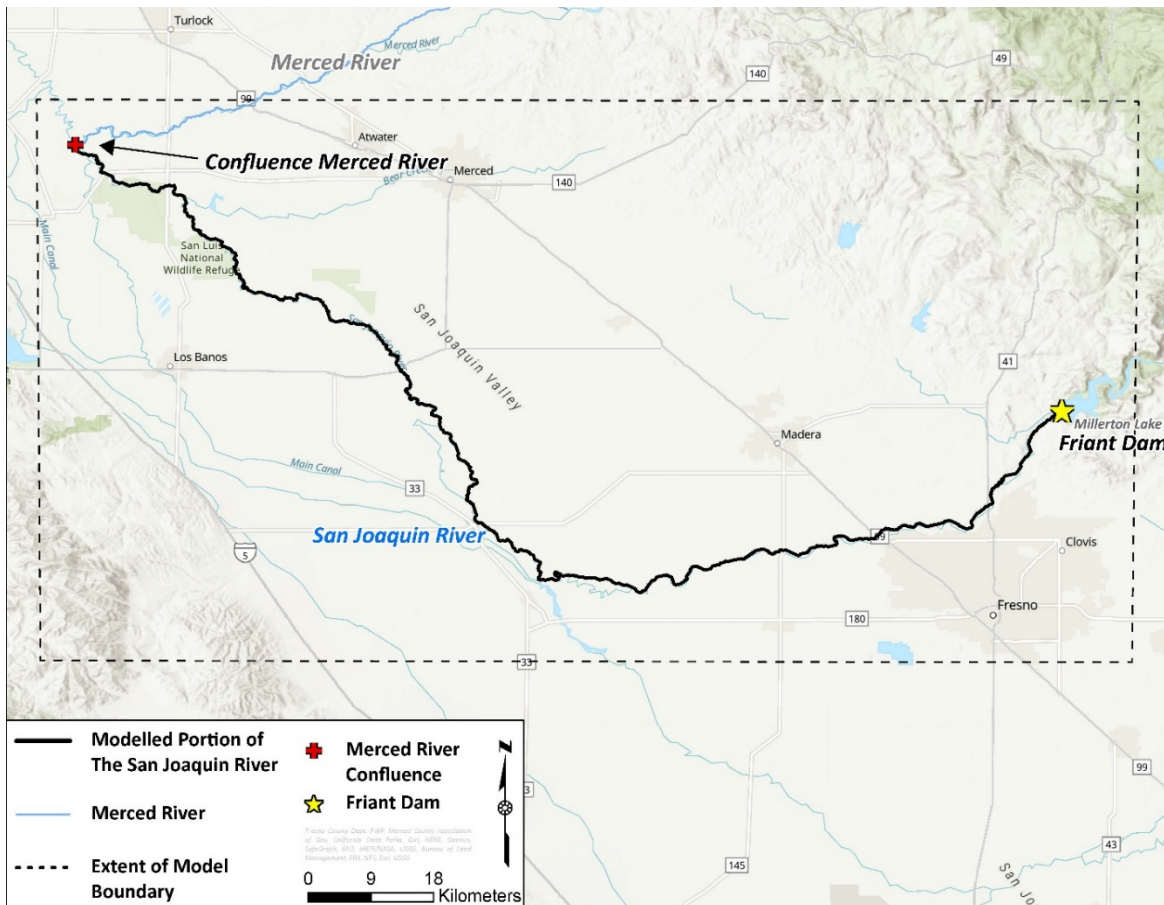


Figure 2. Overview of the Sacramento-San Joaquin River Delta system



**Figure 3. Overview of the model extent. The FLUVIAL-EB model predicts energy fluxes and river temperature from Friant Dam to the confluence of the Merced River**



**Figure 4. Site map of the study area, including the extent of modeled river channel (black line), weather stations (CIMIS, yellow diamonds), stream gauge sites (USGS, USBR, CADWR, CDFW, green triangles), and the location of Friant Dam (yellow star).**

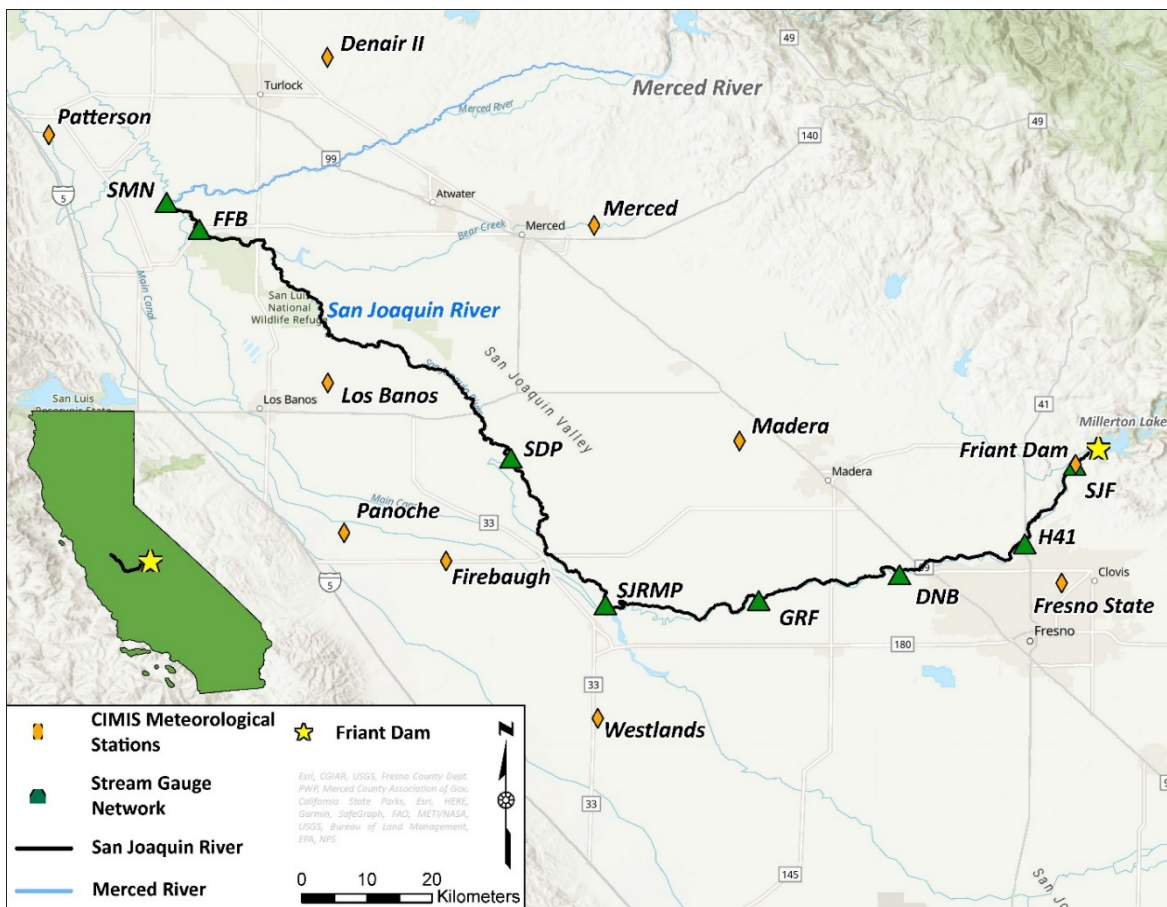


**Figure 5. Perturbation Theory. Perturbed predicted river temperature values are subtracted from baseline predicted river temperature values for each time and distance along the river. The difference is divided by the unique perturbation value. The result is a partial derivate value for each time and distance along the river, representing river temperature sensitivity to an atmospheric variable.**

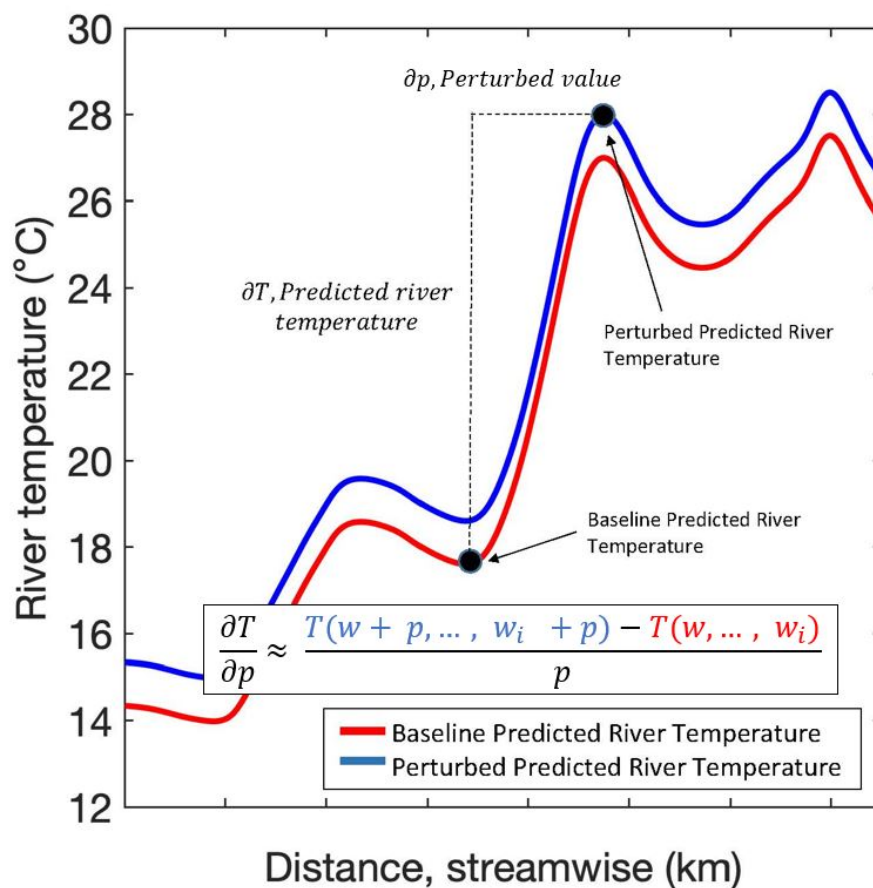


**Figure 6. Scaled partial derivatives representing predicted river temperature sensitivity along river distance for the 7-day DJF (Winter) model simulation period.**

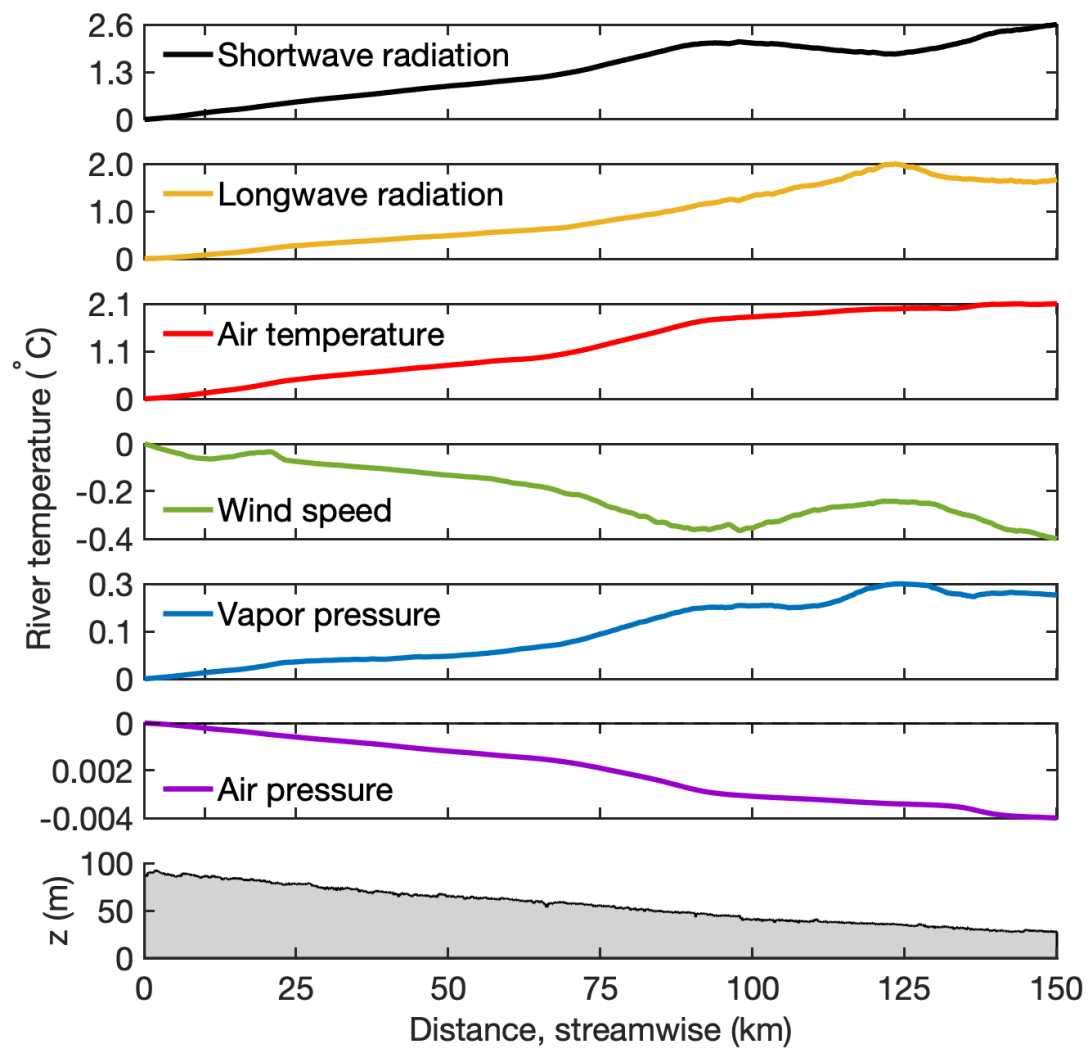
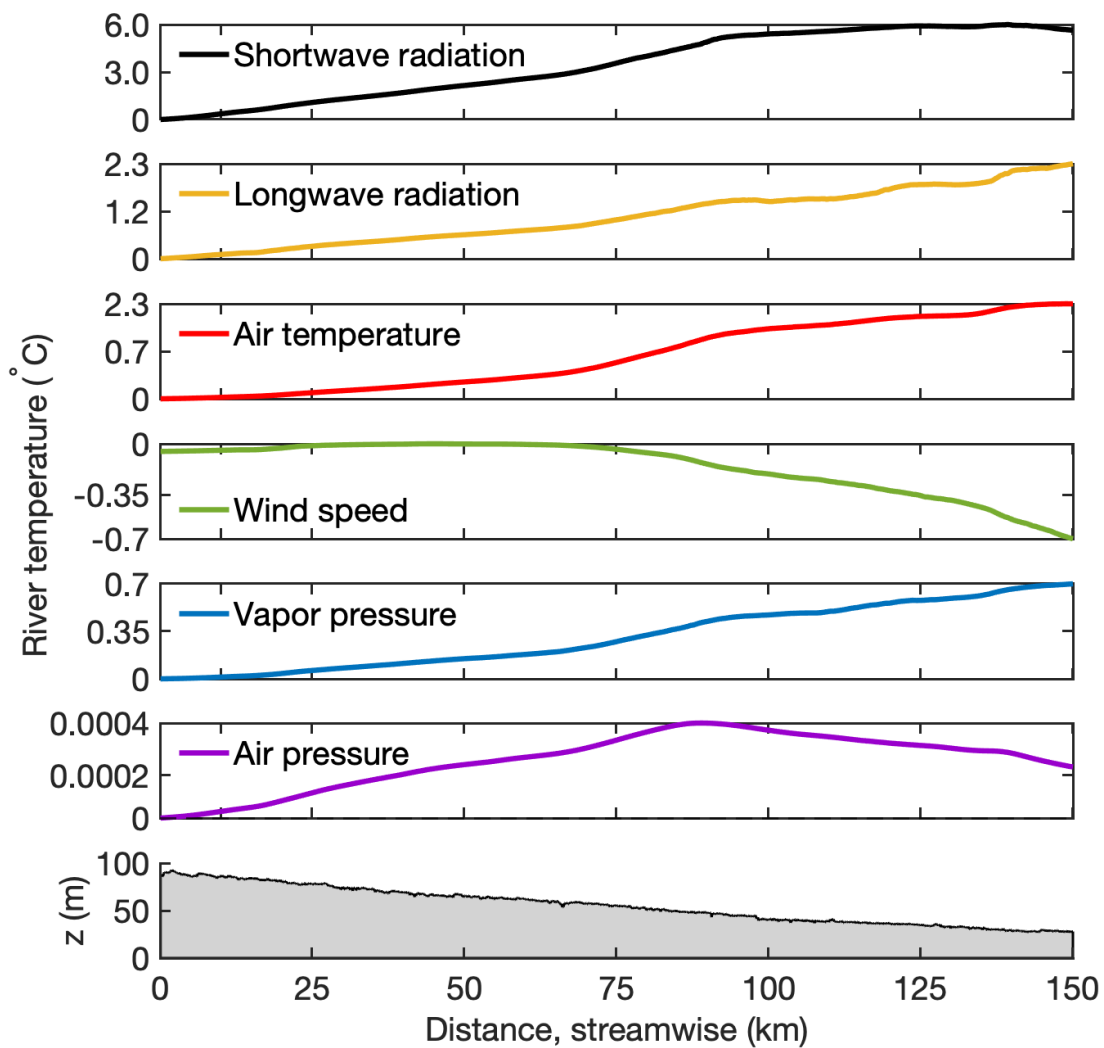
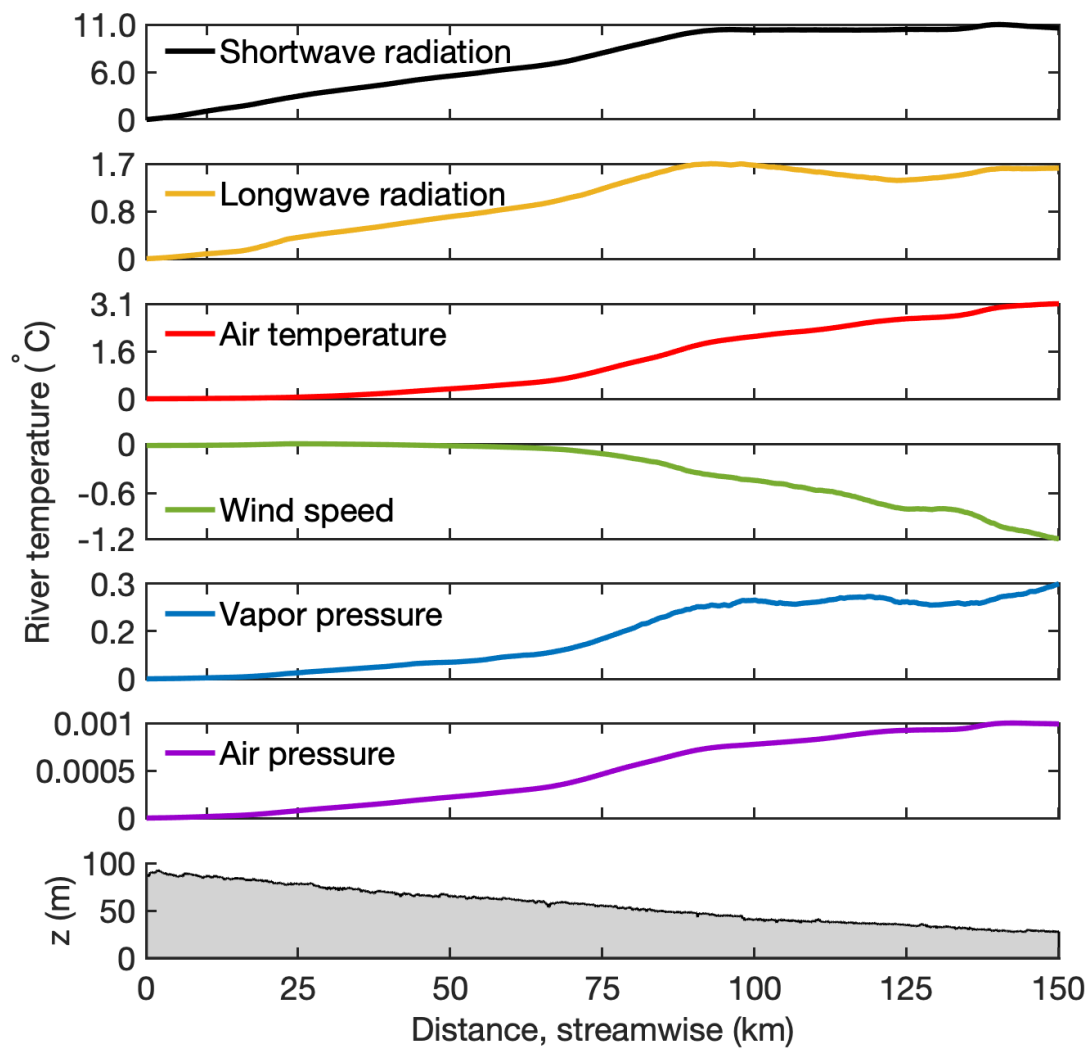


Figure 7. Scaled partial derivatives representing predicted river temperature sensitivity along river distance for the 7-day MAM (Spring) model simulation period.



**Figure 8. Scaled partial derivatives representing predicted river temperature sensitivity along river distance for the 7-day JJA (Summer) model simulation period.**



**Figure 9. Scaled partial derivatives representing predicted river temperature sensitivity along river distance for the 7-day SON (Fall) model simulation period.**

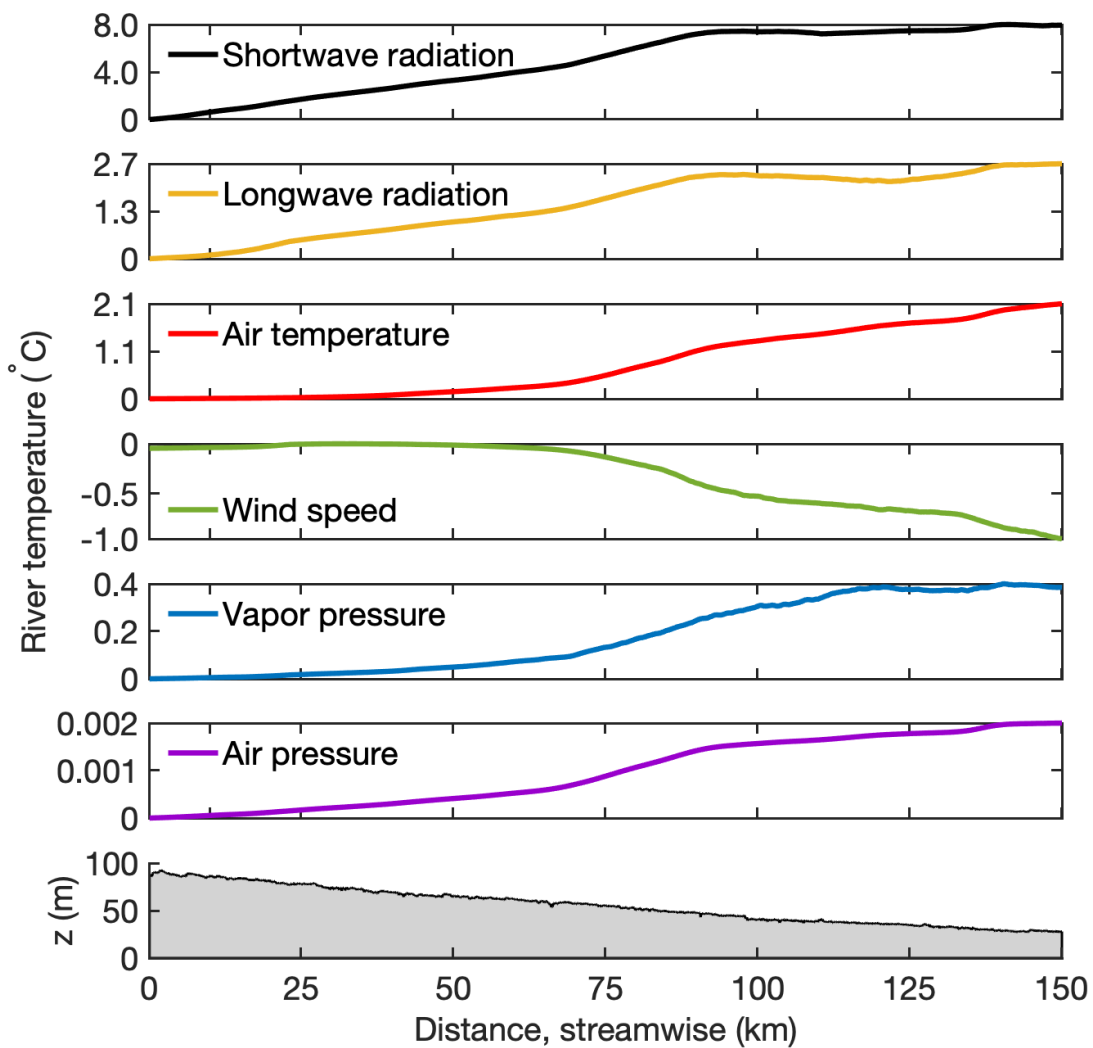


**Figure 10. Normalized partial derivatives representing predicted river temperature sensitivity along river distance for the 7-day DJF (Winter) model simulation period.**

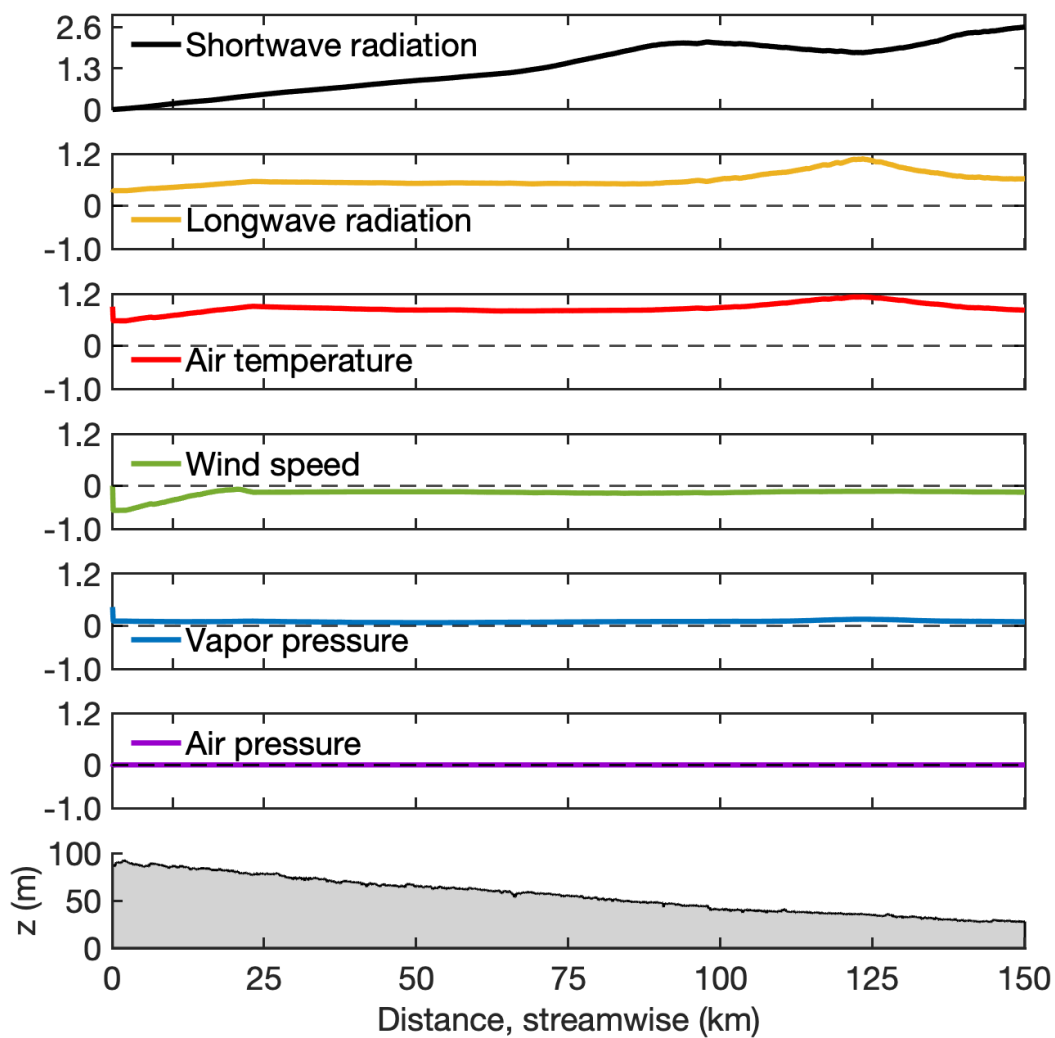


**Figure 11. Normalized partial derivatives representing predicted river temperature sensitivity along river distance for the 7-day MAM (Spring) model simulation period.**

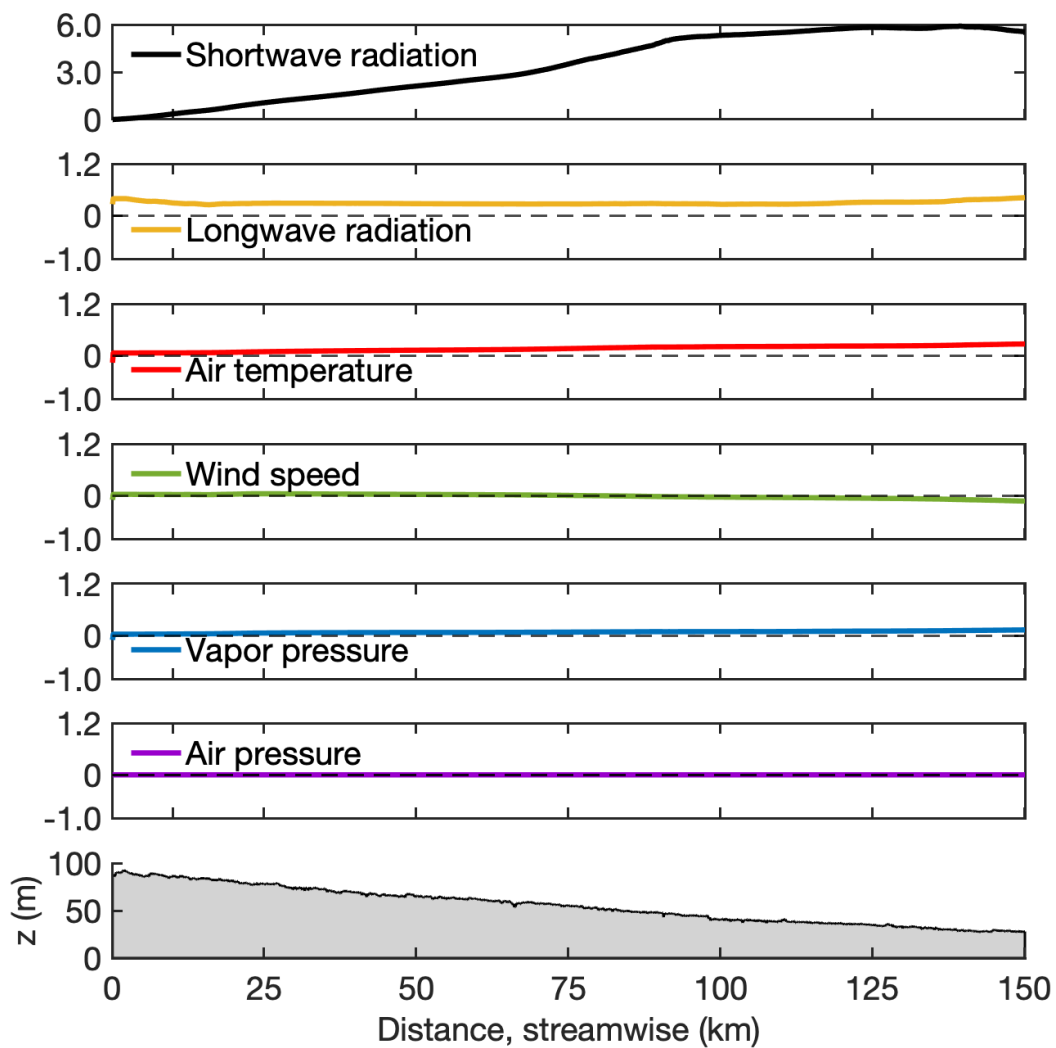


**Figure 12. Normalized partial derivatives representing predicted river temperature sensitivity along river distance for the 7-day JJA (Summer) model simulation period.**

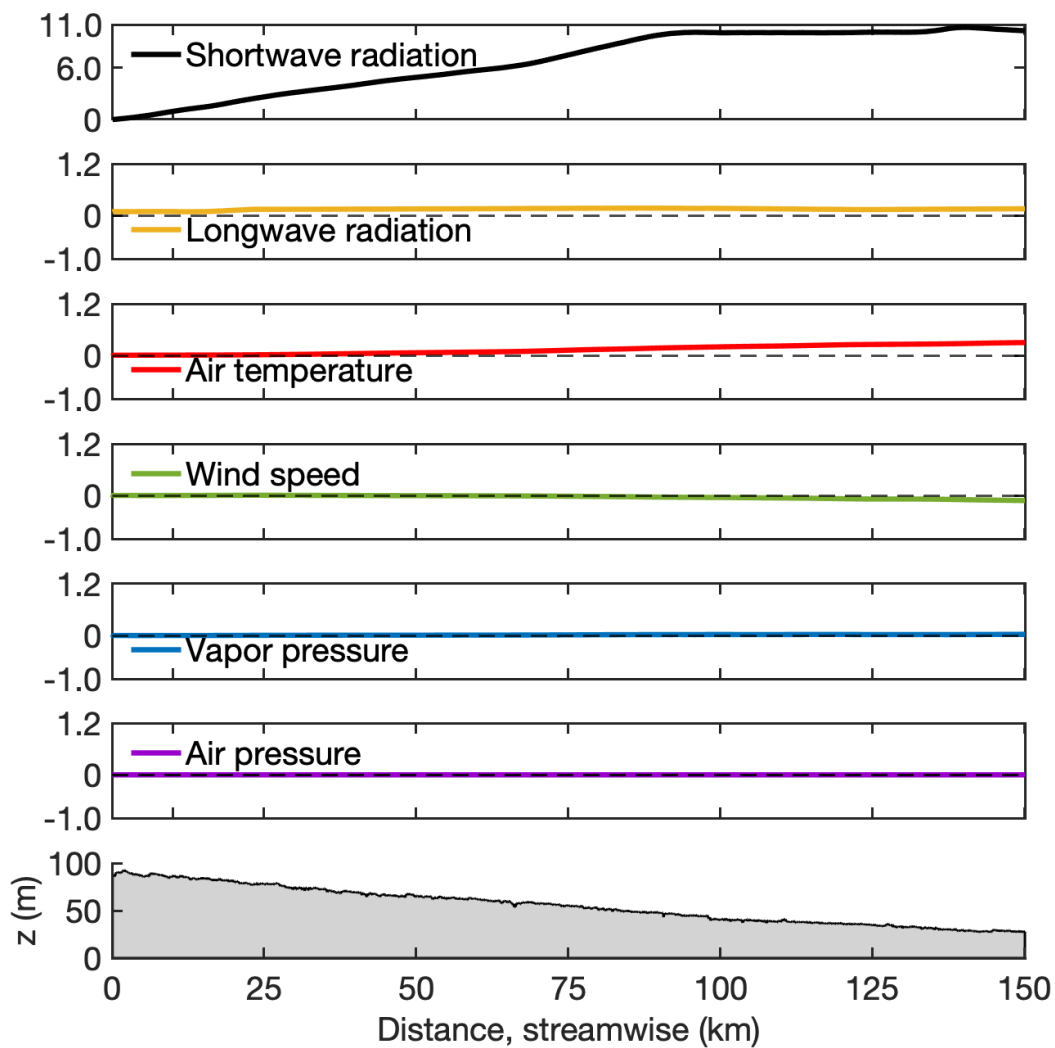


**Figure 13. Normalized partial derivatives representing predicted river temperature sensitivity along river distance for the 7-day SON (Fall) model simulation period.**

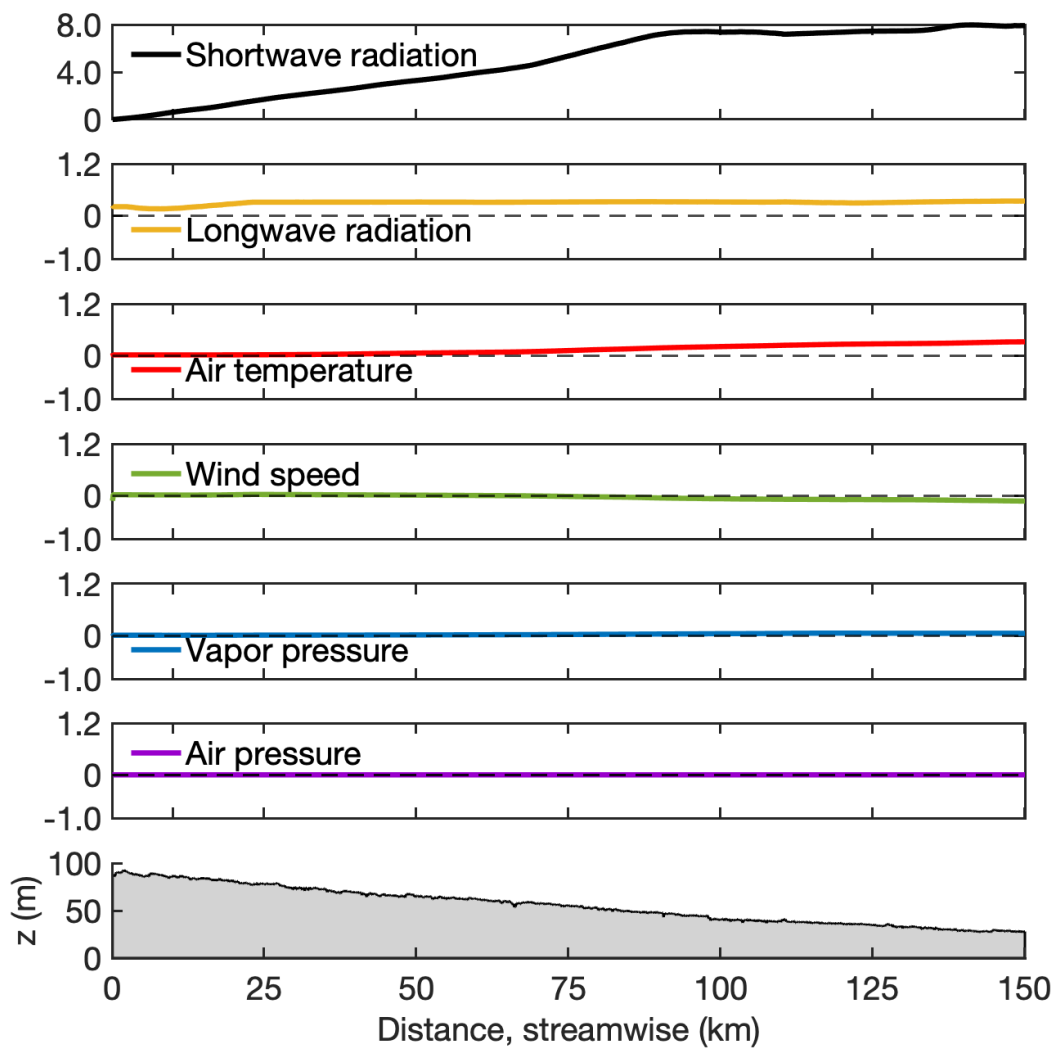
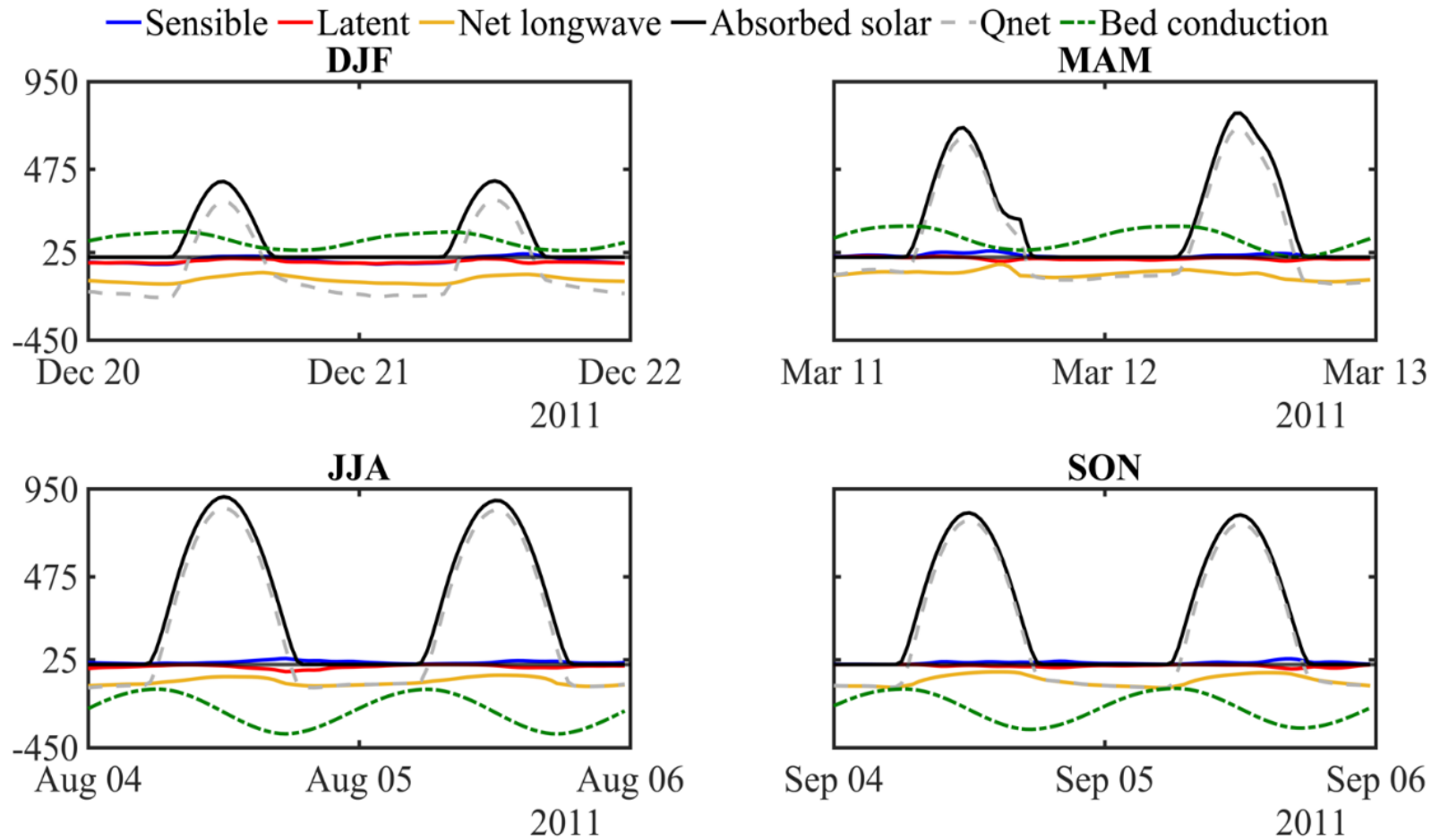
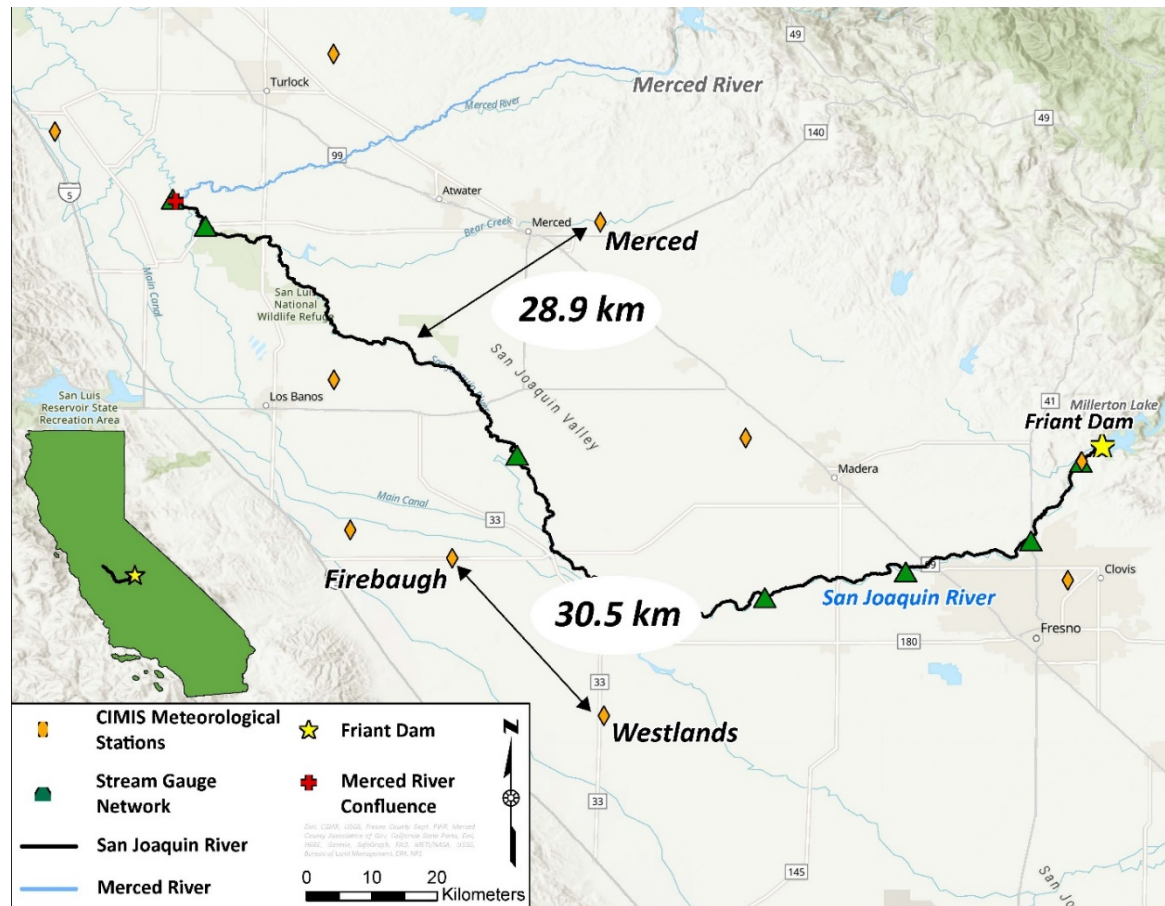


Figure 14. Baseline energy fluxes ( $Wm^{-2}$ ) for each of 4 seasonal simulation periods.



**Figure 15. Methodology map for error due to geographic proximity to the river channel. Weather values from Firebaugh and Westland CIMIS stations are used to calculate the standard error of each weather variable.**



**Figure16. Total standard error due to uncertainties in weather values collected from the CIMIS station network within the study area along river distance and across all seasons.**

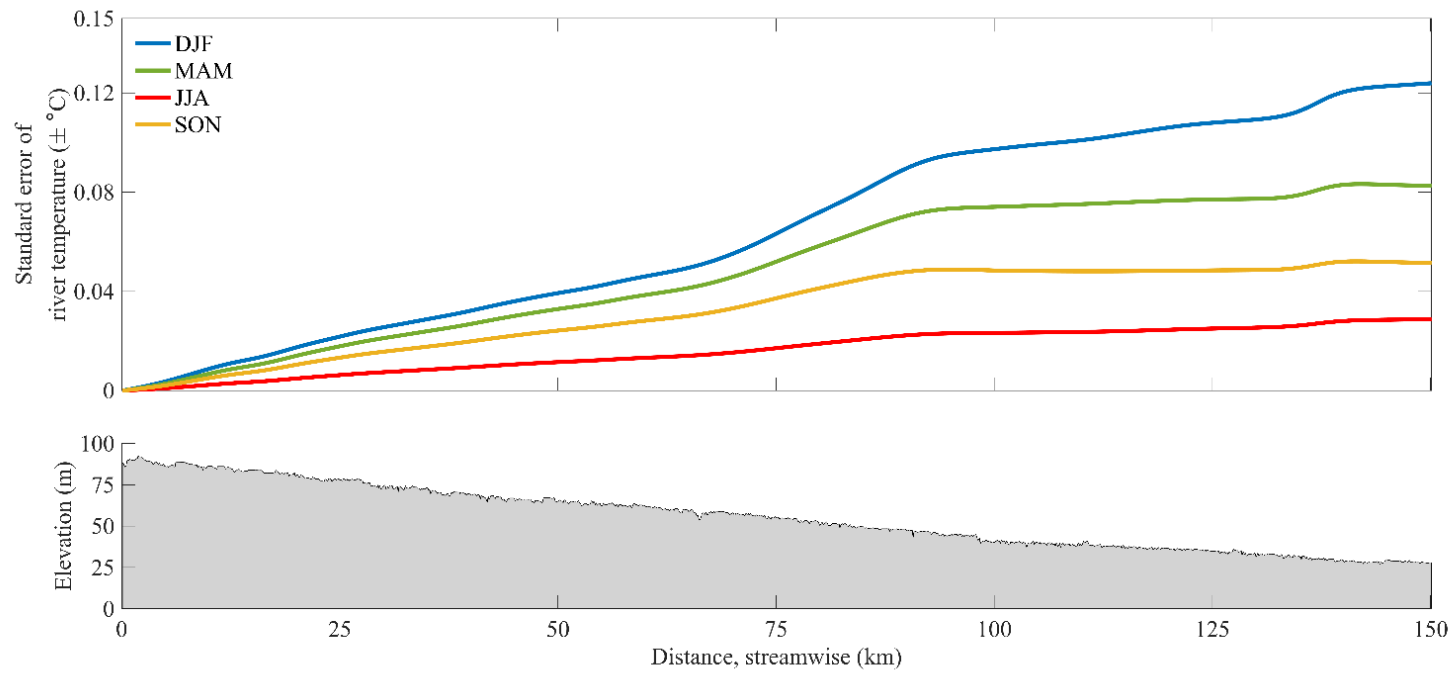
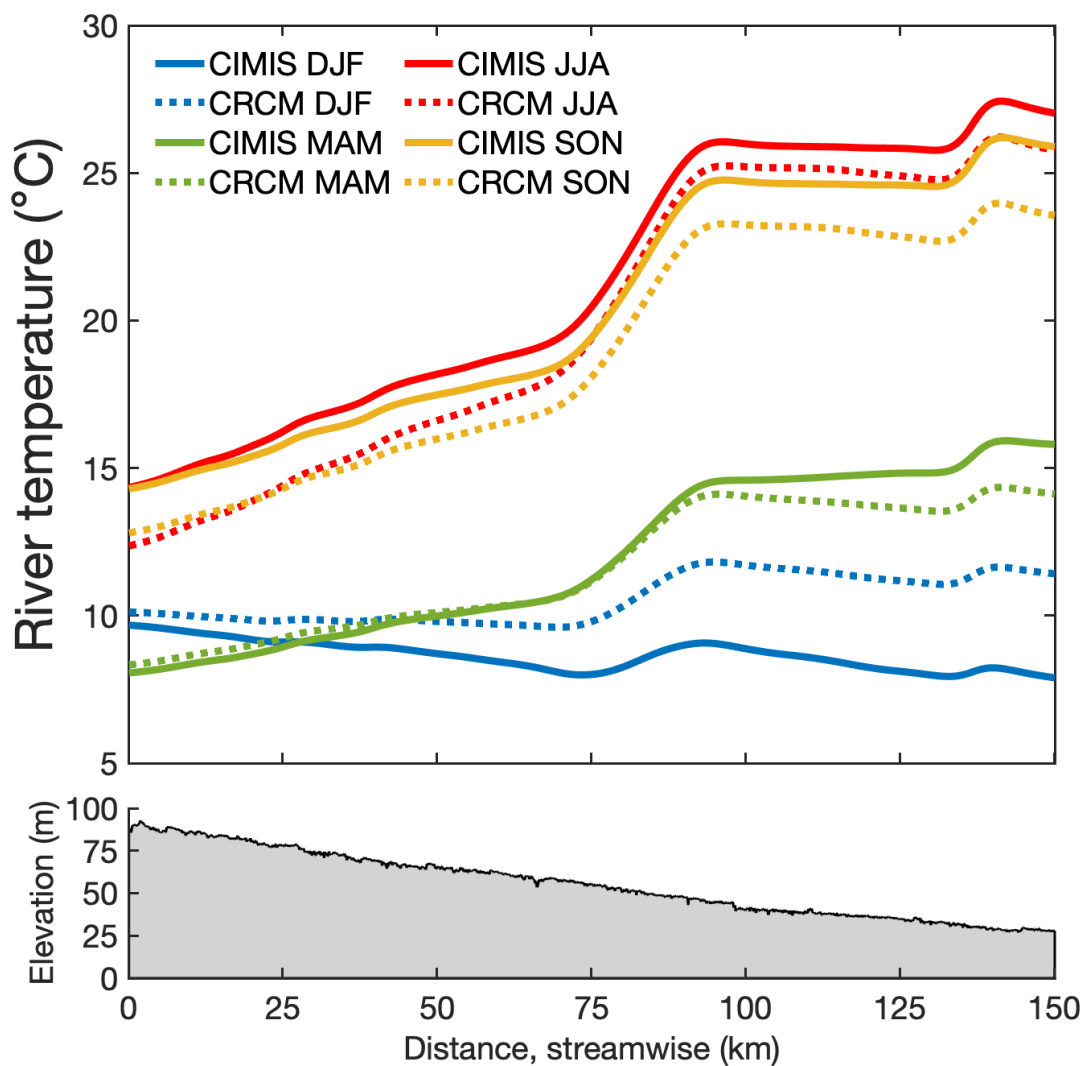


Figure 17. Predicted river temperature calculated using gridded climate data (dashed lines) and predicted river temperature calculated using weather time-series data from the CIMIS station network (solid line) are shown for each season and along river distance.



## Tables

Table 1. Notation Table

<b>Energy Balance</b>		
<b><i>Q</i></b>	<i>river discharge</i>	$m^3 s^{-1}$
<b><i>T</i></b>	<i>water temperature</i>	$^{\circ}K$ or $^{\circ}C$
<b><i>Q<sub>net</sub></i></b>	<i>net energy exchange between the atmosphere, the bed, and the water</i>	$W m^{-2}$
<b><i>F<sub>net</sub></i></b>	<i>net energy transferred into or out from a unit area of the river</i>	$W m^{-2}$
<b><i>S<sub>net</sub></i></b>	<i>net shortwave radiation</i>	$W m^{-2}$
<b><i>Φ<sub>net</sub></i></b>	<i>net longwave radiation</i>	$W m^{-2}$
<b><i>H</i></b>	<i>sensible heat exchange</i>	$W m^{-2}$
<b><i>L</i></b>	<i>latent heat exchange</i>	$W m^{-2}$
<b><i>G</i></b>	<i>heat exchange due to bed conduction</i>	$W m^{-2}$
<b><i>x</i></b>	<i>distance along the river</i>	$m$
<b><i>t</i></b>	<i>time</i>	$s$
<b><i>v</i></b>	<i>water velocity</i>	$m s^{-1}$
<b><i>D</i></b>	<i>physical depth of the water</i>	$m$
<b><i>D<sub>L</sub></i></b>	<i>longitudinal dispersion coefficient</i>	
<b><i>ρ</i></b>	<i>density of water</i>	$kg m^{-3}$
<b><i>c<sub>p</sub></i></b>	<i>specific heat of water</i>	$J kg^{-1} ^{\circ}K^{-1}$
<b>Atmospheric Variables</b>		
<b><i>T</i></b>	<i>water temperature</i>	$^{\circ}C$
<b><i>T<sub>a</sub></i></b>	<i>air temperature</i>	$^{\circ}K$
<b><i>P</i></b>	<i>air pressure</i>	$kPa$
<b><i>Φ<sub>↓</sub></i></b>	<i>net longwave radiation emitted by the atmosphere</i>	$W m^{-2}$
<b><i>S</i></b>	<i>shortwave radiation incident upon the water's surface</i>	$W m^{-2}$
<b><i>e<sub>0</sub></i></b>	<i>vapor pressure</i>	$kPa$
<b><i>U</i></b>	<i>windspeed</i>	$m s^{-1}$
<b>Sensitivity Analysis</b>		
<b><i>w</i></b>	<i>weather variable</i>	<i>unit of variable</i>
<b><i>CV</i></b>	<i>coefficient of variation</i>	<i>unit of variable</i>
<b><i>p</i></b>	<i>perturbation value</i>	<i>unit of variable</i>
<b><i>σ</i></b>	<i>standard deviation</i>	<i>unit of variable</i>
<b><i>IQR</i></b>	<i>interquartile range</i>	<i>unit of variable</i>
<b><i>SE</i></b>	<i>standard error</i>	<i>unit of variable</i>
<b><i>n</i></b>	<i>sample size</i>	-
<b><i>r</i></b>	<i>Pearson's correlation coefficient</i>	-

**Table 2. Observed hydrometeorological data from 11 sites and observed water temperature from 8 sites used to predict the energy balance continuously along the San Joaquin River, CA, USA. Denair II and Patterson are not within the study area and therefore are not considered part of the standard error calculations. Data sources include the California Irrigation Management Information System (CIMIS), the US Bureau of Reclamation (USBR), the US Geological Survey (USGS), the CA Dept. of Fish and Game (CADFG), the CA Dept. of Water Resources (CADWR), and the California Data Exchange Center (CDEC)**

<b>Observed Water Temperature Data</b>						
ID	Latitude	Longitude	Elevation (m)	Distance from Friant Dam (km)	Agency	Source
SJF	36.9844	-119.7243	89	2.24	USGS	CDEC
H41	36.8762	-119.7932	78	19.43	USBR	CDEC
DNB	36.8335	-119.9658	64	42.12	USBR	CDEC
GRF	36.7980	-120.1600	55	64.03	USBR	CDEC
SJRMP	36.7921	-120.3712	41	101.07	USBR/CDFW	USBR
SDP	36.9940	-120.5015	33	137.86	CADWR	CDEC
FFB	37.3099	-120.9310	16	228.11	USGS	CDEC
SMN	37.3472	-120.9762	12	239.35	USGS	CDEC
<b>Observed Meteorological Data</b>						
ID	Latitude	Longitude	Elevation (m)	Distance from channel (km)	Station Name	Source
FRT	36.9840	-119.7230	176	0.1	Friant Dam	USBR
080	36.8208	-119.7423	103	7.33	Fresno State	CIMIS
145	37.0165	-120.1864	70	22.97	Madera	CIMIS
148	37.3141	-120.3867	61	28.9	Merced	CIMIS
105	36.6340	-120.3818	58	16.92	Westlands	CIMIS
007	36.8512	-120.5909	56	12.01	Firebaugh	CIMIS
124	36.8901	-120.7314	56	22.65	Panoche	CIMIS
161	37.4389	-121.1385	49	17.45	Patterson	CIMIS
206	37.5459	-120.7545	46	29.3	Denair II	CIMIS
056	37.0967	-120.7539	29	6.65	Los Banos	CIMIS

**Table 3. Periods of consistent flow from SJF stream gauge data.**

<b>Periods of Consistent Flow</b>			
Start Date	End Date	Flow ( $\pm 30$ (cfs))	Season
1/1/09 0:00	2/15/09 17:30	96.6	DJF
2/15/09 17:45	3/7/09 7:45	94.6	DJF
3/7/09 15:15	3/18/09 7:45	109	MAM
3/25/09 16:30	4/20/09 8:30	144	MAM
5/1/09 15:15	6/5/09 6:15	180	MAM
7/10/09 6:30	7/21/09 2:30	180	JJA
7/21/09 2:45	8/28/09 22:30	210	JJA
8/28/09 22:45	9/9/09 7:00	180	JJA
9/7/09 9:30	9/18/09 15:45	190	SON
10/9/09 17:00	10/23/09 7:00	365	SON
10/23/09 9:00	11/1/09 10:30	389	SON
11/11/09 14:00	11/21/09 10:30	353	SON
11/21/09 13:30	12/22/09 8:00	96.4	SON
12/22/09 13:15	1/22/10 7:15	92.8	DJF
2/11/10 16:00	2/23/10 7:00	410	DJF
3/29/10 17:00	4/12/10 15:15	1300	MAM
5/1/10 18:00	5/13/10 13:15	1670	MAM
5/28/10 13:00	6/8/10 11:15	866	MAM
6/8/10 15:15	7/17/10 2:30	372	JJA
7/17/10 2:45	8/13/10 15:45	339	JJA
8/13/10 20:00	8/23/10 12:00	331	JJA
8/27/10 19:00	10/8/10 7:00	331	JJA
10/15/10 16:00	11/15/10 15:30	335	SON
2/1/11 11:15	2/11/11 6:15	221	DJF
3/4/11 16:15	3/19/11 20:15	700	MAM
7/17/11 1:00	8/12/11 10:30	310	JJA
8/12/11 21:30	9/12/11 6:15	320	SON
11/18/11 10:30	12/5/11 9:45	96.8	DJF
12/8/11 20:15	12/28/11 7:15	96.8	DJF

**Table 4. Selected periods of consistent flow from SJF stream gauge station. Start and end times will be used for model simulation.**

<b>Select 2011 Periods of Consistent Flow</b>			
Start Date	End Date	Flow ( $\pm 30$ (cfs))	Season
12/8/11 20:15	12/28/11 7:15	96.8	DJF
3/4/11 16:15	3/19/11 20:15	700	MAM
7/17/11 1:00	8/12/11 10:30	310	JJA
8/12/11 21:30	9/12/11 6:15	320	SON

**Table 5. Mean water temperature values from USGS station: SJF for initial boundary conditions across all seasons.**

<b>Water Temperatures for FLUVIAL-EB Initial Boundary Conditions</b>	
<b>Season</b>	<b>Water Temperature (°C)</b>
DJF	9.5
MAM	8.0
JJA	14.5
SON	14.5

**Table 6. FLUVIAL-EB model run commands for prescribed flow profile, temporal range, spatial and temporal resolution, and initial and boundary temperatures specified**

<b>FLUVIAL-EB Model Run Parameters</b>								
Season	Model Start Time	Model End Time	Selected Time Range	Flow Profile (cfs)	Distance Resolution (m)	Temporal Resolution (sec)	Boundary Temperature (°C)	Initial Temperature (°C)
DJF	12/15/2011	12/28/2011	12/20/2011 - 12/28/2011	1530	100	30	9.7	11
MAM	03/4/2011	03/19/2011	03/11/2011 - 03/19/2011	1530	100	30	8.1	11
JJA	07/29/2011	08/12/2011	08/04/2011 - 08/12/2011	1530	100	30	14.3	11
SON	08/30/2011	09/12/2011	09/04/2011 - 09/12/2012	1530	100	30	14.2	11

**Table 7. Scaled sensitivity terms along river distance and across seasons for each atmospheric variable. Scaled 7-day mean partial derivative terms at different distances along the river for the 7-day DJF, MAM, JJA, and SON model simulation periods. Color gradient corresponds to negative terms (green) and positive terms (red).**

will be reformatted to fit on one page:

DJF		0 km	10 km	25 km	50 km	75 km	100 km	125 km	150 km
	Shortwave radiation ( $^{\circ}\text{C}_{\text{river}}$ )	0.000	0.186	0.482	0.916	1.474	2.099	2.832	3.606
	Longwave radiation ( $^{\circ}\text{C}_{\text{river}}$ )	0.000	0.079	0.267	0.471	0.732	1.283	1.894	2.620
	Air temperature ( $^{\circ}\text{C}_{\text{river}}$ )	0.000	0.131	0.434	0.754	1.193	1.843	2.633	3.440
	Wind speed ( $^{\circ}\text{C}_{\text{river}}$ )	0.000	-0.062	-0.074	-0.131	-0.246	-0.330	-0.243	-0.396
	Vapor pressure ( $^{\circ}\text{C}_{\text{river}}$ )	0.000	0.018	0.048	0.084	0.127	0.206	0.267	0.236
	Air pressure ( $^{\circ}\text{C}_{\text{river}}$ )	0.000	0.000	-0.001	-0.001	-0.002	-0.003	-0.004	-0.004
MAM		0 km	10 km	25 km	50 km	75 km	100 km	125 km	150 km
	Shortwave radiation ( $^{\circ}\text{C}_{\text{river}}$ )	0.000	0.358	1.063	2.113	3.509	5.317	5.813	5.348
	Longwave radiation ( $^{\circ}\text{C}_{\text{river}}$ )	0.000	0.104	0.303	0.581	0.944	1.387	1.798	2.301
	Air temperature ( $^{\circ}\text{C}_{\text{river}}$ )	0.000	0.023	0.096	0.264	0.571	1.100	1.395	1.492
	Wind speed ( $^{\circ}\text{C}_{\text{river}}$ )	0.000	0.009	0.046	0.060	0.017	-0.182	-0.356	-0.703
	Vapor pressure ( $^{\circ}\text{C}_{\text{river}}$ )	0.000	0.014	0.065	0.157	0.290	0.498	0.611	0.740
	Air pressure ( $^{\circ}\text{C}_{\text{river}}$ )	0.000	0.000	0.000	0.000	0.000	0.000	0.000	0.000
JJA		0 km	10 km	25 km	50 km	75 km	100 km	125 km	150 km
	Shortwave radiation ( $^{\circ}\text{C}_{\text{river}}$ )	0.000	0.955	2.633	4.885	7.488	10.049	10.121	10.279
	Longwave radiation ( $^{\circ}\text{C}_{\text{river}}$ )	0.000	0.089	0.382	0.751	1.251	1.668	1.405	1.618
	Air temperature ( $^{\circ}\text{C}_{\text{river}}$ )	0.000	0.011	0.054	0.324	0.940	2.037	2.612	3.101
	Wind speed ( $^{\circ}\text{C}_{\text{river}}$ )	0.000	0.003	0.021	-0.004	-0.104	-0.439	-0.798	-1.172
	Vapor pressure ( $^{\circ}\text{C}_{\text{river}}$ )	0.000	0.003	0.021	0.056	0.136	0.267	0.261	0.322
	Air pressure ( $^{\circ}\text{C}_{\text{river}}$ )	0.000	0.000	0.000	0.000	0.001	0.001	0.001	0.001
SON		0 km	10 km	25 km	50 km	75 km	100 km	125 km	150 km
	Shortwave radiation ( $^{\circ}\text{C}_{\text{river}}$ )	0.000	0.624	1.705	3.285	5.353	7.364	7.439	7.907
	Longwave radiation ( $^{\circ}\text{C}_{\text{river}}$ )	0.000	0.104	0.528	1.028	1.688	2.319	2.209	2.653
	Air temperature ( $^{\circ}\text{C}_{\text{river}}$ )	0.000	0.010	0.033	0.189	0.625	1.541	2.015	2.528
	Wind speed ( $^{\circ}\text{C}_{\text{river}}$ )	0.000	0.009	0.046	0.036	-0.097	-0.528	-0.688	-0.997
	Vapor pressure ( $^{\circ}\text{C}_{\text{river}}$ )	0.000	0.006	0.020	0.055	0.149	0.342	0.420	0.430
	Air pressure ( $^{\circ}\text{C}_{\text{river}}$ )	0.000	0.000	0.000	0.001	0.001	0.002	0.002	0.003



**Table 9. Summary of perturbation values for sensitivity analysis.**

DJF	Coefficient of Variation (CV) Method	Rakovec et al., (2014) Method
Shortwave radiation ( $W m^{-2}$ )	1.548	1.012
Longwave radiation ( $W m^{-2}$ )	0.084	2.364
Air temperature ( $^{\circ}C$ )	1.314	0.038
Windspeed ( $m s^{-1}$ )	0.271	0.014
Vapor pressure (hPa)	0.183	0.006
Air pressure (hPa)	0.005	1.015

MAM	Coefficient of Variation (CV) Method	Rakovec et al., (2014) Method
Shortwave radiation ( $W m^{-2}$ )	1.387	1.700
Longwave radiation ( $W m^{-2}$ )	0.100	2.955
Air temperature ( $^{\circ}C$ )	0.374	0.124
Windspeed ( $m s^{-1}$ )	0.471	0.020
Vapor pressure (hPa)	0.236	0.010
Air pressure (hPa)	0.002	1.010

JJA	Coefficient of Variation (CV) Method	Rakovec et al., (2014) Method
Shortwave radiation ( $W m^{-2}$ )	1.136	3.135
Longwave radiation ( $W m^{-2}$ )	0.082	3.092
Air temperature ( $^{\circ}C$ )	0.271	0.238
Windspeed ( $m s^{-1}$ )	0.297	0.020
Vapor pressure (hPa)	0.074	0.014
Air pressure (hPa)	0.001	1.000

SON	Coefficient of Variation (CV) Method	Rakovec et al., (2014) Method
Shortwave radiation ( $W m^{-2}$ )	1.267	2.400
Longwave radiation ( $W m^{-2}$ )	0.115	3.280
Air temperature ( $^{\circ}C$ )	0.252	0.246
Windspeed ( $m s^{-1}$ )	0.318	0.020
Vapor pressure (hPa)	0.130	0.014
Air pressure (hPa)	0.003	1.000

**Table 10. Standard error values across all seasons and select distances along the river.**

	0 km	10 km	25 km	50 km	75 km	100 km	125 km	150 km
DJF ( $\pm^{\circ}\text{C}$ )	0.000	0.009	0.022	0.039	0.063	0.097	0.108	0.124
MAM ( $\pm^{\circ}\text{C}$ )	0.000	0.007	0.018	0.033	0.052	0.074	0.077	0.083
JJA ( $\pm^{\circ}\text{C}$ )	0.000	0.002	0.006	0.012	0.017	0.023	0.025	0.029
SON ( $\pm^{\circ}\text{C}$ )	0.000	0.005	0.013	0.024	0.037	0.048	0.049	0.052

**Table 11. CRCM5 gridded climate data.**

Model	Experiment type	Spatial Resolution	Temporal resolution	Simulation period
CRCM5	ERA-interim	0.11 deg	3 hourly	2010
CRCM5	ERA-interim	0.22 deg	3 hourly	2010
CRCM5	ERA-interim	0.44 deg	3 hourly	2010
CRCM5	ERA-interim	0.11 deg	3 hourly	2009
CRCM5	ERA-interim	0.22 deg	3 hourly	2009
CRCM5	ERA-interim	0.44 deg	3 hourly	2009
CRCM5	Historical	0.44 deg	3 hourly	1950 -2005
CRCM5	RCP 8.5	0.44 deg	3 hourly	1950 – 2100
RCP 8.5 greenhouse forcings begin in 2006 for future projection experiment.				

## Appendices

**Appendix A: Auxiliary Figures**

**Figure A1. Interpolated weather values at distance along the river for a mean 7-day model simulation period for the DJF season.**

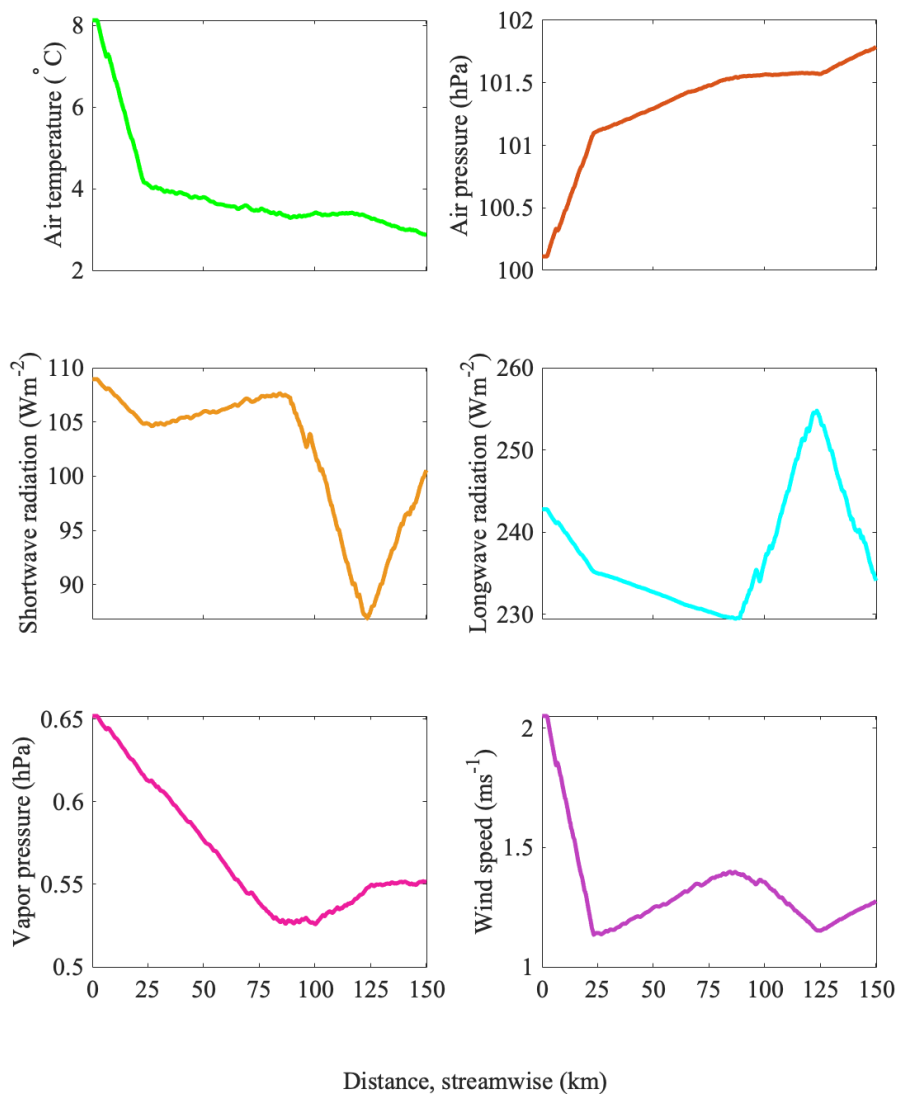


**Figure A2. Interpolated weather values at distance along the river for a mean 7-day model simulation period for the MAM season.**

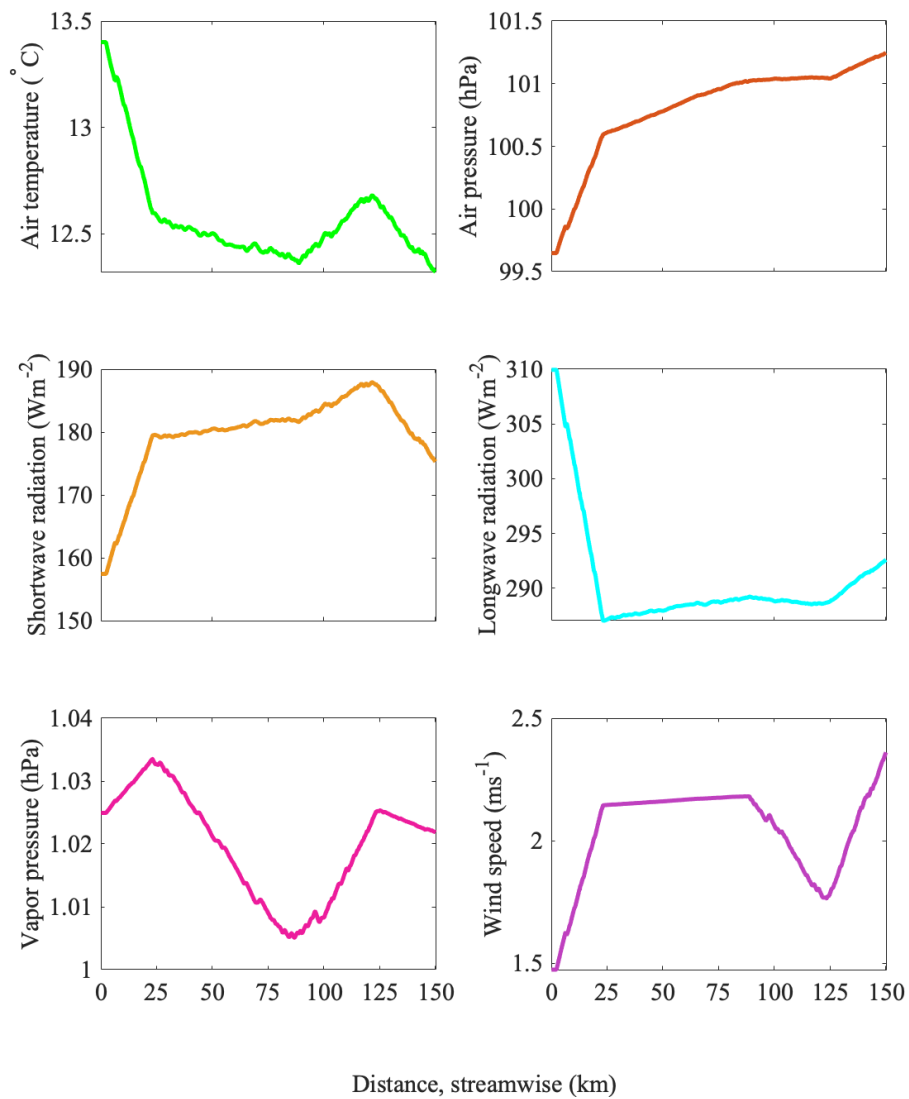


**Figure A3. Interpolated weather values at distance along the river for a mean 7-day model simulation period for the JJA season.**

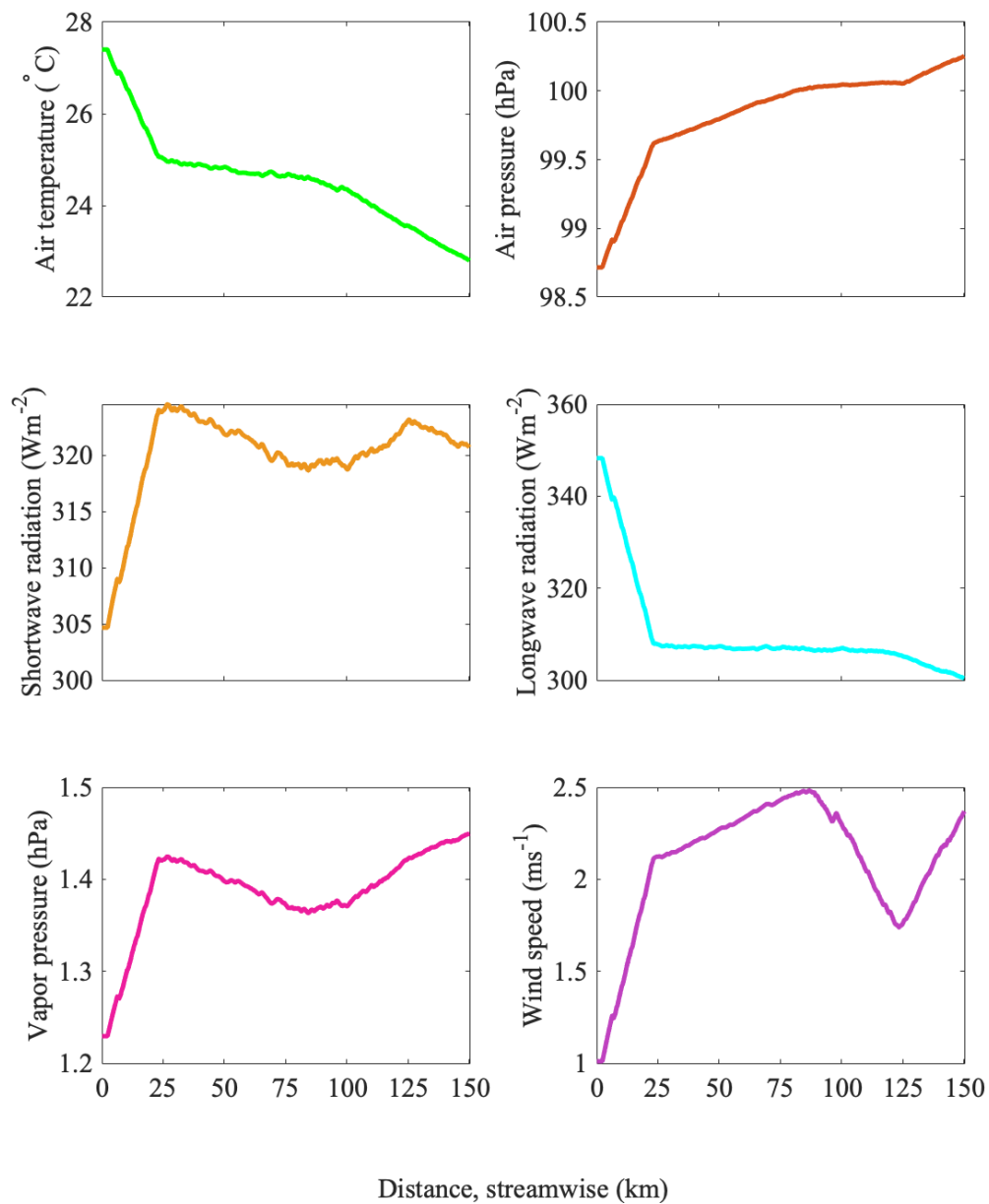


**Figure A4. Interpolated weather values at distance along the river for a mean 7-day model simulation period for the SON season.**

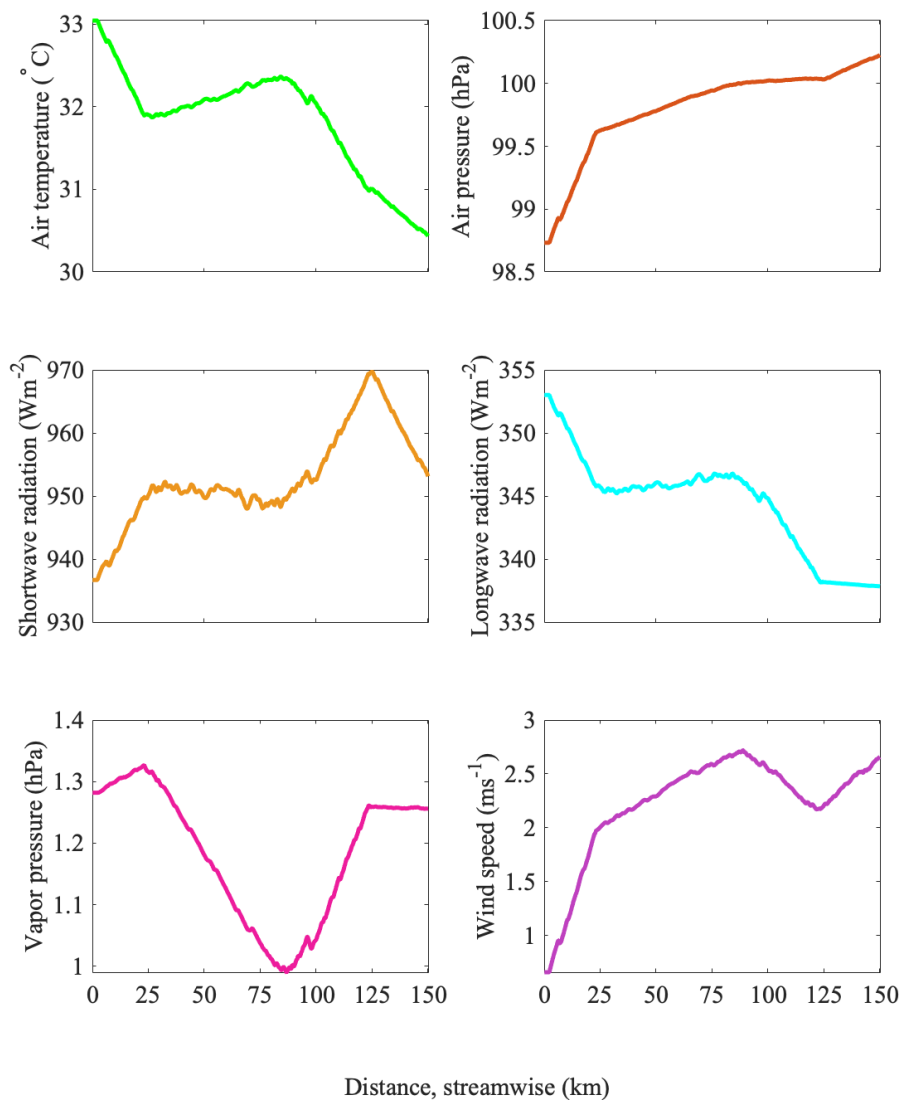


**Figure A5. Partial derivatives representing predicted river temperature sensitivity along river distance for the 7-day DJF (Winter) model simulation period.**

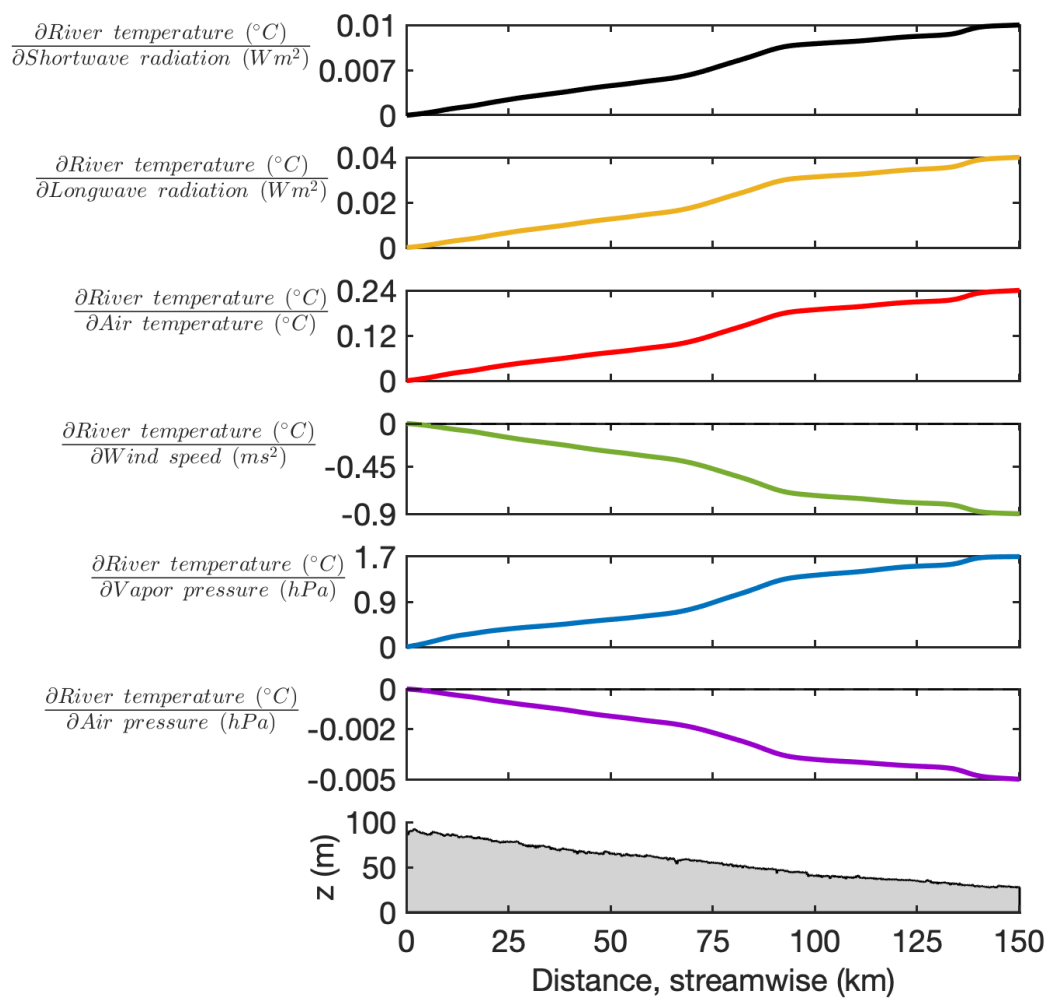


**Figure A6. Partial derivatives representing predicted river temperature sensitivity along river distance for the 7-day MAM (Spring) model simulation period.**

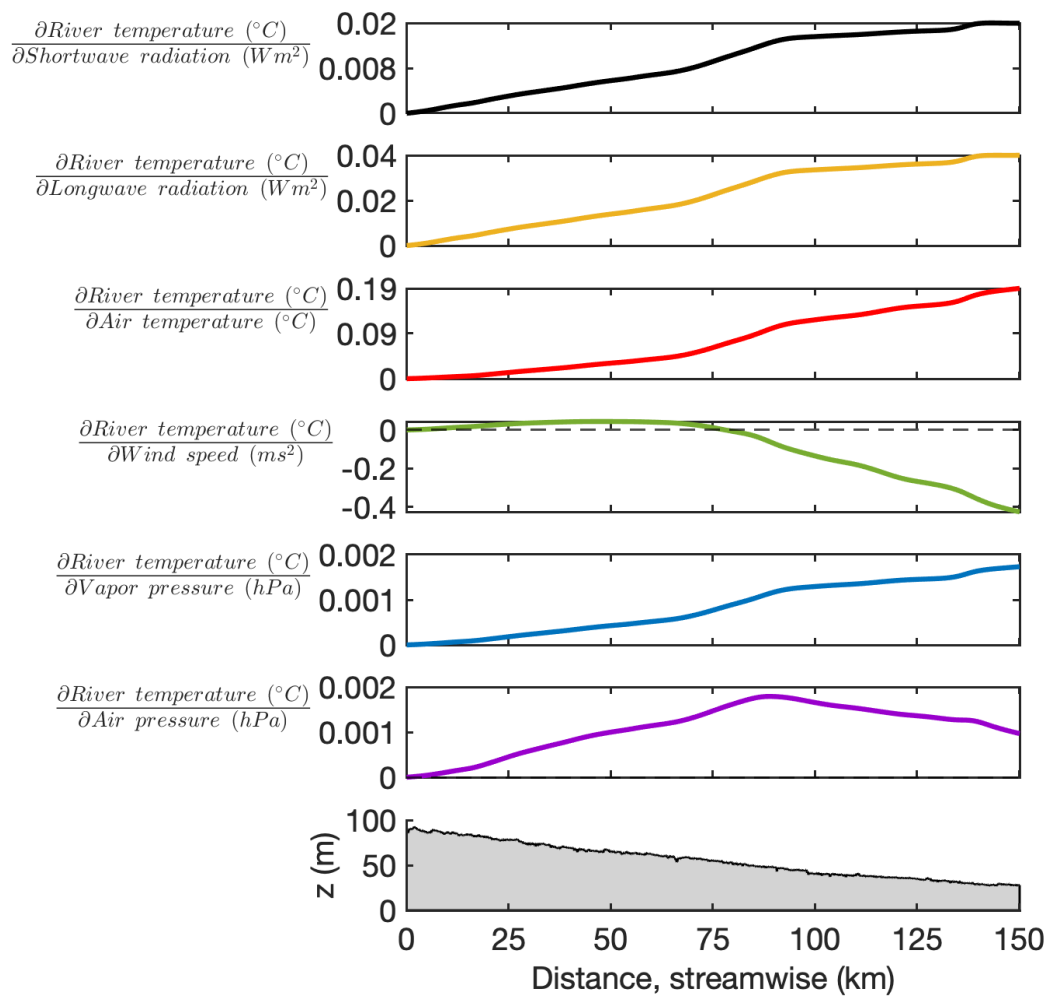


**Figure A7. Partial derivatives representing predicted river temperature sensitivity along river distance for the 7-day JJA (Summer) model simulation period.**

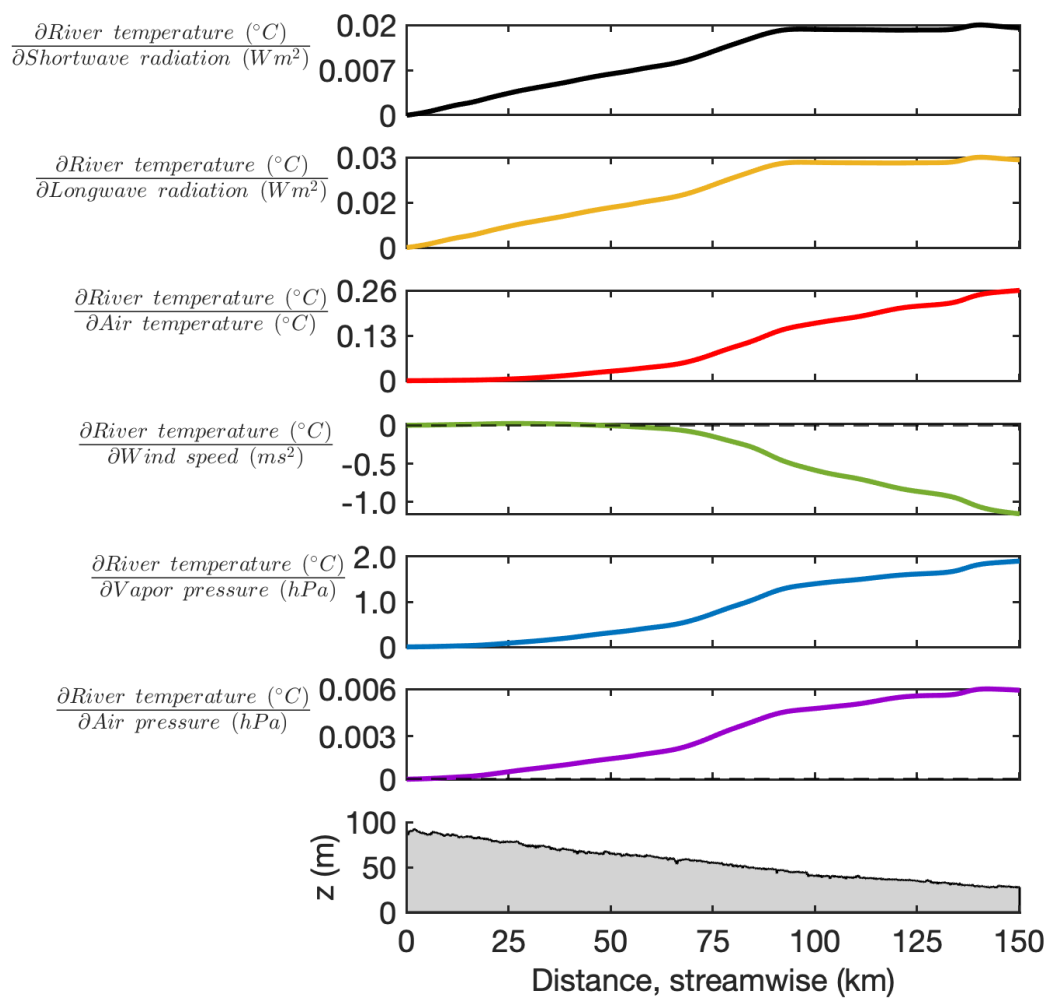


**Figure A8. Partial derivatives representing predicted river temperature sensitivity along river distance for the 7-day SON (Fall) model simulation period.**

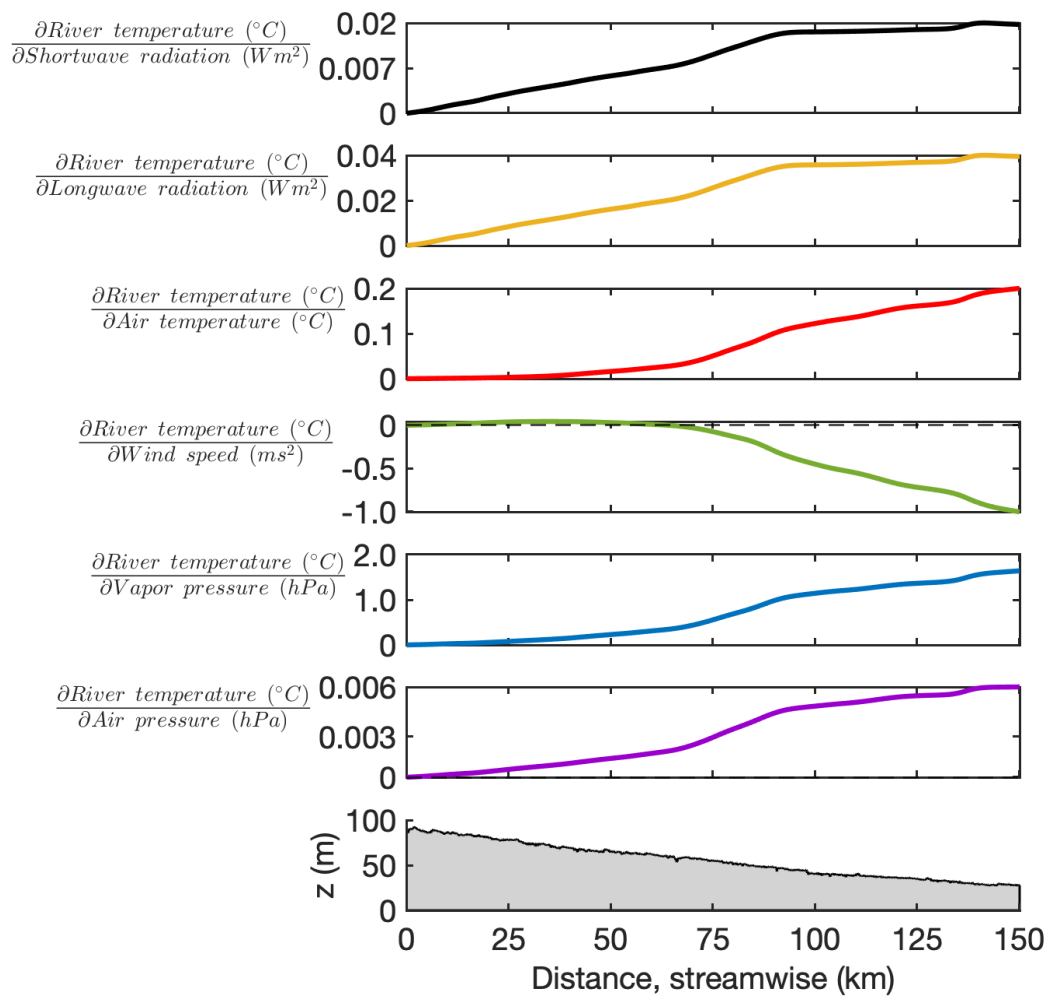
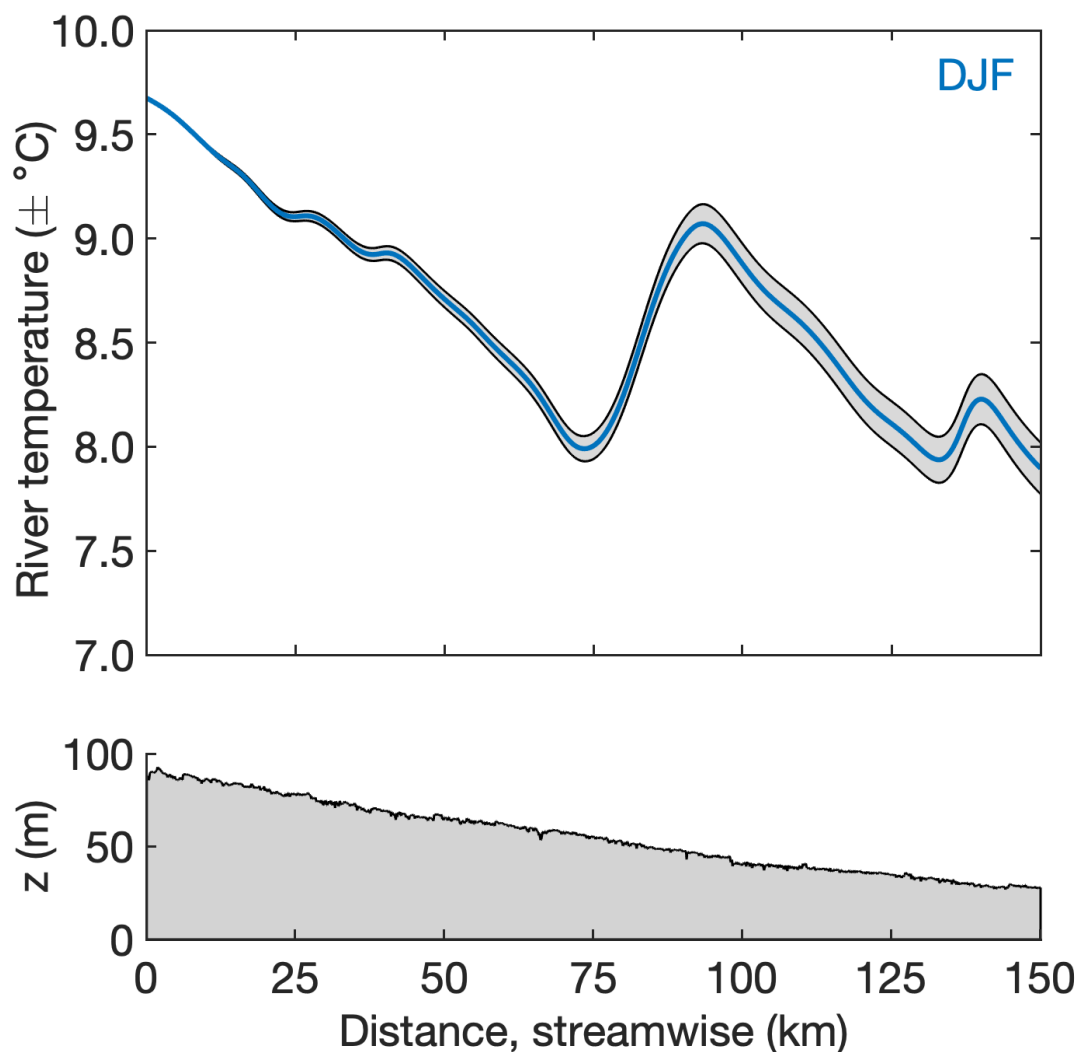


**Figure A9. Predicted river temperature (blue line) simulated during the winter (DJF) season. Grey area represents how confident we are in predicted river temperature ( $\pm^{\circ}\text{C}$ ) for the DJF seasons assuming that predicted river is only a function of the six atmosphere variables used in this study and uncertainty in predictions only come from error due to geographic proximity between weather station and channel.**



**Appendix B: Auxiliary Tables**

**Table 7. Sensitivity terms along river distance and across seasons for each atmospheric variable. Scaled 7-day mean partial derivative terms at different distances along the river for the 7-day DJF, MAM, JJA, and SON model simulation periods. Color gradient corresponds to negative terms (green) and positive terms (red).**

DJF	0 km	10 km	25 km	50 km	75 km	100 km	125 km	150 km
shortwave radiation ( $\frac{\partial T}{\partial S}, \frac{^{\circ}\text{C}_{\text{river}}}{\text{Wm}^{-2}}$ )	0.000	0.001	0.002	0.004	0.007	0.010	0.011	0.013
longwave radiation ( $\frac{\partial T}{\partial \text{ql}}, \frac{^{\circ}\text{C}_{\text{river}}}{\text{Wm}^{-2}}$ )	0.000	0.003	0.008	0.014	0.023	0.036	0.040	0.046
air temperature ( $\frac{\partial T}{\partial T_a}, \frac{^{\circ}\text{C}_{\text{river}}}{^{\circ}\text{C}_{\text{air}}}$ )	0.000	0.017	0.043	0.076	0.122	0.190	0.211	0.241
wind speed ( $\frac{\partial T}{\partial U}, \frac{^{\circ}\text{C}_{\text{river}}}{\text{ms}^{-1}}$ )	0.000	-0.051	-0.147	-0.295	-0.476	-0.755	-0.833	-0.947
vapor pressure ( $\frac{\partial T}{\partial e_0}, \frac{^{\circ}\text{C}_{\text{river}}}{\text{hPa}}$ )	0.000	0.174	0.340	0.518	0.839	1.356	1.527	1.708
air pressure ( $\frac{\partial T}{\partial p}, \frac{^{\circ}\text{C}_{\text{river}}}{\text{hPa}}$ )	0.000	0.000	-0.001	-0.001	-0.002	-0.004	-0.004	-0.005

MAM	0 km	10 km	25 km	50 km	75 km	100 km	125 km	150 km
shortwave radiation ( $\frac{\partial T}{\partial S}, \frac{^{\circ}\text{C}_{\text{river}}}{\text{Wm}^{-2}}$ )	0.000	0.001	0.003	0.006	0.009	0.014	0.015	0.016
longwave radiation ( $\frac{\partial T}{\partial \text{ql}}, \frac{^{\circ}\text{C}_{\text{river}}}{\text{Wm}^{-2}}$ )	0.000	0.003	0.008	0.015	0.024	0.036	0.038	0.043
air temperature ( $\frac{\partial T}{\partial T_a}, \frac{^{\circ}\text{C}_{\text{river}}}{^{\circ}\text{C}_{\text{air}}}$ )	0.000	0.004	0.013	0.033	0.067	0.127	0.156	0.194
wind speed ( $\frac{\partial T}{\partial U}, \frac{^{\circ}\text{C}_{\text{river}}}{\text{ms}^{-1}}$ )	0.000	0.011	0.023	0.044	0.012	-0.135	-0.268	-0.426
vapor pressure ( $\frac{\partial T}{\partial e_0}, \frac{^{\circ}\text{C}_{\text{river}}}{\text{hPa}}$ )	0.000	0.052	0.181	0.427	0.770	1.294	1.452	1.731
air pressure ( $\frac{\partial T}{\partial p}, \frac{^{\circ}\text{C}_{\text{river}}}{\text{hPa}}$ )	0.000	0.000	0.000	0.001	0.001	0.002	0.001	0.001

JJA	0 km	10 km	25 km	50 km	75 km	100 km	125 km	150 km
shortwave radiation ( $\frac{\partial T}{\partial S}, \frac{^{\circ}\text{C}_{\text{river}}}{\text{Wm}^{-2}}$ )	0.000	0.001	0.004	0.007	0.011	0.015	0.015	0.015
longwave radiation ( $\frac{\partial T}{\partial \text{ql}}, \frac{^{\circ}\text{C}_{\text{river}}}{\text{Wm}^{-2}}$ )	0.000	0.003	0.008	0.015	0.023	0.031	0.031	0.032
air temperature ( $\frac{\partial T}{\partial T_a}, \frac{^{\circ}\text{C}_{\text{river}}}{^{\circ}\text{C}_{\text{air}}}$ )	0.000	0.001	0.005	0.027	0.075	0.163	0.211	0.256
wind speed ( $\frac{\partial T}{\partial U}, \frac{^{\circ}\text{C}_{\text{river}}}{\text{ms}^{-1}}$ )	0.000	0.007	0.031	-0.006	-0.147	-0.587	-0.862	-1.155
vapor pressure ( $\frac{\partial T}{\partial e_0}, \frac{^{\circ}\text{C}_{\text{river}}}{\text{hPa}}$ )	0.000	0.016	0.084	0.315	0.740	1.399	1.614	1.901
air pressure ( $\frac{\partial T}{\partial p}, \frac{^{\circ}\text{C}_{\text{river}}}{\text{hPa}}$ )	0.000	0.000	0.001	0.001	0.003	0.005	0.006	0.006

SON	0 km	10 km	25 km	50 km	75 km	100 km	125 km	150 km
shortwave radiation ( $\frac{\partial T}{\partial S}, \frac{^{\circ}\text{C}_{\text{river}}}{\text{Wm}^{-2}}$ )	0.000	0.001	0.003	0.007	0.010	0.014	0.015	0.016
longwave radiation ( $\frac{\partial T}{\partial \text{ql}}, \frac{^{\circ}\text{C}_{\text{river}}}{\text{Wm}^{-2}}$ )	0.000	0.003	0.008	0.015	0.024	0.033	0.034	0.037
air temperature ( $\frac{\partial T}{\partial T_a}, \frac{^{\circ}\text{C}_{\text{river}}}{^{\circ}\text{C}_{\text{air}}}$ )	0.000	0.001	0.003	0.018	0.057	0.139	0.183	0.227
wind speed ( $\frac{\partial T}{\partial U}, \frac{^{\circ}\text{C}_{\text{river}}}{\text{ms}^{-1}}$ )	0.000	0.013	0.038	0.030	-0.075	-0.451	-0.718	-1.001
vapor pressure ( $\frac{\partial T}{\partial e_0}, \frac{^{\circ}\text{C}_{\text{river}}}{\text{hPa}}$ )	0.000	0.024	0.077	0.230	0.557	1.144	1.365	1.641
air pressure ( $\frac{\partial T}{\partial p}, \frac{^{\circ}\text{C}_{\text{river}}}{\text{hPa}}$ )	0.000	0.000	0.001	0.001	0.003	0.005	0.006	0.007

## References

- Arnold, N., Richards, K., Willis, I., & Sharp, M. (1998). Initial results from a distributed, physically based model of glacier hydrology. *Hydrological Processes*, 12.
- B.W. Webb, Y. Z. (1997). Spatial and Seasonal Variability in the Components of the River Heat Budget.
- Baker, C. (1994). *The quality control of long-term climatological data using objective data analysis*. Paper presented at the AMS Ninth Conference on Applied Climatology, Dallas, TX., January 15-20, 1995.
- Beven, K. (1989). Changing ideas in hydrology — The case of physically-based models. *Journal of Hydrology*, 105(1-2), 157-172. doi:10.1016/0022-1694(89)90101-7
- Bobba, A. G., Singh, V. P., & Bengtsson, L. (1995). Application of uncertainty analysis to groundwater pollution modeling. *Environmental Geology*, 26(2), 89-96. doi:10.1007/bf00768321
- Bray, E. N., Dozier, J., & Dunne, T. (2017). Mechanics of the energy balance in large lowland rivers, and why the bed matters. *Geophysical Research Letters*, 44(17), 8910-8918. doi:10.1002/2017GL075317
- Brown, G. W. (1969). Predicting Temperatures of Small Streams. *Water Resources Research*, 5(1), 68-75. doi:10.1029/WR005i001p00068
- Bukovsky, M. S., & Mearns, L. O. (2020). Regional climate change projections from NA-CORDEX and their relation to climate sensitivity. *Climatic Change*, 162(2), 645-665. doi:10.1007/s10584-020-02835-x
- Bunn, S. E., & Arthington, A. H. (2002). Basic Principles and Ecological Consequences of Altered Flow Regimes for Aquatic Biodiversity. *Environmental Management*, 30(4), 492-507. doi:10.1007/s00267-002-2737-0
- Caissie, D. (2006). The thermal regime of rivers: a review. *Freshwater Biology*, 51(8), 1389-1406. doi:10.1111/j.1365-2427.2006.01597.x
- Cardenas, M. B., Doering, M., Rivas, D. S., Galdeano, C., Neilson, B. T., & Robinson, C. T. (2014). Analysis of the temperature dynamics of a proglacial river using time-lapse thermal imaging and energy balance modeling. *Journal of Hydrology*, 519, 1963-1973. doi:10.1016/j.jhydrol.2014.09.079
- Choi, W., Moore, A., & Rasmussen, P. F. (2007). Evaluation of Temperature and Precipitation Data from NCEP-NCAR Global and Regional Reanalyses for Hydrological Modeling in Manitoba. 1-10.
- Christian E. Torgersen, R. N. F., Bruce A. McIntosh, Nathan J. Poage, Douglas J. Norton. (2000). Airborne Thermal Remote Sensing for Water Temperature Assessment in Rivers and Streams.
- Crawford, N. H., & Linsley, R. K. (1966). Digital Simulation in Hydrology'Stanford Watershed Model 4.
- Crawford, T. M., & Duchon, C. E. (1999). An Improved Parameterization for Estimating Effective Atmospheric Emissivity for Use in Calculating Daytime Downwelling Longwave Radiation. *Journal of Applied Meteorology*, 38(4), 474-480. doi:10.1175/1520-0450(1999)038<0474:aipfee>2.0.co;2

- Daly, C. (2006). Guidelines for Assessing the Suitability of Spatial Climate Data Sets. *International Journal of Climatology*, 26. doi:10.1002/joc.1322
- Daniels, M. E., & Danner, E. M. (2020). The Drivers of River Temperatures Below a Large Dam. *Water resources research.*, 56(5). doi:10.1029/2019WR026751
- Datt, P., Srivastava, P. K., Negi, P. S., & Satyawali, P. K. (2008). Surface energy balance of seasonal snow cover for snow-melt estimation in N–W Himalaya. *Journal of Earth Systems*, 567-573.
- Dee, D. P., Uppala, S. M., Simmons, A. J., Berrisford, P., Poli, P., Kobayashi, S., . . . Vitart, F. (2011). The ERA-Interim reanalysis: Configuration and performance of the data assimilation system. *Quarterly Journal of the Royal Meteorological Society*, 137(656), 553-597. doi:10.1002/qj.828
- Devak, M., & Dhanya, C. T. (2017). Sensitivity analysis of hydrological models: review and way forward. *Journal of Water and Climate Change*, 8(4), 557-575. doi:10.2166/wcc.2017.149
- Dilley, A. C., & O'Brien, D. M. (1997). Estimating downward clear sky long-wave irradiance at the surface from screen temperature and precipitable water.
- Dugdale, S. J., Hannah, D. M., & Malcolm, I. A. (2017). River temperature modelling: A review of process-based approaches and future directions. In (Vol. 175, pp. 97-113): Elsevier B.V.
- Eum, H.-I., Dibike, Y., Prowse, T., & Bonsal, B. (2014). Inter-comparison of high-resolution gridded climate data sets and their implication on hydrological model simulation over the Athabasca Watershed, Canada. *Hydrological Processes*, 28(14), 4250-4271. doi:10.1002/hyp.10236
- Fernandez-Bou, A. S., Ortiz-Partida, J. P., Pells, C., Classen-Rodriguez, L. M., Espinoza, V., Rodríguez-Flores, J. M., . . . Azuara, J. M. n.-. (2021). *Regional Report for the San Joaquin Valley Region on Impacts of Climate Change*. California Natural Resources Agency. Retrieved from
- Freeze, R. A., & Harlan, R. L. (1969). Blueprint for a Physically-Based, Digitally-Simulated Hydrologic Response Model.
- Gleick, P. H. (1989). Climate Change, Hydrology, and Water Resources.
- Griessinger, N., Schirmera, M., Helbiga, N., Winstrala, A., Michelc, A., & Jonasa, T. (2019). Implications of observation-enhanced energy-balance snowmelt simulations for runoff modeling of Alpine catchments. *Advances in Water Resources*. doi:10.1016/j.advwatres.2019.103410
- Hannah, D. M., & Garner, G. (2015). River water temperature in the United Kingdom: Changes over the 20th century and possible changes over the 21st century. *Progress in Physical Geography: Earth and Environment*, 39(1), 68-92. doi:10.1177/0309133314550669
- Hardy, B. (1998). *ITS-90 formulations for vapor pressure, frostpoint temperature, dewpoint temperature, and enhancement factors in the range -100 to + 100 C*. Paper presented at the The proceedings of the third international symposium on Humidity & Moisture, Teddington, London, England.

- Horton, P., Schaefli, B., & Kauzlaric, M. (2022). Why do we have so many different hydrological models? A review based on the case of Switzerland. *WIREs Water*, 9(1), e1574. doi:<https://doi.org/10.1002/wat2.1574>
- Lettenmaier, D. P., & Gan, T. Y. (1990). Hydrologic Sensitivities of the Sacramento-San Joaquin River Basin, California, to Global Warming.
- Li, D., Marshall, L., Liang, Z., Sharma, A., & Zhou, Y. (2021). Bayesian LSTM with stochastic variational inference for estimating model uncertainty in process-based hydrological models. *Water Resources Research*, 57(e2021WR029772). doi:<https://doi.org/10.1029/2021WR029772>
- Martynov, A., Laprise, R., Sushama, L., Winger, K., Šeparović, L., & Dugas, B. (2013). Reanalysis-driven climate simulation over CORDEX North America domain using the Canadian Regional Climate Model, version 5: Model performance evaluation. *Climate Dynamics*, 41(11-12), 2973-3005. doi:10.1007/s00382-013-1778-9
- Mussetter Engineering, I. (2006). *Evaluation of Bar Morphology, Distribution and Dynamics as Indices of Fluvial Processes in the Middel Rio Grande, New Mexico* Retrieved from Norman H. Crawford, S. J. B. (2004). History of the Stanford Watershed Model.
- Null, S. E., Ligare, S. T., & Viers, J. H. (2013). A Method to Consider Whether Dams Mitigate Climate Change Effects on Stream Temperatures. *JAWRA Journal of the American Water Resources Association*, 49(6), 1456-1472. doi:10.1111/jawr.12102
- Ortiz-Partida, J. P., Pells, C., Classen-Rodriguez, L. M., Espinoza, V., Rodríguez-Flores, J. M., Medellín-Azuara, J., . . . Westerling, L. (2022). San Joaquin Valley Region Report.
- Pechlivanidis, I. G., Jackson, B. M., & McIntyre, N. R. (2011). Catchment scale hydrological modelling: A review of model types calibration approached and uncertainty analysis methods.
- Pike, A., Danner, E., Boughton, D., Melton, F., Nemani, R., Rajagopalan, B., & Lindley, S. (2013). Forecasting river temperatures in real time using a stochastic dynamics approach. *Water Resources Research*, 49(9), 5168-5182. doi:10.1002/wrcr.20389
- Prata, A. J. (1996). A new long-wave formula for estimating downward clear-sky radiation at the surface. *Quarterly Journal of the Royal Meteorological Society*, 122(533), 1127-1151. doi:<https://doi.org/10.1002/qj.49712253306>
- Rakovec, O., Hill, M. C., Clark, M. P., Weerts, A. H., Teuling, A. J., & Uijlenhoet, R. (2014). Distributed Evaluation of Local Sensitivity Analysis (DELSA), with application to hydrologic models. *Water Resources Research*, 50(1), 409-426. doi:10.1002/2013wr014063
- Riahi, K., Rao, S., Krey, V., Cho, C., Chirkov, V., Fischer, G., . . . Rafaj, P. (2011). RCP 8.5—A scenario of comparatively high greenhouse gas emissions. doi:10.1007/s10584-011-0149-y
- Rivington, M., Matthews, K. B., Bellocchi, G., & Buchan, K. (2006). Evaluating uncertainty introduced to process-based simulation model estimates by alternative sources of meteorological data. *Agricultural Systems*, 88(2-3), 451-471. doi:10.1016/j.agsy.2005.07.004
- Rosbjerg, D., & Rodda, J. (2019). IAHS: a brief history of hydrology. *History of Geo- and Space Sciences*, 10(1), 109-118. doi:10.5194/hgss-10-109-2019

- Rummukainen, M. (2010). State-of-the-art with regional climate models. *I*. doi:10.1002/wcc.008
- Seck, A., Welty, C., & Maxwell, R. M. (2015). Spin-up behavior and effects of initial conditions for an integrated hydrologic model. *Water Resources Research*, *51*(4), 2188-2210. doi:10.1002/2014wr016371
- Simmons, C. T. (2008). Henry Darcy (1803–1858): Immortalised by his scientific legacy. *Hydrogeology Journal*, *16*(6), 1023-1038. doi:10.1007/s10040-008-0304-3
- Sridhar, V., Sansone, A. L., LaMarche, J., Dubin, T., & Lettenmaier, D. P. (2004). Prediction of stream temperature in forested watersheds. *Journal of the American Water Resources Association*, *40*(1), 197-213. doi:10.1111/j.1752-1688.2004.tb01019.x
- St-Hilaire, A. (2017). TEMPERATURE SUPPORT TOOLS CALIFORNIA'S CENTRAL VALLEY.
- Sun, J., Salvucci, G. D., Entekhabi, D., & Farhadi, L. (2011). Parameter estimation of coupled water and energy balance models based on stationary constraints of surface states. *Water Resources Research*, *47*(2). doi:<https://doi.org/10.1029/2010WR009293>
- Taheri, M., Mohammadian, A., Ganji, F., Bigdeli, M., & Nasserli, M. (2022). Energy-Based Approaches in Estimating Actual Evapotranspiration Focusing on Land Surface Temperature: A Review of Methods, Concepts, and Challenges. *Energies*, *15*(4), 1264. doi:10.3390/en15041264
- Verburg, P., & Antenucci, J. P. (2010). Persistent unstable atmospheric boundary layer enhances sensible and latent heat loss in a tropical great lake: Lake Tanganyika. *Journal of Geophysical Research Atmospheres*, *115*(11), 1-13. doi:10.1029/2009JD012839
- Wang, D., Zhan, Y., Yu, T., Liu, Y., Jin, X., Ren, X., . . . Liu, Q. (2020). Improving Meteorological Input for Surface Energy Balance System Utilizing Mesoscale Weather Research and Forecasting Model for Estimating Daily Actual Evapotranspiration. *Water*, *12*(1), 9. Retrieved from <https://www.mdpi.com/2073-4441/12/1/9>
- Webb, B. W., Hannah, D. M., Moore, R. D., Brown, L. E., & Nobilis, F. (2008). Recent advances in stream and river temperature research. *Hydrological Processes*, *22*(7), 902-918. doi:<https://doi.org/10.1002/hyp.6994>
- Westhoff, M. C., Savenije, H. H. G., Luxemburg, W. M. J., Stelling, G. S., Van De Giesen, N. C., Selker, J. S., . . . Uhlenbrook, S. (2007). A distributed stream temperature model using high resolution temperature observations. *Hydrology and Earth System Sciences*, *11*(4), 1469-1480. doi:10.5194/hess-11-1469-2007
- Whan, K., & Zwiers, F. (2014). Evaluation of extreme rainfall and temperature over North America in CanRCM4 and CRCM5. doi:10.1007/s00382-015-2807-7
- Willey, R. (1986). *HEC-5Q: System water quality modeling*: US Army Corps of Engineers, Hydrologic Engineering Center.